Biomimetic and bioactive plasma polymer surfaces

Richard P. Garrod

Biomimetic and Bioactive Plasma Polymer Surfaces

Richard P. Garrod

Chemistry Department

University of Durham

Durham

DH1 3LE

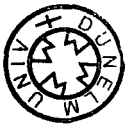

To Gran

Summary

Plasma polymer surfaces have been produced and analysed to evaluate their suitability as biomimetic and bioactive surfaces. The conclusions drawn are listed below:

- Plasma patterning of surfaces can be achieved by both an "ink and lift-off" or "emboss and lift-off" approaches.
- Plasma patterning using the "emboss and lift-off" approach improves with increasing force used to emboss the aperture containing device.
- Plasma polymer patterned surfaces can be used to mimic naturally occurring micro-condensers and a combination of super-hydrophobic and super-hydrophilic surfaces results in the optimal micro-condenser.
- Super-hydrophilic plasma polymer surfaces are superior in cell adhesion tests to polymers at higher contact angles.
- Plasma patterning of super-hydrophilic spots onto protein resistant backgrounds leads to patterning of cell growth.

Declaration

This thesis is a presentation of my original research work. Wherever contributions of others are involved, every effort is made to indicate this clearly, with due reference to the literature, and acknowledgement of collaborative research and discussions.
The work was completed under the guidance of Professor Badyal at Durham University.

Acknowledgements

From Durham University, I wish to express my thanks to Professor Badyal for his financial support and guidance in this project. From Lab 98 I would like to thank Luke Ward, Wayne Schofield and Declan Teare for all their help and guidance over the four years I spent in the group.

From Lab 98 I should also like to thank both Tom Bradley and later Lee Harris for producing the AFM imaging, to all the members of the Lab for preparing the hundreds of cell samples.

I would like to thank Victoria Christie and Dr. Pryzborski for their help in culturing Stem cells and Heather Long and Dr. Määttä for their assistance with culturing the MCF7 cells.

I should also like to thank both my parents and Michael Cannon for proofreading.

Resulting Literature:

This research has lead to the publication of the following literature:

- Mimicking a Stenocara Beetle's Back for Micro-Condensation. Garrod, R. P.; Schofield, W. C. E.; McGettrick, J; Teare, D. O. H.; Badyal, J. P. S. Winner of Durham University Chemistry Department Poster Competition 2005.
- Mimicking a Stenocara Beetle's Back for Microcondensation Using Plasmachemical Patterned Superhydrophobic-Superhydrophilic Surfaces. Garrod, R. P.; Harris, L. G.; Schofield, W. C. E.; McGettrick, J.; Ward, L. J.; Teare, D. O. H.; Badyal, J. P. S. Langmuir; 2007; 23(2); 689-693
- Substrate-Independent Approach for Polymer Brush Growth by Surface Atom Transfer Radical Polymerization. Teare, D. O. H.; Barwick, D. C.; Schofield, W. C. E.; Garrod, R. P.; Ward, L. J.; Badyal, J. P. S. Langmuir; 2005; 21(24); 11425-11430
- Poly(N-acryloylsarcosine methyl ester) Protein-Resistant Surfaces. Teare, D. O. H.; Schofield, W. C. E.; Garrod, R. P.; Badyal, J. P. S. J. Phys. Chem. B.; 2005; 109(44); 20923-20928
- Functionalization of Solid Surfaces with Thermoresponsive Protein-Resistant Films. Teare, D. O. H.; Barwick, D. C.; Schofield, W. C. E.; Garrod, R. P.; Beeby, A.; Badyal, J. P. S. J. Phys. Chem. B.; 2005; 109(47); 22407-22412
- Electroless Metallization onto Pulsed Plasma Deposited Poly(4-vinylpyridine) Surfaces. Bradley, T. J.; Schofield, W. C. E.; Garrod, R. P.; Badyal, J. P. S. Langmuir; 2006; 22(18); 7552-7555
- Rapid Polymer Brush Growth by TEMPO-Mediated Controlled Free-Radical Polymerization from Swollen Plasma Deposited Poly(maleic anhydride) Initiator Surfaces. Teare, D. O. H.; Schofield, W. C. E.; Garrod, R. P.; Badyal, J. P. S. Langmuir; 2005; 21(23); 10818-10824

List of Abbreviations used

3-VBA	- 3-vinylbenzaldehdye
4-VA	- 4-vinyl aniline
4-VP	- 4-vinyl pyridine
AFM	- Atomic Force Microscopy
AM	- Allyl Mecaptan
BEA	- 2-bromoethyl acrylate
CAE	- Constant Analyzer Energy
CCD	- Charge-coupled device
CHA	- Concentric Hemispherical Analyser
CMA	- Cylindrical Mirror Analyser
CRR	- Constant Retard Ratio
CW 4-VP	- Continuous Wave 4-vinyl pyridine
CW AA	- Continuous Wave acrylic acid
CW DMS	- Continuous Wave Dimethyl sulphate
CW HEMA	- Continuous Wave 2-hydroxyethyl methacrylate
DMEM	- Dulbecco's modified eagle's medium
DMS	- Dimethyl sulphate
DNA	- Deoxyribonucleic Acid
EC	- Embryonic carcinoma
ECM	- Extra-cellular Matrix
EEDF	- Electron Energy Distribution Function
ESCA	- Electronic Spectroscopy for Chemical Analysis
FAT	- Fixed Analyzer Transmission
FRR	- Fixed Retard Ratio
FT-IR	- Fourier Transform Infrared
FWHM	- Full-Width At Half Maximum Of The Peak
GMA	- Glycidyl methacrylate
He-Ne	- Helium-Neon
MA	- Maleic anhydride
MCF7	- Human Breast Adenocarcinoma Cell Line
MIMIC	- Micro-Moulding In Capillaries
MW	- Molecular Weight
NASME	- N-acryloylsarcosine methyl ester
PBD	- Polybutadiene
PBS	- Phosphate buffered saline
PDMS	- Polydimethysiloxane
PFAC-6	- 1H,1H,2H,2H-perfluorooctyl acrylate
PMMA	- Polymethylmethacrylate
PS	- Styrene
PTFE	- Polytetrafluoroethylene
RAIRS	- Reflection-absorption infrared spectroscopy
RF	- Radio Frequency
RIE	- Reactive Ion Etching
S/N	- Signal To Noise
SAM	- Self Assembled Monolayer
SDS	- Sodium Dodecyl Sulphate
SPR	- Surface Plasmon Resonance
STM	- Scanning Tunnelling Microscope
SWR	- Standing Wave Ratio
TEMPO	- 2,2,6,6-Tetramethylpiperidine-1-oxyl
t_{off}	- Plasma Time Off
t_{on}	- Plasma Time On
UA	- 10-Undecenal
UHV	- Ultra-high Vacuum
UV	- Ultraviolet
v/v	- Volume/volume
VBC	- 4-vinylbenzyl chloride
VUV	- Vacuum Ultraviolet
w/v	- Weight/volume
XPS	- X-Ray Photoelectron Spectroscopy
µCP	- Micro-Contact Printing
µTM	- Micro-Transfer Moulding

Table of Contents

Table of Figures

Table of Tables

1. Plasmas and Experimental Techniques

1.1. Plasma

1.1.1. Introduction to Plasmas

Plasma is defined as "a gaseous complex that may be composed of electrons, ions of either polarity, gas atoms, and molecules in the ground or any higher stats of any form of excitation, as well as light quanta".[1] This definition excludes it from being either a solid, liquid or gas and is often referred to as the fourth state.[2] Often quoted examples include naturally occurring plasma in the interior of stars and within lightning strikes.

1.1.2. Types of Plasma

Plasmas are split into three categories depending on the method of ionisation and their properties:[3]

- Complete Thermal Equilibrium Plasma: Exists in total thermal equilibrium, all the individual components (*e.g.* the electrons and atoms) are at the same temperature. This is not possible in controlled laboratory experiments but occurs in stars.
- Local Thermodynamic Equilibrium Plasma: Occurs when radiation from the plasma is at a lower temperature to the rest of the plasma but the ignition is still caused by intense heat. Common examples are an electric arc or a lightning strike.
- Non-Local Thermodynamic Equilibrium Plasma: Also known as a non-equilibrium plasma since there is no thermodynamic equilibrium present. The energy of the electrons is much greater than that of the other species present. The temperature of the plasma gas is relatively low. Non-equilibrium plasmas are the most common plasmas used in chemistry laboratories.[4,5]

1.1.3. Plasma Physics

Plasmas are ignited when the available energy density present is greater than the ionisation energy of the gas of vapour molecules in the chamber. Once initiated the ionisation is sustained by the applied potential because the reactions within the plasma create a cascade effect of reactive species. The applied potential varies from a few volts at low pressure (0.2 mbar)[6] to greater than 100 V at higher pressure.[7]

Plasma comprises a collection of charged particles with overall electronic neutrality. These charged particles enable electrical conductivity, mainly through the movement of electrons, but this movement must be countered by charge movement by the opposite polarity species. For the plasma to be sustainable, it must occupy a greater volume than the Debye length. The Debye length, λ_D, is the shortest dimension a plasma can exist in, for the non-equilibrium plasmas used in this research, the Debye length is less than 100 μm.

1.1.4. Plasma Processes

All species in a plasma are in constant motion and collisions are readily occurring. Electrons are the lightest species present and the most easily accelerated. The electrons have a range of energies determined by the electron energy distribution function, EEDF:

$$F(E) = \left(\frac{2E^{1/2}}{n^{1/2} kT^{3/2}} \right) e^{\left(\frac{-E}{kT} \right)} \qquad (1)$$

Where E = electron energy, T = electron temperature, k = Boltzmann constant. This distribution function explains why ionisation can occur; the few electrons at the highest energies have enough kinetic energy to break chemical bonds and activate plasma gases.

- Ionisation - Occurs when an electron collision with an atom or molecule produces a positive ion and two electrons. This is the most common form of ionisation within a plasma. Recombination, the reverse of ionisation, also occurs.
- Excitation - An electron collision promotes an electron from the atom or molecule ground state into a higher energy level.

- Relaxation - Atoms or molecules excited by collision emit a quantum of light as the promoted electron relaxes into its ground state. Relaxation is the process that causes plasmas to emit light over a range of frequencies from ultraviolet to infrared.
- Dissociation - Electron collision causes the splitting of a molecule to create reactive radicals. Dissociation to radicals can also be caused by photon impact
- Electron attachment - An electron is absorbed into the molecule during collision and a radical species is emitted.

1.1.4.1. Other Processes

There are several other processes occurring in plasmas including charge transfer and collisions between molecules that have already been excited. Molecules, atoms and the excited species created are also in frequent collision with the walls of the reactor and any samples present. These interactions result in even more reactions including sputtering, polymerisation or ion implantation.

1.1.5. Plasma Polymerisation

Polymerisation by conventional methodologies produces long chain polymers with consistent repeat units and high molar mass. Plasma polymerisation occurs in a higher energy environment and the abundance of different reactive species leads to polymers that are highly branched and cross-linked. Plasma polymerisation is characterised by several features:

- Absence of repeat units.
- Varying properties depending on plasma conditions.
- Functional groups such as double bonds are not essential for polymerisation to occur.

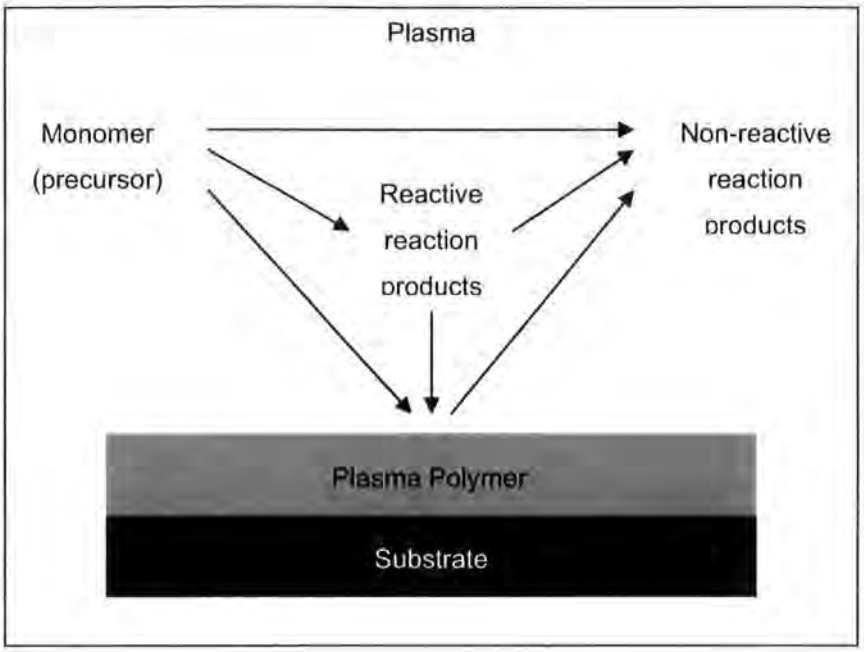

Figure 1: Plasma polymerisation process

1.1.5.1. Continuous Wave Plasma Polymerisation

Continuous wave plasma causes the complete breakdown of the plasma gas or vapours and results in extremely reactive high-energy species. Commonly used for etching or modification,[8] deposition can occur but unless the treatment time is short, etching or modification will damage the surface layer.

1.1.5.2. Pulsed Plasma Polymerisation

By using a pulse generator the potential applied to the reactor can be pulsed to reduce the overall power applied to the plasma. The plasma is first ignited and sustained for a short period, typically in the microsecond range, before the potential is switched off and the plasma exponentially decays, typically in the millisecond range. This technique has several advantages of continuous wave polymerisation:[9]

- Better structural retention.
- Control over cross-linking.
- Longer chain growth.
- Absence of surface modification.

The average power is defined by:

$$\langle P \rangle = P_P \left(\frac{t_{on}}{t_{on} + t_{off}} \right) \quad (2)$$

<P> is the average power, P_p the peak power, t_{on} the plasma on time and t_{off} the plasma off time.

1.1.6. Plasma Reactors

A plasma reactor is quite simple, it must have the ability to emit and contain the gas or vapour, whilst withstand reduced pressures and be coupled to an energy source to sustain the plasma. They can be grouped into three main types depending on their method of sustaining the plasma discharge:

- Microwave or high frequency.
- Internal, *e.g.* parallel plate.
- External, *e.g.* coils.

The potential source must be capable of producing powers from 1 W to 5 kW. Microwave reactors also require a waveguide to transfer the power to the reactor.

A matching unit is required which matches the resistance capacitance or inductance of the power supply with that of the gas or vapour being used. This allows greater efficiency in power dissipation. The chamber must also be capable of controlling the inlet of gas, the pressure and flow-rate.

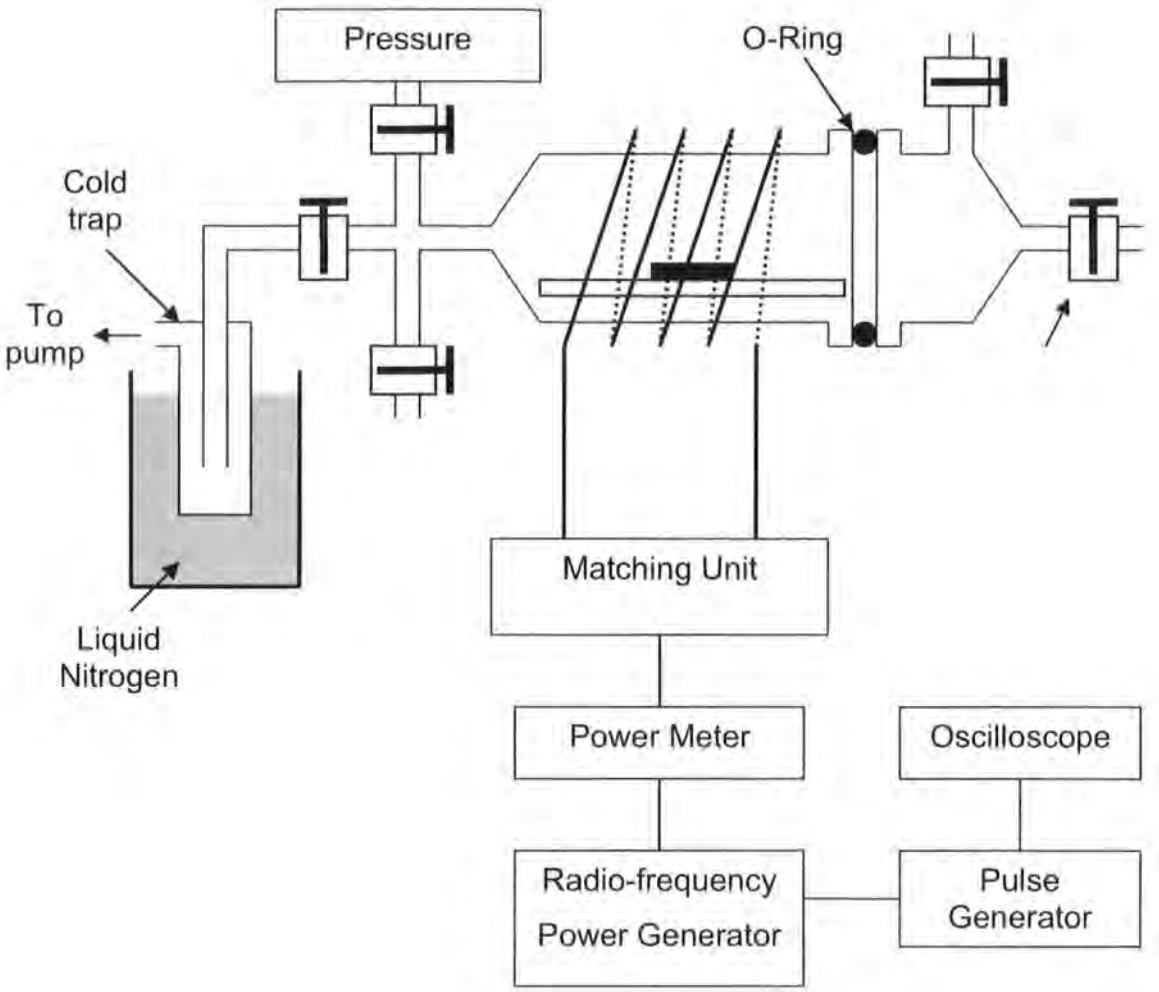

Figure 2: The apparatus used during this work

1.2. X-Ray Photoelectron Spectroscopy

1.2.1. Introduction

X-Ray Photoelectron Spectroscopy, XPS, or Electronic Spectroscopy for Chemical Analysis, ESCA, is a method for determining the elements on a surface and quantifying the chemical composition. The sample is excited by an X-ray source, which causes photo-ionisation of atoms in the surface of the sample. This leads to photoelectron emission and by interpreting the kinetic energy of these photoelectrons, the elemental composition of the surface.

1.2.2. Electron Emission

X-ray photons have a known energy due to Planck's Equation:

$$E = h\nu \quad (3)$$

h is Planck's constant and ν is the frequency. These photons excite the sample and cause photoemission of electrons with kinetic energy, E_k. These photo-emitted electrons leave a hole in the core level which is filled by an electron dropping down from a higher level. Either the energy released by this electron will be emitted as a photon (X-ray fluorescence) or it can be transferred to another electron (an Auger electron) which is ejected from the atom.

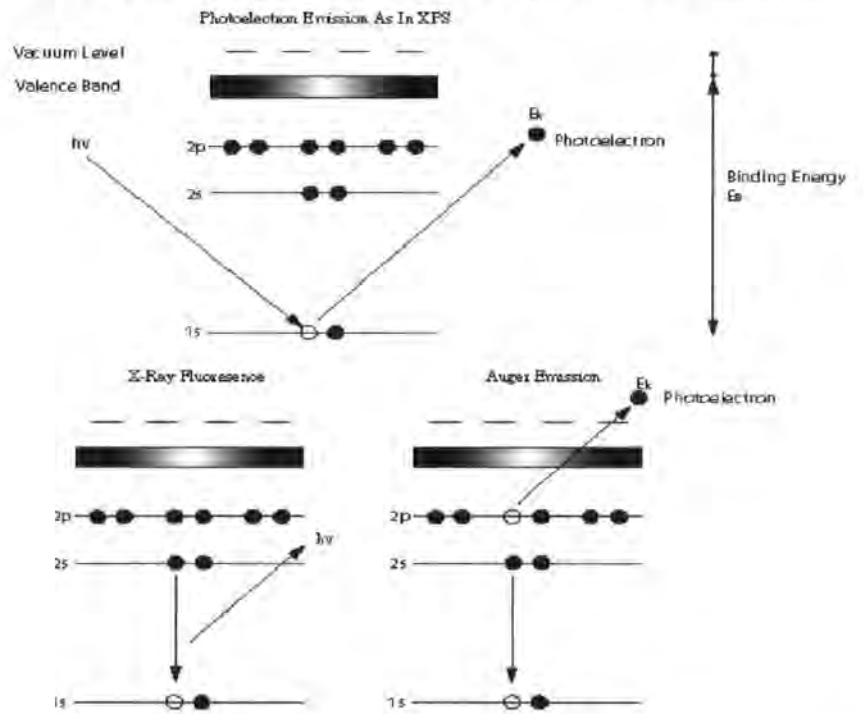

Figure 3: Photoemission of a core electron following exposure to an X-ray Source[10]

The energy of the emitted photoelectron is calculated by combining Planck's equation with laws on the conservation of energy:

$$E_k = h\nu - E_B - \Phi \quad (4)$$

E_k is the kinetic energy of the emitted electron (eV), E_B is the binding energy of the nucleus (eV) and F is the work function (eV). The work function is a property of both the sample and the spectrometer and quantifies the energy required for the electron to get from the core level to the spectrometer detector.

In a normal sample, the work function is substantially smaller than the binding energy so the equation can be simplified and rearranged to:

$$E_B = h\nu - E_k \quad (5)$$

No two elements have the same binding energy;[11] this allows XPS to be used to differentiate between elements. Small changes in the chemical environment of atoms cause a shift in the binding energy. With a high-resolution spectrometer, this allows the determination of the bonding of the elements present. The intensity of photoelectron emission is proportional to the elemental composition of the sample; so with calibration of the spectrometer the sample can be quantitatively analysed.

The depth of measurement in XPS is dependant on the inelastic mean free path of the electron beam. This is the characteristic length that the electron can travel without suffering any energy loss.

1.2.3. Spectrometers

XPS spectrometers do not vary a great deal and all must include the basic components of an X-ray source, an electron energy analyser and an electron detector whilst maintaining ultra-high vacuum.

1.2.3.1. X-Ray Source

X-ray sources emit radiation when bombarded by high-energy electrons. The energy of the X-rays emitted must be large enough to excite core-level electrons (>1 keV). In addition, the line width emitted by the source should be as narrow as possible to limit the signal to noise ratio. The two commonly used X-ray sources are MgK_a ($h\nu$ = 1253.6 eV) and AlK_a ($h\nu$ = 1486.6 eV). Some spectrometers use a diffraction grating to monochromate the source, but this reduces signal intensity and these were not used in this research.

By turning on the filament, X-rays from the anode material are generated by electron bombardment. The soft X-rays generated then pass out through an aperture in the surrounding cylindrical shield. The aperture is covered by a thin aluminium foil that screens the sample from stray electrons from the filament, heating effects and any contamination from the source.

1.2.3.2. Detectors

Photoelectrons emitted from the surface are separated according to their energy and intensity by an electrostatic analyser. There are two main types of electrostatic analyzer: Concentric Hemispherical Analyser, CHA, and the Cylindrical Mirror Analyser, CMA.

The CHA uses two concentrically positioned hemispheres with radii, R_1, inner hemisphere, and R_2, outer hemisphere. Negative potentials are applied to both hemispheres and with V_2 being greater than V_1.

The different voltages are placed on each hemisphere in such a way that there is an electric field between the two hemispheres. Electrons are injected into the gap between the hemispheres, if the electrons are travelling too fast they will collide with the outer hemisphere; if they are travelling too slowly they will be attracted to the inner hemisphere. Only electrons in a narrow energy region (called the pass energy) will get all of the way round the hemispheres to the detector. The fields within the analyser are varied to allow only electrons of a given energy to arrive at the detector slits and into the detector themselves.

A hemispherical analyser and electrostatic lens can be operated in two modes:

- Fixed Analyzer Transmission, FAT, also known as Constant Analyzer Energy, CAE.
- Fixed Retard Ratio, FRR, also known as Constant Retard Ratio, CRR.

In CAE mode, the pass energy of the analyser is held at a constant value and it is the job of the electrostatic lens to retard the given kinetic energy channel to the one accepted by the analyser. In the alternative mode, CRR, the electrons are slowed down by an amount that is a constant ratio of the electron energy to be analysed. If the retard ratio is 10, and 1000 eV electrons are to be detected, then the electrons will be slowed down to 100 eV, and the pass energy will be set to 100 eV. XPS is normally operated in CAE to keep the absolute resolution of the peak constant. The absolute resolution of the peak can be defined as:

$$R = \frac{\Delta E}{E_0} \qquad (6)$$

R is the absolute resolution of the peak, ΔE is the full-width at half maximum of the peak, FWHM, and E_0 is the energy of the peak. The current reaching the slit is too low to be measured so must therefore be amplified. This is done using a

Channeltron as both an electron detector and amplifier. It has a spiral glass tube coated with a highly resistive material on the inside walls and a potential of 3 kV applied to its ends. Incoming electrons collide with the walls and cause an emission of secondary electrons. This induces a cascade of electrons that can be detected.

1.2.3.3. Ultra-High Vacuum

Ultra-high Vacuum, UHV, conditions are essential for XPS. Interaction of electrons with any gaseous species will result in loss of signal, and XPS is extremely sensitive to surface adsorbed species.

1.3. Infrared Spectroscopy

1.3.1. Introduction

Infrared Spectroscopy measures the change of dipole moment during vibrations or stretches of a chemical bond. Different chemical bonds absorb infrared energy at specific and unique frequencies and intensities. Because of this, infrared spectroscopy allows the identification of the different chemical groups in a sample.

Infrared frequencies stretch from 13,000 to 10 cm^{-1} but analysis is typically measured from 4,000 – 700 cm^{-1}. The incident light excites the bonds thereby induces a change in the dipole moment by causing them to stretch, vibrate or rotate. By comparing the transmitted radiation to the incident light, the relative transmission can be calculated. Spectra are recorded by plotting the transmittance as a function of frequency.

$$T = \frac{I}{I_0} \tag{7}$$

T is the relative transmission, I is the intensity of transmitted radiation and I_0 is the intensity of the incident radiation. The wavelength that any vibrational mode absorbs is related to the frequency of the vibration whilst its intensity depends on how well the radiation is adsorbed. Vibrational modes are active only if there is a change in the molecular dipole moment during the vibration; examples

include anti-symmetric vibrations and vibrations involving polar groups (*e.g.* carbonyls).

Infrared spectrometers usually use a material heated to incandescence by an electric current as the activation source. The main materials used are composite oxides of rare earths (Nernst Glower) or a silicon carbide rod (Globar). The source must produce a consistent output and the energy distribution emitted should be as close as possible to that of a theoretical black body. Sources are usually positioned at the focal point of a parabolic mirror so that the reflected light produces a parallel beam.

1.3.2. Michelson Interferometer

A monochromator is positioned between the source and sample to control which wavelengths of the incident light reach the sample. In FT-IR machines, this device is called a Michelson Interferometer, this consists of a beam splitter at 45^0 to a fixed mirror, and at 90^0 to the fixed mirror and perpendicular to the incoming radiation is a moveable mirror. The relative path lengths between the two mirrors and the beam splitter govern whether there is constructive or destructive interference.

By application of a Fourier transform procedure and with reference to a background, it is possible to determine which elements of the signal come from interactions with the sample. The FT-IR method has several advantages over normal infrared spectroscopy:

- The whole spectrum is scanned at once, so the time taken to acquire a spectrum with identical signal to noise, S/N, ratio to a conventional Infrared spectrometer is drastically reduced.
- There are no slits required in the optics of the spectrometer that results in a much higher radiation throughput.
- Resolving power in an FT-IR instrument is constant and does not vary with wavenumber.

The detector measures the intensity of the infrared energy that has passed through the spectrometer and converts it into a measurable electrical current. There are two main types of detector:

- Thermal detectors measure the heating effect of the radiation. Thermal detectors such as triglycine sulphate have good responses over a wide range of infrared frequencies and are relatively cheap in terms of cost.
- Selective detectors respond differently at certain wavelengths. The mercury cadmium telluride detector is a quantum detector that has much better sensitivity and response, but over a smaller range of frequencies and is cooled with liquid nitrogen to improve the S/N ratio.[12]

1.4. Reflectometry

1.4.1. Introduction

Thin films are often deposited onto surfaces of other materials to create insulating covers, gas barriers or wear resistance layers. The thickness of these layers can be particularly important, not least to economise on raw materials. Non-optical measurement of film thickness often requires a destructive technique and these methods are usually slow and inaccurate. Optical techniques are preferred for non-opaque films such as polymers; they measure how the light interacts with film as it passes through the sample. The two most common techniques are Elipsometry and Spectral Reflectometry. Of these, Spectral Reflectometry is simpler and less expensive but is restricted to less complicated surfaces. A comparison of the reflected and transmitted light is made and, using approximations of the physical constants of the film and substrates, a mathematical calculation can be used to determine the thickness.
When light travels through a film, its path is described by optical constants, n, the refractive index ($n>1$) and k, the extinction coefficient. The refractive index is the ratio of the speed of light in a vacuum to the speed of light in the material. The extinction coefficient is a measure of the absorption of light in the material.
Reflection occurs whenever light cross a boundary between two different materials.

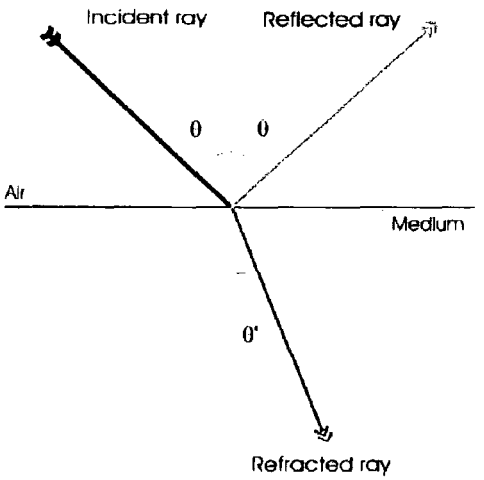

Figure 4: Reflection and refraction at an interface[a]

The fraction of light that is reflected is determined by the changes in *n* and *k* between the two layers.

1.4.2. Reflected and Transmitted Light

If there are several distinct layers to a surface the total reflected light will be the sum of the reflected light from all of the layers. The phase relationship between the reflected beams is directly related to the difference in path lengths of the beams. Using mathematical calculations the depth of the films can be determined from the phase difference and the refractive index and extinction coefficient of the substances being tested. If these are not known accurately then they can be estimated and improved by iterative steps until the mathematical approximation of the phase relationship matches the experimentally determined phase relationship.

1.5. Fluorescence Spectroscopy

1.5.1. Introduction

Fluorescence is a type of luminescence where certain molecules emit quanta of light from an electronically excited state (created by a physical or chemical action). Emission of light quanta following absorption of light is a sub-category

[a] www.aquila-instruments.co.uk

of luminescence termed photoluminescence, of which there are two types, fluorescence and phosphorescence. Fluorescence is the absorption of light at a certain wavelength and immediate (10^{-7} – 10^{-9} s) emission of light at a longer wavelength. Phosphorescence is similar to fluorescence but involves a delayed emission.

1.5.2. Excitation and Emission

In the Jablonski diagram, the process of fluorescence takes a matter of a few billionths of a second. For any particular molecule, several different electron states exist depending on the total electron energy and symmetry. Within each state there are vibrational and rotational energy levels associated with the atomic nuclei and bonding orbitals.

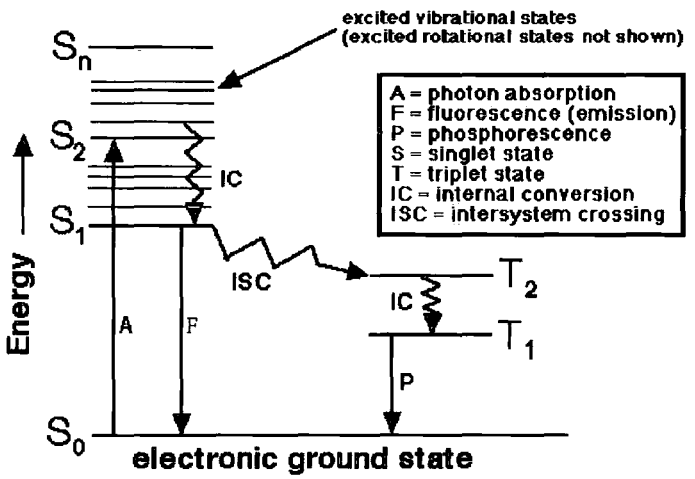

Figure 5: Jablonski Diagram[b]

The absorption of a photon only occurs when the incident light has a wavelength short enough to have enough energy to promote an electron transition. Above this energy, photons are absorbed at wavelengths corresponding to transitions between bands and excess energy is converted into vibrational and rotational energy. Any absorption band is broadened by the energy provided by thermal motion.

Immediately after the photon is absorbed the most probable process is relaxation to the lowest vibrational energy level of the first excited state. The

[b] www.shsu.edu

other possible processes are non-radiative decay and collision with another electron. If relaxation is followed by emission of a photon and return to the ground state then this process is fluorescence. The closely spaced vibrational energy levels of the ground state produce a wide range of photon energies during emission. The emission spectra are usually broad spectra rather than just sharp lines.

Due to the loss of energy to vibrational modes, there is a shift in energy to longer wavelengths in the fluorescence spectra from the absorption spectrum. This phenomenon is known as Stokes Law or Stokes Shift.

1.5.3. Practical Aspects of Fluorescence

To achieve maximum fluorescence intensity the fluorescent species is excited at the wavelength corresponding to the peak of the absorption spectrum. The process of fluorescence can usually be repeated many times prior to bleaching and the loss of fluorescence. The decay of fluorescence intensity as a function of time in a uniform population of molecules excited with a brief pulse of light is described by an exponential function.

$$I(t) = I_0 e^{\left(\frac{-t}{t_0}\right)} \qquad (8)$$

I is the fluorescence intensity, I_0 is the initial intensity of the fluorescence and t is the time.

1.5.4. Fluorophores

Fluorophores are measured by three fundamental parameters:

- Extinction co-efficient - measures the ability of the fluorophore to absorb light
- Quantum yield - a measure of the efficiency of fluorescence emission relative to all of the possible pathways for relaxation. Expressed as a ratio of photons emitted to the number of photons absorbed.
- Fluorescence lifetime - the time that a molecule remains in its excited state prior to returning to the ground state.

1.6. Contact Angle Theory

1.6.1. Introduction

One of the most sensitive and simple surface analysis techniques is the measurement of liquid contact angles on a surface. The different surface energies of compounds create surfaces that range from wettable to water repellent. The free surface energy of a substance comes from the attraction of the bulk molecules to the molecules at the surface. The free surface energy is sometimes called the surface tension. Dupré's equation relates the work of adhesion to the surface tensions of the solid-vapour, liquid-vapour and solid-liquid interface:

$$W_{SL} = \gamma_{SV} + \gamma_{LV} - \gamma_{LS} \quad (9)$$

W_{SL} is the work of adhesion, the work required to separate unit area of solid and liquid in contact, γ_{SV} is the surface - vapour interfacial tension, γ_{LV} is the liquid - vapour interfacial tension and γ_{LS} is the liquid - solid interfacial tension. In an ideal world, if a drop of liquid was placed on a perfectly flat surface it would spread out indefinitely if the following condition was obeyed (Young's Equation):

$$(\gamma_{SV} - \gamma_{SL}) \succ \gamma_{LV} \quad (10)$$

When the reverse is true, the droplet will remain finite and a contact angle will exist. This angle is defined by Adam[13] as:

$$Cos\theta = \frac{(\gamma_{SV} - \gamma_{LS})}{\gamma_{LV}} \quad (11)$$

θ is the contact angle.

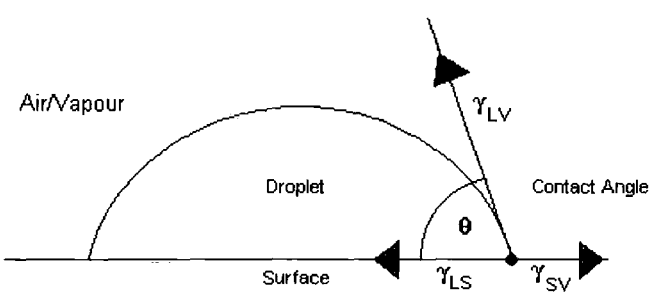

Figure 6: A liquid droplet on a surface showing the contact angle

1.6.2. Roughness

Most surfaces are not ideally flat; Wenzel[14,15] proposed a modification to Young's and Adam's equations accounting for the roughness of a surface.

$$Cos(\theta') = \frac{r(\gamma_{SV} - \gamma_{SL})}{\gamma_{LV}} = r.Cos(\theta) \quad (12)$$

θ' is the real contact angle, r is the roughness ($0 < r < 1$). The roughness factor is defined as the ratio of the actual area of a rough surface to the area of a smooth surface having the same geometric projected shape and dimensions.

$$r = \frac{actual\ surface}{geometric\ surface} \quad (13)$$

Therefore, any surface that is hydrophilic becomes more hydrophilic the rougher the surface becomes, and a surface that is hydrophobic becomes more hydrophobic on increased roughness.

Cassie and Baxter[16] proposed an alternative to Wenzel's equation to give the contact angle at a porous surface. This is useful for rough hydrophobic surfaces when the liquid does not penetrate the surface structure.

$$\cos\theta' = f_1 \cos\theta - f_2 \quad (14)$$

f_1 is the total area of solid-liquid interface, f_2 is the total area of liquid-air interface in a plane. f_1 is the geometrical area of unity parallel to the rough surface. f_2 is equal to zero when the surface is rough but not a composite structure.

In the literature, four different contact angle values are regularly reported:

- The static, or equilibrium, contact angle where a droplet is left for a short period of time and no movement or change in droplet size precedes measurement. This is the most commonly quoted value but contains the least information.
- The advancing contact angle where the three phase boundary has moved outwards recently and is at the limit of moving again. This is often the result of the droplet being increased in size.
- The receding contact angle; where the 3-phase boundary has moved inwards recently and is just about to move again. Often the result of a reduction in the droplet volume.

- The hysteresis; the difference between the advancing and receding contact angles. This value is important in judging the super-hydrophobicity of a surface.

1.6.3. Hysteresis

Shuttleworth and Bailey[17] showed that hysteresis occurs because of the roughness of solid surfaces. They concluded that when a droplet of liquid sits on a surface, it does so at a minimum of the total surface energy. Hysteresis occurs because the liquid rests at different minima after advancing and receding. Other work has attributed hysteresis to the adsorption of the liquid in the solid.[18,19]

An apparent contact angle is observed where the droplet rests on essentially a flat surface and the angle is relative to a horizontal line. However, on a microscopic level the surface is at an angle, there are peaks and troughs similar to a mountainous region. As the triple point (the boundary between the solid, liquid and air) has to move across these regions it requires greater energy to overcome the "obstacles". If the triple point is pushed outwards, away from the centre of the drop, a build up of liquid will occur (i.e. a bulge in the drop) until sufficient energy is present to move the droplet. If the triple point is retracted, enough "pull" from the capillarity effect of water is needed to withdraw the triple point (a flattening of the drop).[20]

In a series of articles, Bartell and Shepard[21,22,23] discussed surface roughness and its relationship to hysteresis of contact angles on a paraffin substrate. They defined roughness in terms of the average height and angle of inclination of the peaks in the substrate. Their results showed the advancing contact angle was found to increase with an increase in the angle of inclination while only a slight decrease, if any, was observed in the receding contact angle. Therefore, an increase in hysteresis was observed with an increase in the angle of inclination but no change was observed with change in the height of the asperities.

Johnson and Dettre[24] theoretically simulated the effect of the surface roughness on the hysteresis of the advancing and receding contact angles. Their analysis concluded that roughness allows for a number of metastable states. The lowest energy states are given by Wenzel's equation for normal surfaces and Cassie

and Baxter's equation for composite surfaces. Between each metastable state an energy barrier exists and hysteresis is at its highest when the energy barriers are at their maximum. Hysteresis on hydrophobic surfaces increases with increasing surface roughness in the low-roughness region but decreases drastically when the roughness becomes large and the composite configuration, in which the liquid does not penetrate into the troughs, is energetically preferred.

1.7. Atomic Force Microscopy

The field of Scanning Probe Microscopes began in 1981 with the Scanning Tunnelling Microscope,[25] STM, for which Binnig and Rohrer shared half the Noble prize in 1986.[c] This microscope was limited to conducting or semi-conducting samples. The Atomic Force Microscopy,[26] AFM, was invented in 1986 and introduced commercially by Digital Instruments in 1989. Both STM and AFM use very sharp tips to scan the surface to measure the 3D topography. AFM has the ability to measure features down to between 2-10 nm because unlike optical microscopy it does not use a lens and is only limited by the size of the probe rather than diffraction effects.

1.7.1. Introduction

AFM uses a small sharp probe mounted at the end of a cantilever arm to raster across the surface, the force between the sample and the probe causes the cantilever to bend according to Hooke's Law:

$$F(z) = -kz \tag{15}$$

F is the force, *k* the spring constant and *z* the distance from rest. The amount of bend can be recorded and converted into a topographical image of the surface. In the first AFMs, the cantilever had a diamond probe and a gold cantilever, with an STM mounted at the end of the cantilever to measure the bend. Modern AFMs use a laser and photodiode to measure the deviation in a reflected light from the end of the cantilever.

---

[c] Binnig and Rohrer shared the 1986 Nobel Prize for Physics with Ernst Ruska (fundamental work in electron optics, and for the design of the first electron microscope).

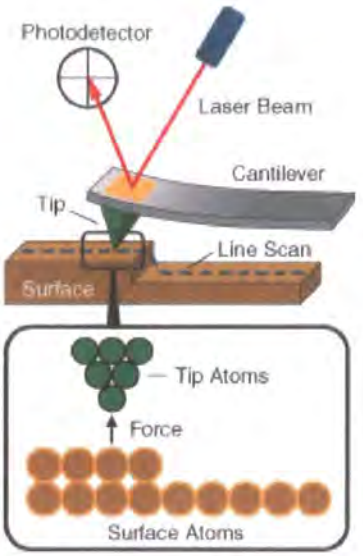

Figure 7: A simple schematic of the AFM process[d]

As the probe is rastered across the surface the beam is reflected onto different sections of the photodiode that converts the signal into electrical current.

The probe is the most important aspect when considering the lateral resolution of AFM. The important value is the radius of curvature of the end of the tip. Commonly this is around 20 nm but can be as small as 10 nm. If the size of the tip is the same size as features being measured it is common to see broadening of features caused by the side of the tip hitting the feature before the end of the tip. The aspect ratio of a tip can be improved to reduce this problem; especially important if the feature is a crevice or depression.

Figure 8: An AFM tip, an inverted pyramid of 3 µm height and 10 nm tip radius, usually made with Si or Si_3N_4[e]**. Scale bar is 3 µm.**

[d] www.molec.com

[e] http://stm2.nrl.navy.mil/

1.7.2. Modes of Operation

AFM can operated in different modes depending on how the tip interacts with the sample and how the feedback loop is used to control the process.

1.7.2.1. Tapping Mode

Tapping mode is a combination of contact and non-contact mode. The probe tip is alternately in contact with the sample then lifted away at a frequency of 50-500 kHz. This allows for high resolution topographical images without causing damage to the surface. It achieves this by oscillating the tip at or close to the resonant frequency of the cantilever using a piezoelectric motor. The amplitude of oscillation is around 20 nm and at the bottom of the oscillation it contacts gently the sample surface, causing a loss of energy and a reduction in amplitude. This reduction in amplitude allows the identification and measurement of features on the surface. During tapping mode the amplitude of oscillation is maintained by the feedback loop and the force is pre-determined and maintained at the lowest level possible.

1.7.3. Phase Imaging

Tapping mode allows for the interpretation of the different composition of the surface. This is achieved by measuring the phase difference between the applied cantilever oscillation and the measured cantilever oscillation. The phase lag is sensitive to variations in material properties such as adhesion and viscoelasticity. Lateral resolution is approximately 10 nm, similar to tapping mode. Phase imaging is used to show the contrast between composite surfaces.

1.8. Surface Plasmon Resonance

Surface Plasmon Resonance, SPR, is a method for measuring the refractive index of very thin layers of material absorbed onto a metal surface. When a beam of light hits the interface between a material of high refractive index and one with a low refractive index there is an angle (θ_c) above which the light is totally internally reflected. When one of the substances is glass and that glass is coated with a thin film of metal (usually gold) then the reflection is not total,

some of the light is absorbed into the metal. Above the angle for total internal reflectance the loss of light is greatest at a second angle. This angle is the angle of surface plasmon resonance. It is caused by the free sea of electrons that exist at a metals surface which are oscillating at a certain frequency. When this frequency is matched by the incident light the free electrons begin to resonate, which causes a loss of reflected light from the sample. The electrons oscillating at the surfaces emit an evanescent electromagnetic wave that decays exponentially away from the surface. In gold and silver films the fields associated with the surface plasmon are large enough to extend into the media immediately adjacent to a thin metal film. Because of this the surface plasmon in these metals is sensitive to changes in the nature of the adjacent field. This can be used this to measure the effect of binding cells or proteins.

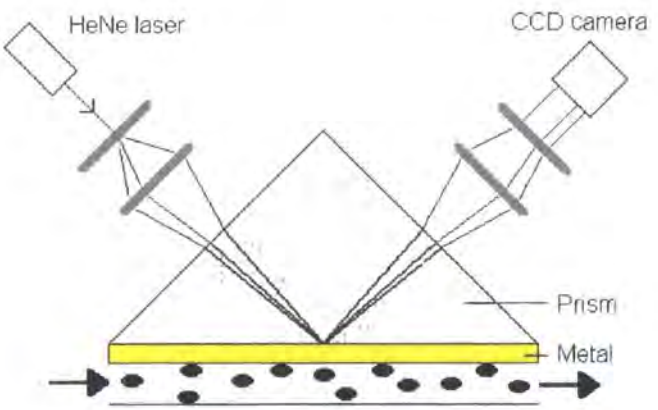

Figure 9: Kretschmann configuration of a glass prism adjacent to the thin gold film[f]

Shining a light at the reverse side of the coated gold film near the required conditions (wavelength and angle) for surface plasmon resonance to occur produces a sensitive reflected response dependant on the film refractivity. A key advantage of this technique over other binding experiments is the lack of labelling required on the target molecules (i.e. proteins).

[f] www.inano.dk

1.9. General Experimental Methods

1.9.1. Plasma Deposition

Plasma deposition was carried out in a cylindrical glass reactor (5 cm diameter, 470 cm^3 volume) connected to a two-stage rotary pump *via* a liquid nitrogen cold trap with a base pressure of 2 x 10^{-3} mbar and a leak rate better than 7 x 10^{-9} mol s^{-1}.[34] An L-C matching unit was used to minimize the standing wave ratio (SWR) of the power transmitted from a 13.56 MHz radio frequency (RF) generator to a copper coil externally wound around the glass reactor. A signal generator was used to trigger the RF supply. Prior to each plasma treatment, the chamber was scrubbed with detergent, rinsed in propan-2-ol, and further cleaned using a 50 W air plasma for 30 minutes. Precursor was loaded into a sealable glass tube and further purified by several freeze-pump-thaw cycles. Samples were then inserted into the centre of the plasma reactor, followed by evacuation to base pressure. Next, precursor vapour was admitted into the system *via* a fine control needle valve at a pressure of 0.2 mbar and purged for 5 minutes. At this stage, the electrical discharge was ignited at the appropriate peak power and a duty cycle.[35] Upon completion of deposition, the power supply was switched off and the monomer was allowed to continue to purge through the system for a further 5 minutes.

1.9.2. Fluorescent mapping

Fluorescence maps of cresyl violet perchlorate (Aldrich) derivatized poly(glycidyl methacrylate) patterned surfaces was collected using a Raman microscope system (LABRAM, Jobin Yvon). This entailed focusing an unattenuated 633 nm He-Ne laser (20 mW, attenuated to 1% transmission) onto the sample using a microscope objective (x50) and collecting the fluorescence signal at 633 nm through the same objective *via* a back-scattering configuration with a cooled CCD detector (diffraction grating was set to 300 g/mm grating). The sample was mounted onto a computerized X-Y translational mapping stage and the surface rastered using 1 μm steps. Corresponding optical images of the surface were taken using the same Raman microscope and objective lens.

1.9.3. XPS Spectra

XPS spectra of the polymer films were recorded on a VG Escalab MkII spectrometer equipped with an un-monochromatized MgK_a X-Ray source (1253.6 eV) and a concentric hemispherical analyzer. Photo-emitted core level electrons were collected at a fixed take-off angle with electron detection in constant analyzer energy (CAE) mode operating at 20 eV pass energy. XPS core level spectra were fitted using Marquardt minimisation computer software assuming a linear background and equal full-width-at-half-maximum (FWHM) for all Gaussian component peaks Experimentally determined elemental sensitivity (multiplication) factors were taken as being C(1s) : F(1s) : O(1s) : N(1s) : Br(3d) = 1.00 : 0.29 : 0.46 : 0.69 : 0.29. No spectral deterioration due to X-ray radiation damage of the surface was observed during the timescale of the data acquisition. The absence of any Si(2p) signal from the underlying silicon substrate was taken as being indicative of continuous plasma polymer film coverage of thickness greater than the XPS sampling depth (2- 5 nm).[27]

1.9.4. AFM imaging

AFM micrographs were acquired in tapping mode operating in air at room temperature using a Nanoscope III (Digital Instruments Nanoscope III control module, extender electronics, and signal access module, Santa Barbara, CA), images were recorded over 50 μm by 50 μm sections using a Si_3N_4 tip (Nanoprobe) with a spring constant of 42 - 83 Nm^{-1}.

1.9.5. Contact Angle Measurements

Sessile drop contact angle measurements were made at 20 $^{\circ}C$ using a video capture apparatus (A.S.T. Products VCA 2500 XE) and 2 μl high purity water droplets (BS 3978 Grade 1). Advancing and receding contact angle values were determined by increasing or decreasing the probe liquid volume at the surface.[28]

1.9.6. Film Thickness Measurements

Film thickness measurements were carried out using a spectrophotometer (Aquila Instruments Ltd, model nkd-6000). The obtained transmittance-

reflectance curves (350-1000 nm wavelength range) were fitted to a Cauchy model for dielectric materials using a modified Levenburg-Marquardt method.[29]

1.9.7. Infrared Spectra

Fourier transform infrared (FTIR) analysis of the films at each stage of reaction was carried out using a Perkin Elmer Spectrum One spectrometer equipped with a liquid nitrogen cooled MCT detector operating across the 700 – 4000 cm^{-1} range. Reflection-absorption (RAIRS) measurements were performed using a variable angle SPECAC accessory set at 66° with a KRS-5 polarizer fitted to remove the s-polarized component. All spectra were averaged over 128 scans at a resolution of 4 cm^{-1}.

Optical images taken from the mapping stage of the Infrared microscope (Perkin-Elmer Spectrum One FTIR) were recorded by rastering the camera across the sample and recording 50 µm by 50 µm still images at each step.

2. Plasma Patterning

2.1. Introduction

Polymers have been patterned in a variety of ways to create surfaces with multi-functional areas. Each technique has its own advantages and disadvantages with no one technique being suitable for every application. Polymers can now be physically patterned using a wide variety of techniques including soft lithography,[30,31] photo/optical lithography,[32] electron-beam writing[33] and ion beam techniques.[34] Applications of functionalised patterned surface include engineering templates,[35] arrays,[36] small scale electronic devices[37] and biosensors.[38]

2.1.1. Photolithography

Photolithography is the process of creating an image by selectively exposing a surface to radiation. The irradiation of the surface to the radiation causes physical and/or chemical changes. It has been used for UV patterning thiol-terminated siloxane films[39] and in biology by linking proteins to photosensitive

groups[40] and to control growth of neurons.[41] The technique has been developed over a number of years to produce very accurate pattern dimensions.[42] However the equipment is expensive and the technique cannot produce specific chemical functionalities[43] or be used in delicate biological processes as some of the reagents can be toxic.

There are two main ways of patterning a surface using photolithography. Either a mask can be placed between the light source and the surface to selectively block the radiation or the radiation can be focused to a point on the surface and then rastered across the surface to form the pattern. Using a mask is quicker and cheaper but focusing the beam on the surface allows a wider variety of patterns to be formed.

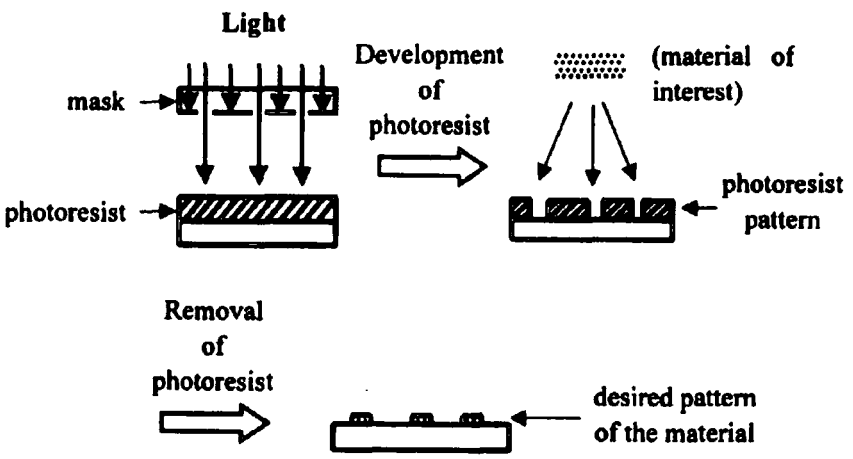

Figure 10: Schematic of photolithography process using a mask[44]

A photoresist is exposed to UV light through the mask which has the appropriate pattern. The exposed part of the photoresist is then solubilised in a developer solution, resulting in a photoresist pattern. Subsequently the functionalised material is applied to the pattern and the photoresist is then lifted off.

The dimensions of a photoresist pattern are limited by the wavelength of the incident radiation.[45] Electron beams, with shorter wavelengths than light, are used to create the smallest features.[46,47]

Ion-Beam lithography is another alternative to standard lithography requiring fewer steps and enables the surface chemistry to be tailored to the

requirements of the user. Other lithographic techniques involve neutral atoms or particles.

The resolution, R, of any lithographic technique is directly related to the wavelength, λ, of the radiation or particle source used. The resolution is also inversely affected by the numerical aperture of the system.[48]

$$R = \frac{k_1 \lambda}{NA} \tag{16}$$

NA is the numerical aperture, λ the wavelength and k_1 is a constant. However reducing the wavelength to improve the resolution will have a detrimental effect on the depth of focus of the technique.

$$Depth\,of\ focus = \frac{k_2 \lambda}{(NA)^2} \tag{17}$$

k_2 is a constant. When treating rougher or non-planar surfaces it is important for the system to have a large depth of focus. Therefore, a compromise between the resolution and the depth of focus must be reached.

2.1.2. Soft Lithography

Soft lithography[43,49,50] generally uses polydimethysiloxane, PDMS, moulds to physically pattern soft materials, usually polymers, without using light, ions or electrons. The PDMS stamp is itself created using photolithography.

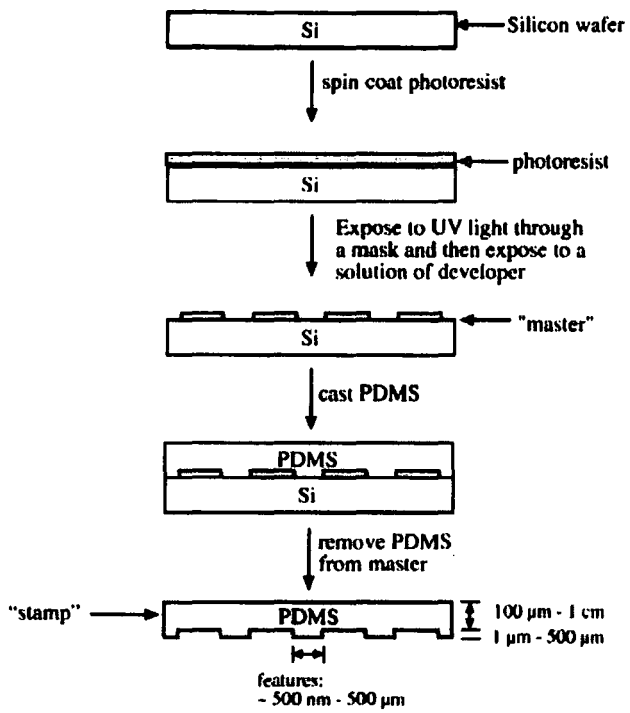

Figure 11: Schematic illustration of the procedure used to fabricate a PDMS stamp from a photolithographic master having relief structures in photoresist on its surface[43]

Variants of soft lithography include micro-contact printing, μCP, replica moulding, micro-transfer moulding, μTM, and micro-moulding in capillaries, MIMIC. These methods are capable of generating patterns down to <100 nm as shown in Table 1.

Table 1: Comparison of feature sizes produced by different patterning techniques

Technique	Feature size (nm)
Photolithography	180
Neutral atom lithography	70
Electron-beam writing	5-6
Replica Moulding	30
Micro-contact Printing	100
Micro-moulding in capillaries	1000
Micro-transfer moulding	700
Laser Ablation	1000

2.1.3. Micro-Contact Printing

Micro-contact printing, μCP, is a well known conceptually simple lithographic technique that utilises PDMS stamps of the type described previously[51,52,53,54] Patterns with feature size >200 nm are easily formed by this method, although chemical etching can reduce this to around 100 nm.

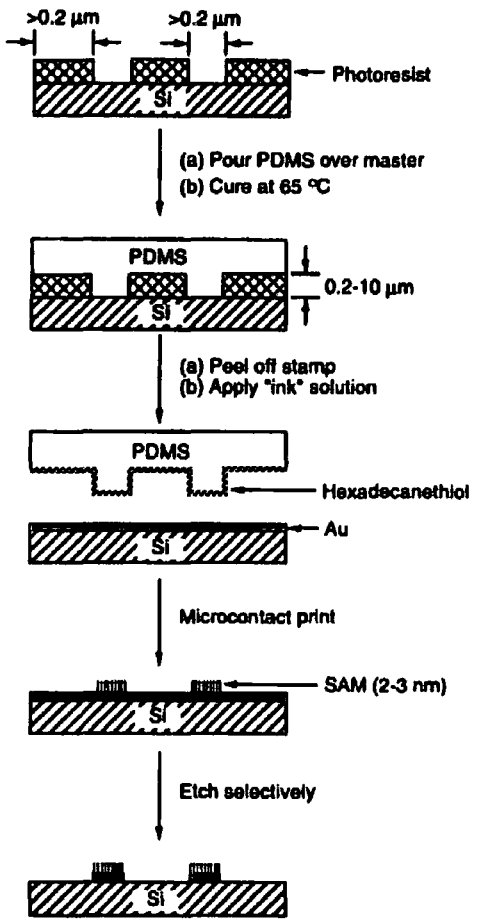

Figure 12: Schematic illustration of the procedure for microcontact printing a self assembled monolayer, SAM[55]

A patterned PDMS stamp coated with the ink (the material with the required functionality) is first bought into contact with the substrate. Only regions where the stamp makes contact with the substrate transfer the ink to the surface. The ink is then dried or cured and further modification can be made to either region of the sample, *e.g.* Self Assembled Monolayers, can be grown on the exposed regions to create further functionality.[56]

2.1.4. Replica Moulding

Replica moulding utilises a stamp moulded from a rigid master that can then be used to mould numerous patterned organic surfaces. The stamp is made of an elastomer allowing easy separation from the moulded surface. Patterns with features around 50 nm are easily formed by this method and by using

mechanical compression, bending, or stretching the technique is flexible enough to reduce patterns down to 30 nm.[57]

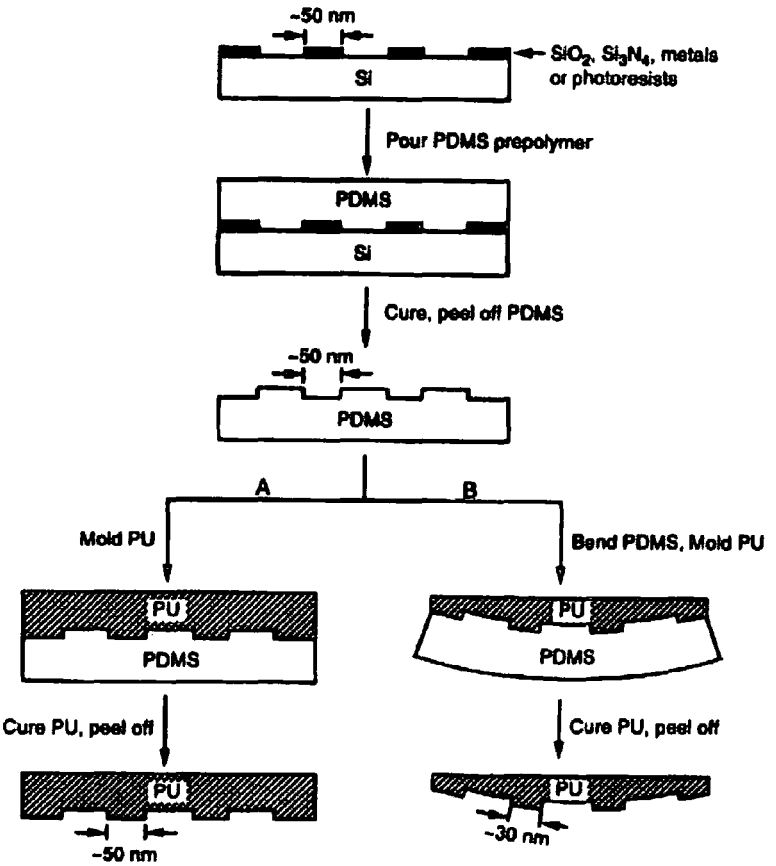

Figure 13: Schematic procedure for carrying out replica moulding against an elastomeric PDMS mould

The PDMS mould is fabricated by casting against nanometre-sized relief structures fabricated using X-ray lithography or electron-beam writing. Replica moulding can also be conducted while the PDMS mould is deformed, *e.g.* by mechanical bending.[55]

2.1.5. Micro-Transfer Moulding

This technique also uses an elastomeric mould; prepolymer is dropped into the mould and any excess is removed. The substrate is then placed in contact with the mould and the polymer is cured. The mould is then removed, leaving the polymer forming a physical structure on the substrate surface. This technique

can be used on non-planar substrates and also used to form 3 dimensional structures with layer after layer added to the surface.

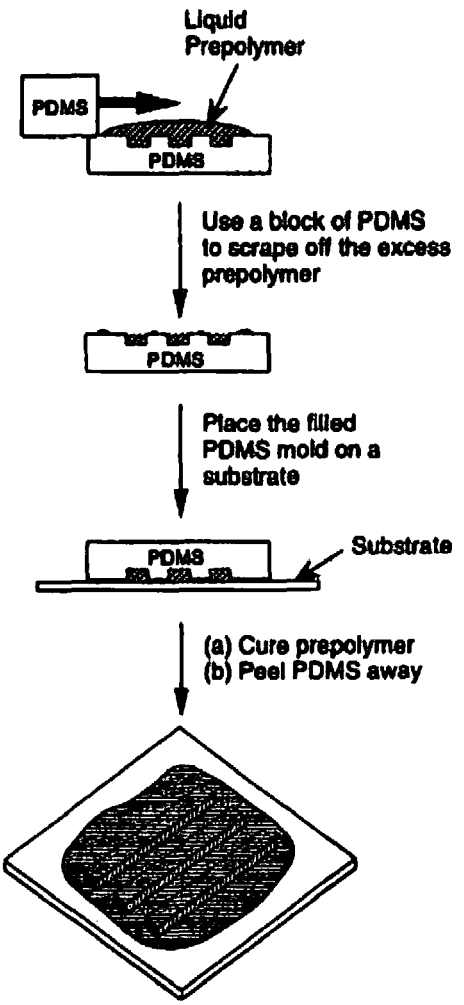

Figure 14: Schematic of the micro-transfer moulding process

A drop of prepolymer is applied on the patterned surface of a PDMS mould. The excess prepolymer is scraped away using a piece of flat PDMS, leaving a filled PDMS mould. The filled mould is then brought into contact with a substrate and the prepolymer is allowed to solidify *in situ*. Patterned microstructures are obtained after the PDMS mould is removed. The process can be repeated on a substrate whose surface has already been patterned with a layer of relief structure to build a multilayer structure layer by layer.[55]

2.1.6. Micro-Moulding in Capillaries

Micro-moulding in capillaries[58] uses capillary action to draw a low viscosity pre-polymer through the open end of a mould placed on the surface of the substrate. The mould must have a network of channels and grooves to allow the liquid to be drawn through the mould. Once the mould is filled then the prepolymer fluid is cured and the mould is removed. Patterns with biological[59] and inorganic applications[60] have been prepared by this method.

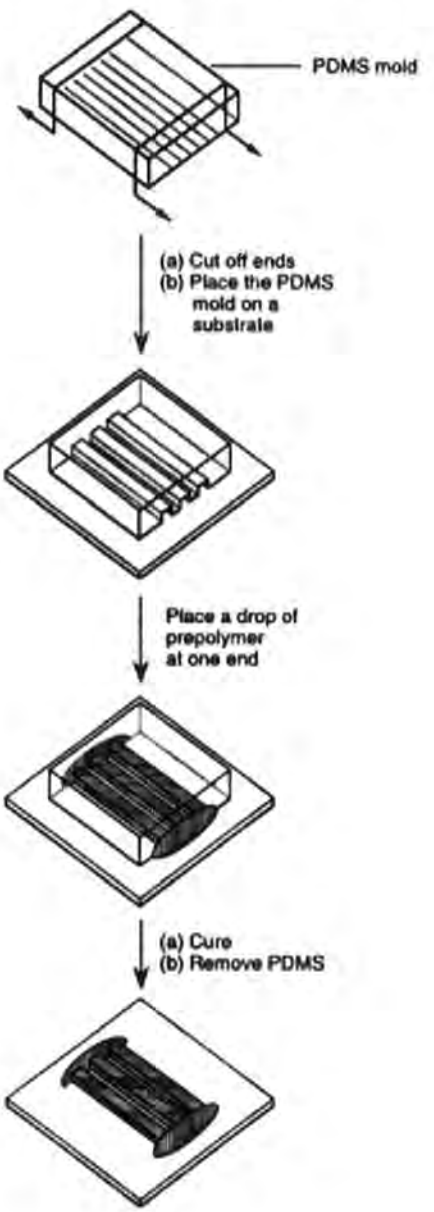

Figure 15: Schematic of the micro-moulding in capillaries procedure

This technique relies on a conformal contact formed between a support and an elastomeric PDMS mould with relief features on its surface to create a network of microchannels.[55]

2.1.7. Laser Ablation

Laser ablation was used by Griesser *et al*[61] to pattern a surface to allow the control of cell attachment; the advantage of this procedure is the single step patterning process. Allyl amine was used to attach cells and poly(ethylene oxide) was used to reduce protein absorption.

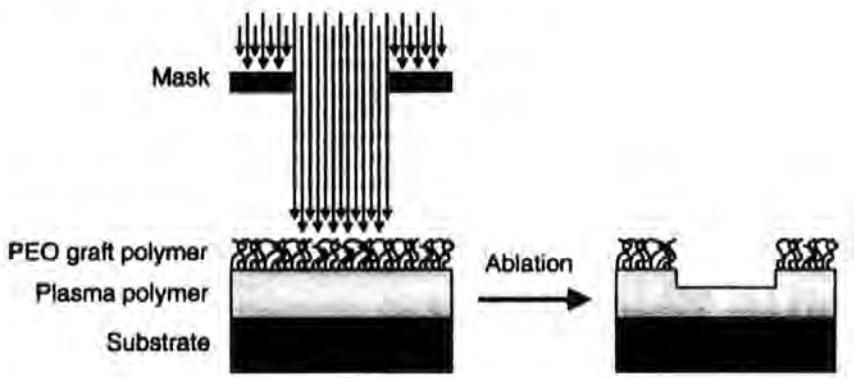

Figure 16: The principle of two-dimensional patterning of the surface chemistry *via* excimer laser ablation[61]

2.1.8. Self-Assembled Monolayers

Self-assembled monolayers (SAMs) are an increasingly popular method of functionalizing a surface. The SAM molecules are generally alkyl chains with 2 distinct end groups: one end reacts with the surface linker pattern and the other end group provides the desired surface functionality. The surface linker pattern may be formed by any of the means mentioned in the previous section, including μCP[62] and photolithography[63] but the functionality comes from the terminal group on an alkyl chain. Once the surface is patterned and the linker group functionality is in place, the SAM molecules assemble themselves onto the pattern. This assembly requires no user input as the molecule is designed to guide itself into the correct position. In addition, once one pattern is introduced by SAMs, further patterning or functionality is possible on the untreated regions or using the treated regions as a substrate for a new reaction.

The major limiting factor of SAMs is the requirement of certain substrates and linking groups:

- Gold; uses thiols or disulfides
- Silicon; uses chlorosilanes and alkoxysilanes
- Glass; uses silanes
- Mica; uses silanes

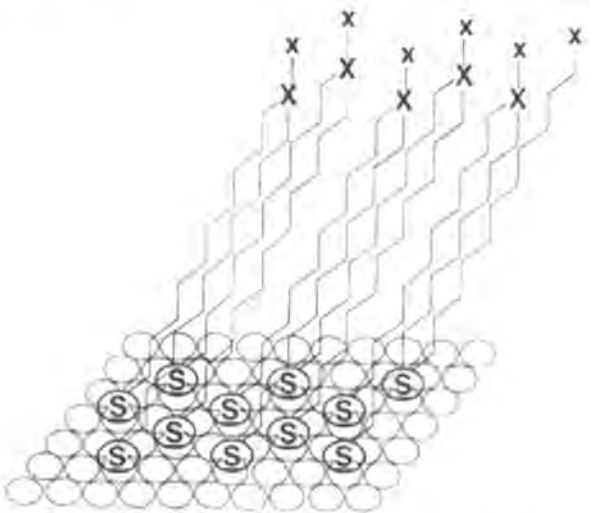

Figure 17: Schematic of a SAM of an alkanethiolate on gold, the surface properties of the film are largely determined by the chemical properties of the terminal group, X[43]

2.1.9. Plasma Functionalisation

Dai, Grieseer and Mau[64] used a combination of plasmas and grids to pattern functionality onto surfaces. This process is similar to photolithography except that it uses a plasma gas to modify the surface, see Figure 18.

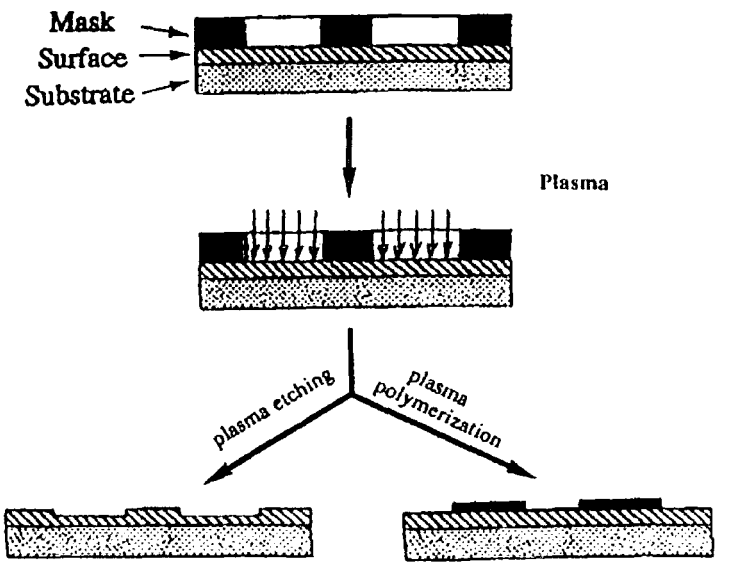

Figure 18: Schematic representation of pattern formation by the radio frequency glow-discharge plasma technique[4]

Their work showed that grids allow patterns with features as small as a 25 μm square. Etched patterns were produced using a methanol plasma and conducting patterns by polymerizing a pyrrole monomer.[65]

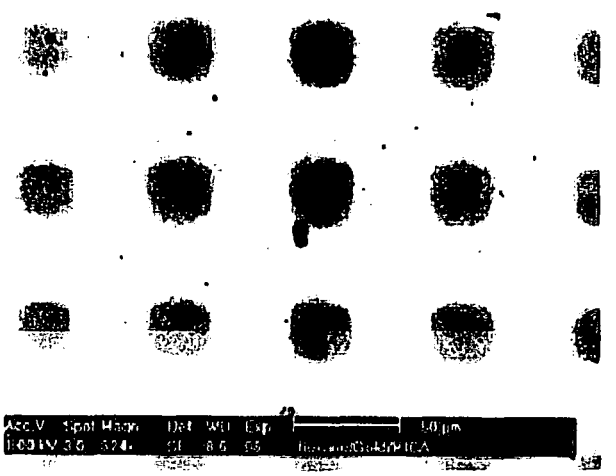

Figure 19: SEM micrograph of gold-coated mica sheets patterned with n-hexane-plasma polymer using a TEM grid consisting of square windows as the mask[4]

Chan *et al*[66] reviewed the effect of polymer surface modifications by plasma polymerisation, photochemical and chemical reactions, and pulsed UV-laser radiation. Table 1 shows the characteristics of plasma gases, these properties can be used in conjunction with lithography to introduce functionality onto polymer surfaces.

Table 2: Plasma Gases and their properties[66]

Plasma Gas	Effects	Comments
Argon (and other noble gases)	Ablates hydrogen and improves the adhesive characteristics of polymers.	Argon is the most common inert gas used in industry since it is inexpensive. Used for cleaning substrates, sputtering processes and crosslinking.
Nitrogen	Improves wettability, printability, adhesion and biocompatibility.	Introduces both nitrogen and oxygen containing groups into the surface.
Ammonia	Primary amine groups produced.	Pure nitrogen plasma does not add these groups.
Carbon monoxide	Surface energy increased.	Can be on its own or coupled with other gases to increase surface energy.
Oxygen	Introduces oxygen groups and etches the polymer surface.	Operational parameters define which process occurs predominantly.
Carbon Dioxide	Introduces oxygen groups.	Milder oxidative attack on substrate than O_2 plasma.
CO_2 + Acrylic acid	Introduces carboxylic groups.	Acidic oxygen containing groups formed on surface.
Water	Incorporates hydroxyl functionality.	Usually oxidative rather than reductive reactions.
CFx	Promotes polymerisation and fluorination.	Surface reactions, etching and polymerisation can occur simultaneously.
Hydrogen	Abstraction of fluorine from polytetrafluoroethylene.	Can be used to lower the concentration of fluorine involved in the plasma process.

2.1.10. Uses of Patterned Surfaces

Functionalised surfaces can be used for a variety of purposes. The smaller scale (<1 μm) μCP is used for electronic applications whilst the larger scale applications in the biological field include DNA arrays or cell attachment.[67] DNA arrays can include attachment of the material either directly or using microspheres. The dimensions of such arrays are in the region of 1-100 μm.

2.1.10.1. Arrays

Ostuni *et al*[68] used soft lithography and selective deposition to create patterned microwell arrays that spatially controlled direct protein and cell attachment. They used PDMS as a substrate and coated the walls and wells with protein repelling and adhesive compounds respectively.

Arrays using microspheres have also been a popular area over the past few years. Suspension arrays are discussed by Nolan and Sklar,[69] surface based microsphere arrays were patented by Krishan *et al*[70] and Harvey.[71] Microsphere arrays attached to fiber optic tubes were discussed by Epstein *et al.*[72] They achieved a feature size of 3 μm, the smallest reproducible DNA array currently published.

Biological arrays have shrunk rapidly in recent years; advances in Bubble-jet technology allow features down to ~75 μm to be produced. For a detailed review of micro-arrays see Blohm and Guiseppi-Elie.[73]

Solid particle arrays were investigated by Whitesides *et al.*[74] By using μCP to create the pattern, self assembly to produce the functionality, and crystallization or precipitation to deposit the solid material, both inorganic and organic solids could be arrayed using this method.

2.1.10.2. Microfluidic Devices

Patterned surfaces are also used in microfluidic devices and micro-condensers. Becker and Gärtner[75] have discussed and reviewed the various methods of producing microfluidic devices. Boone *et al* published a more recent review discussing microfluidic devices[76] where they discussed the concepts and uses of such devices.

Polymer micro-condensers arose from a study in Nature[77] discussing the physical and chemical properties of a desert beetle that uses its back to collect water. The article also discussed the formation of a surface to mimic this patterning with a wax substrate and glass beads acting as the hydrophobic and hydrophilic regions respectively. The beetle tilts its back into the wind and the water vapour condenses onto it. It collects water in hydrophilic regions but water

gets blown across the hydrophobic regions till it hits a hydrophilic region. This patterning prevents evaporation of the water before it can be collected.

2.1.10.3. Conducting Patterns

Conducting material patterns have applications as integrated circuits, field-effect transistors, optical memory storage devices and electroluminescent and electrochemical displays.[78]

Conducting polymer patterns have been produced by Dai, Griesser and Mau[4] using plasma patterning and by Whitesides' group using MIMIC.[79] The area has been reviewed by Gardner and Bartlett[80] and Horowitz.[81] In most cases the conducting polymer which is used has to be modified to work with the patterning technique. The most commonly used polymer is poly(aniline) due to it's stability in air.

Non-ordered nano-patterns can be formed by combining conducting polymers with inorganic particles to produce nano-composites. These exhibit several interesting physical properties; including altered magnetic susceptibility, charge storage capability, and optical activity. This area was reviewed by Gangopadhyay and De.[82]

Metal attachment onto polymer surfaces is another active area of research at present. The majority of papers use fluoropolymers as the substrate; as they offer the advantage of being excellent insulators on which to create the conducting pattern. However, their low surface energy often results in poor adhesion between the polymer and the metal. Many solutions to this problem have been investigated, including: plasma processing,[83] chemical treatment,[84] IR and Excimer VUV photon treatment,[85] and the graft copolymerisation of vinyl pyridine.[86]

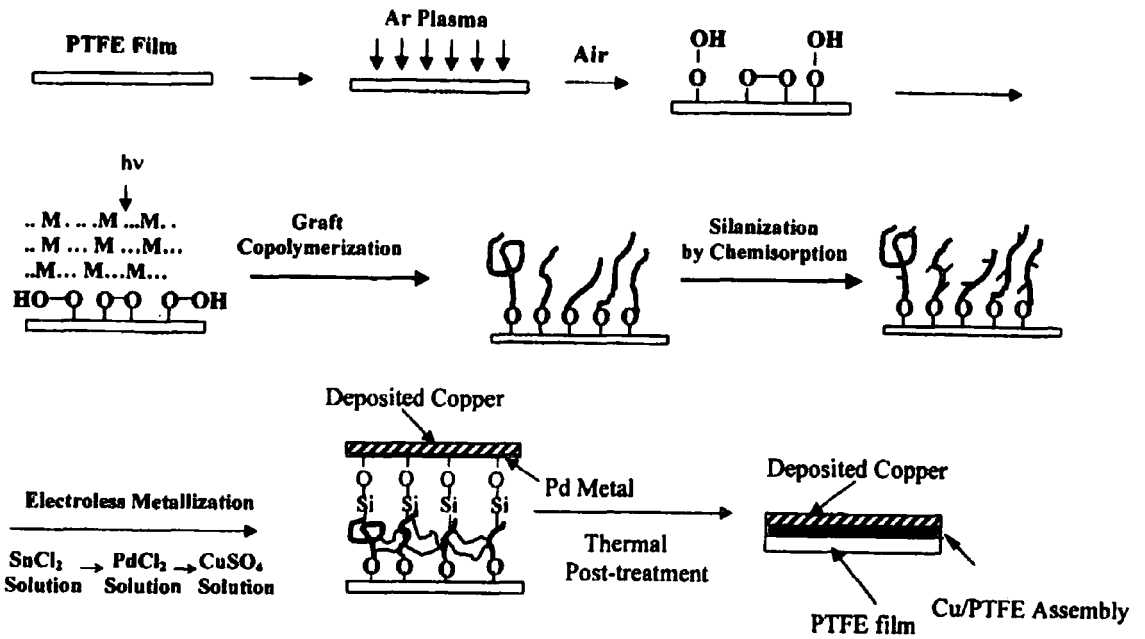

Figure 20: Schematic illustrating the processes of graft copolymerisation, silanisation, sensitisation and electroless metal deposition on the polytetrafluoroethylene film[89]

Starting with a paper in 1996, Kang, Tan and co-workers produced a series of papers detailing their progress towards the adhesion of metals onto polytetrafluoroethylene. Initially they used an Argon plasma treatment to introduce oxygen functionality into the surface.[87] They then used graft-copolymerisation to attach a nitrogen-containing vinyl monomer[88] and finally used the functionalised surface to deposit copper[89, 90] and nickel.[86]

2.2. Functionalized Embossed Surfaces

2.2.1. Introduction

Creating multi-functional chemical patterns on solid surfaces is important for many technological fields such as thin film transistors,[91] solar cells,[92] genomics,[93] proteomics,[94] microelectronics,[95] sensors[96] and microfluidics.[97] Typical methods employed to pattern surfaces include: photolithography,[98,99] laser ablation,[100] plasma patterning,[4,101] block co-polymers[102,103] and soft-lithography[104,43] including micro-contact printing[74,105,106,107] and embossing.[108] Current lithographic techniques have many limitations, including surface suitability, geometry and are restricted to 2 dimensional designs. Similar restrictions apply to soft-lithographic techniques including poor quality over a large substrate.

Lithographic techniques that involve an embossing step have been shown to produce physical patterns down to 25 nm.[109] Most embossing processes use relatively high temperatures and thermoplastic polymeric materials. These processes use a solid master, usually made from PDMS, patterned by a variety of methods from photolithography to laser ablation. The master; a mould, stamp or mask, is embossed into the substrate whilst the system is at a raised temperature and cooled to seal in the physical structure. Room-temperature imprint techniques are possible but feature sizes are limited to 80 nm.[110] The process needs to be coupled with another process to produce functionalized surfaces; the simplest is self-assembly using embossing to transfer the pattern. Mask technology is used in a variety of process, including; deposition of metal for semi-conducting patterns,[111] circuit boards,[112] reactive ion etching (RIE)[113] and patterning photoactive polymers.[114]

Embossed patterned surfaces are used in cell growth by Turner *et al*[115] and conducting polymer arrays have been produced by Wang *et al.*[116] Optical polymer films are also embossed to create films with differing refractive indices.[117] The requirement for a specific surface chemical functionality for a given substrate has tended to limit the more widespread application of embossing techniques for the preparation of chemically patterned surfaces.

Plasma deposition through a grid is a common process, used to pattern carbon nanotubes,[118] conducting polymers[4] and biological cells.[119] These techniques require flat substrates (*e.g.* silica or glass) to ensure close contact with the mask. Better resolution patterns are formed the closer and more evenly the grid is in contact with the substrate. Other methods of plasma patterning have been studied using lift-off processes,[101] nanosphere lithography[120] or photolithography. [101]

In this section a technique is described to show how embossing an aperture-containing template (*e.g.* metal grid) onto non-planar substrates - prior to plasma deposition followed by template removal - can yield high-definition chemically patterned surfaces, Figure 21. Pulsed plasma polymerization has been selected as the surface functionalization technique of choice since it is solventless, produces pin-hole free films, and is amenable to a whole range of substrate materials and geometries, and can be employed to deposit a variety of chemical groups, *e.g.* hydroxyl,[121] perfluoroalkyl,[122] epoxide,[123] anhydride,[124] carboxylic acid,[125] cyano,[126] amine,[127] halide,[128] furfuryl,[129] and thiol[130]

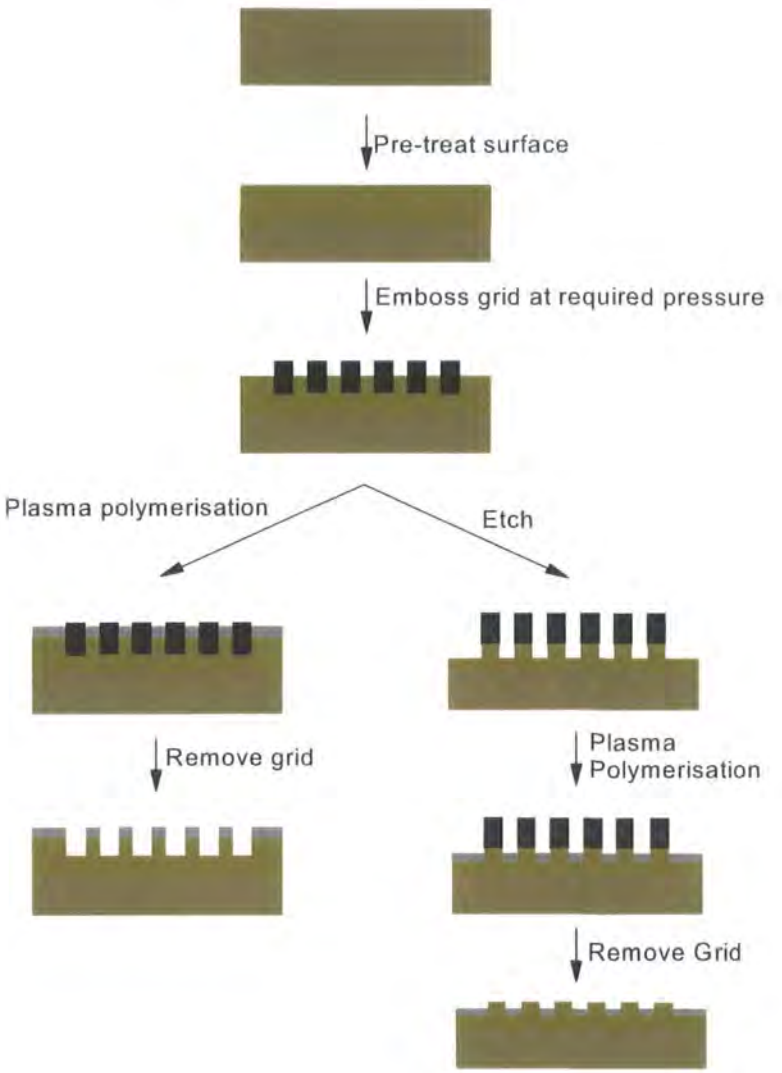

Figure 21: Schematic of plasmachemical embossing process

2.2.2. Experimental

Plaques (10 mm x 10 mm) of polytetrafluoroethylene (Goodfellows, 0.1 mm thick film) were ultrasonically cleaned in a 50/50 cyclohexane/propan-2-ol (Aldrich) mixture for 10 minutes in order to remove surface contaminants. Nickel grids (3.05 mm diameter, Agar Scientific) were embossed into the sheets of polytetrafluoroethylene by placing between two polished aluminium plates (75 mm diameter) in a hydraulic press (Moores Press) and applying a force between 10 kN and 60 kN (an approximate pressure of 100–600 MPa).

Plasma deposition was carried out as detailed previously (section 1.9.1) with glycidyl methacrylate (97%, Aldrich) used as the precursor and grid-embossed polytetrafluoroethylene plaque as the samples.

Functionalized microwells were fabricated in the same reactor, using an embossed nickel grid (2000 Mesh, 7.5 μm squares, 5 μm bars) embossed using a force of 20 kN. In this case, prior to plasmachemical deposition, a 97.5% argon (99% purity, Air Products) and 2.5% oxygen (99% purity, Air Products) gas mixture was flushed through the system for 5 minutes at a pressure of 0.2 mbar and the plasma ignited at a continuous power of 50 W for 2 hours. This gave rise to approximately 5 μm deep wells. Plasmachemical functionalization of these microwells with epoxide groups was then carried out as described previously (section 1.9.1).

Surface dye attachment to the epoxide centres entailed immersion of the patterned poly(glycidyl methacrylate) substrate into a 1% w/v solution of cresyl violet perchlorate (Aldrich) dissolved in high purity water (BS 3978 Grade 1). for 1 hour. Afterwards, the surface was rinsed with high purity water (BS 3978 Grade 1) for 2 hours and dried in air. A fluorescence map was obtained as described previously (section 1.9.2)

2.2.3. Results

Polytetrafluoroethylene films were embossed with metallic grids to create physical structures in the substrate, Figure 22. The difference in contrast between the raised regions (shown as dark patches) and the lighter lower regions is merely an effect of the reflected light. XPS measurements showed no change in the chemical composition of the samples following embossing. The image also shows the underlying roughness of the polytetrafluoroethylene substrate; if a smoother substrate, such as polyethylene terephthalate, was used then the final image would be more accurate.

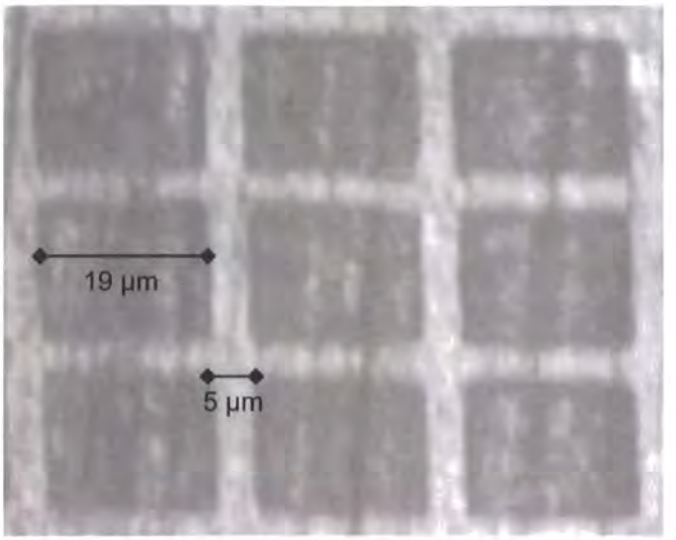

Figure 22: An embossed polytetrafluoroethylene surface.

The darker regions are at a higher level than the lighter bars. The graininess is caused by underlying roughness in the polytetrafluoroethylene substrate. The squares are 19 µm wide and the grid is 5 µm in width

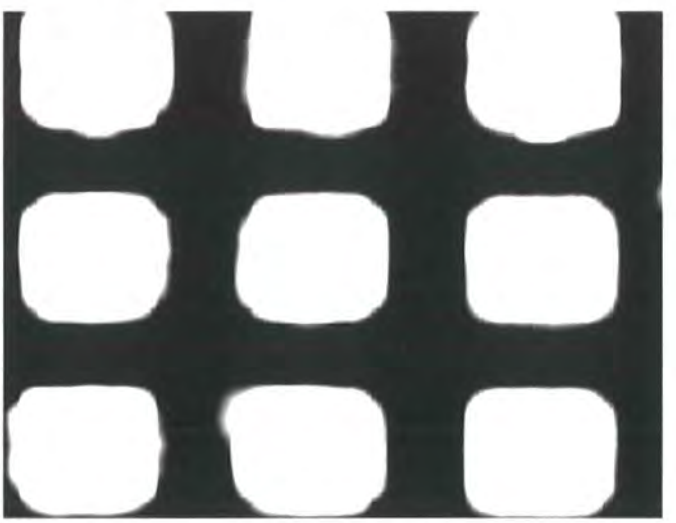

Figure 23: A fluorescence micrograph of a cresyl violet perchlorate tagged pulse plasma polymerised pattern of glycidyl methacrylate on a polytetrafluoroethylene substrate

The squares are 7.5 µm in diameter and the grid is 5 µm.

The physical definition of the embossed pattern in the polytetrafluoroethylene films was found to improve with increasing pressure, Figure 24. The difference in contrast between the raised regions (seen as light patches) and the darker lower regions is merely an effect of the reflected light. XPS characterization showed no change in surface chemistry following embossing. The underlying roughness of the polytetrafluoroethylene substrate is also discernible.

Plasmachemical deposition through an embossed gird was highly effective for functionalizing the substrate. In the case of pulsed plasma deposited poly(glycidyl methacrylate), an aqueous solution of cresyl violet perchlorate was used to identify the location of epoxide layers on the surface. Dye attachment was observed in an array in agreement with the original placement of the grid, Figure 23. Both the regularity and the definition of the array features are clearly seen to improve with increasing embossing pressure.

Chemical patterns have been created by plasma treating through a grid before[118,4,119] but these rely only on close contact between the grid and the flat substrate. Figure 24 and Figure 25 show the effect on the definition of the pattern as you increase the force used to emboss the grid into the surface. Physically and chemically the pattern becomes more clearly defined. At a force of 40 kN the grid appears to be completely pressed into the surface and higher forces do not alter the physical definition. However these higher forces do appear to have an affect on the deposition of the plasma polymer and subsequent derivatization.

Embossing was also shown to have an effect when the substrate was plasma etched using an oxygen/argon plasma rather than plasma functionalized. Figure 26 shows the difference in pattern definition of embossing a grid rather than simply etching the substrate through a grid. Both the depth and the definition of the pattern were more regular for the embossed samples, Figure 27. The wells created in the polytetrafluoroethylene substrate were further treated by plasma polymerizing glycidyl methacrylate prior to removing the grid and then reacting the whole surface with the fluorescent molecule cresyl violet perchlorate. This again showed the difference in quality of the pattern created following embossing a substrate prior to treatment. Because of the non-anisotropic nature of the plasma etching the pattern of fluorescence created following plasma polymerization into the wells is not as well defined as the simple emboss and functionalize treatment shown in Figure 28.

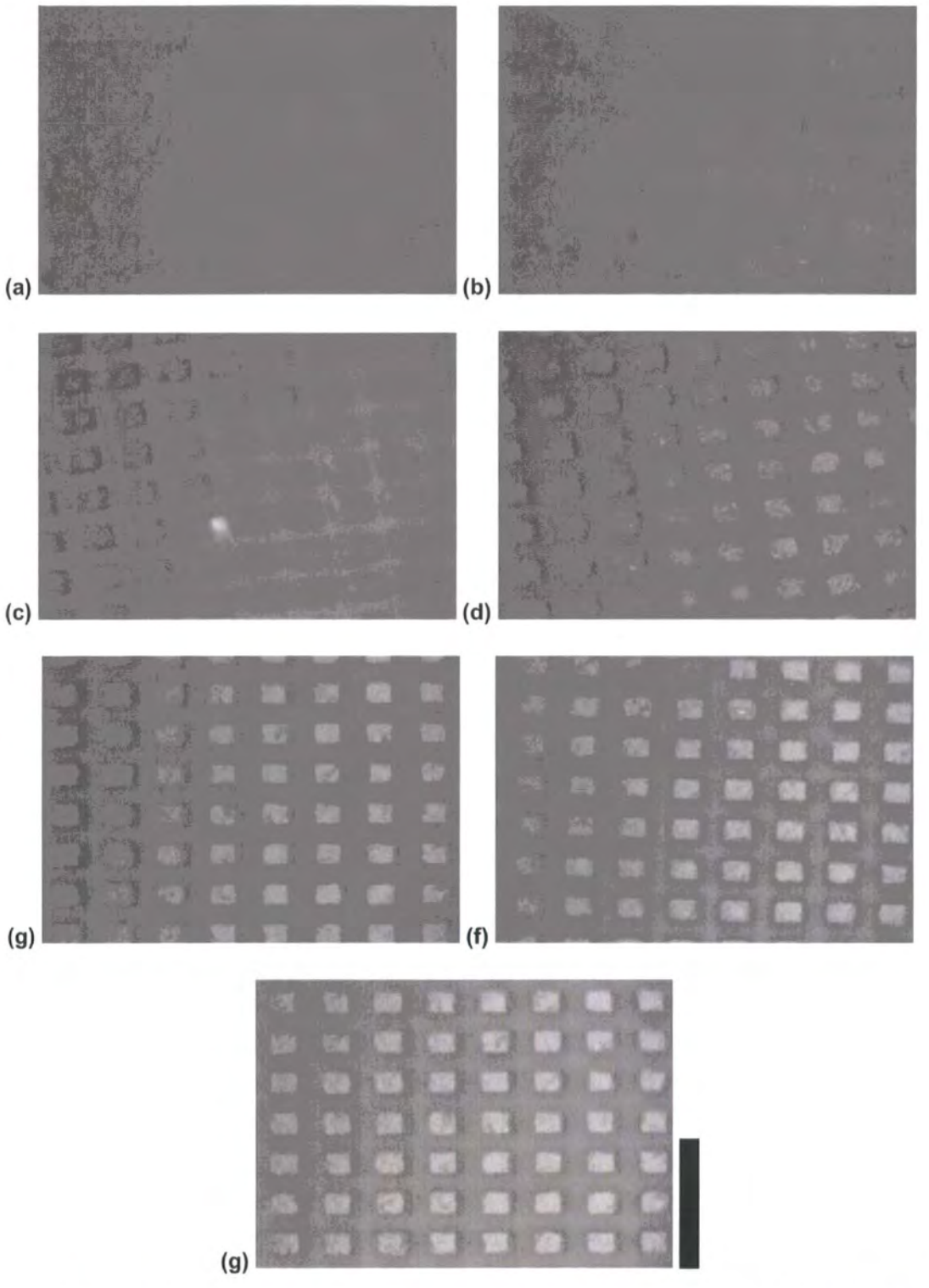

Figure 24: Optical Micrographs Showing the Physical Effect of Embossing a Grid (2000 Mesh, 7.5 µm Square, 5 µm Bar) into a polytetrafluoroethylene Surface

(a) 0 MPa, (b) 100 MPa, (c) 200 MPa, (d) 300 MPa, (e) 400 MPa, (f) 500 MPa, (g) 600 MPa. Scale bar is 40 µm.

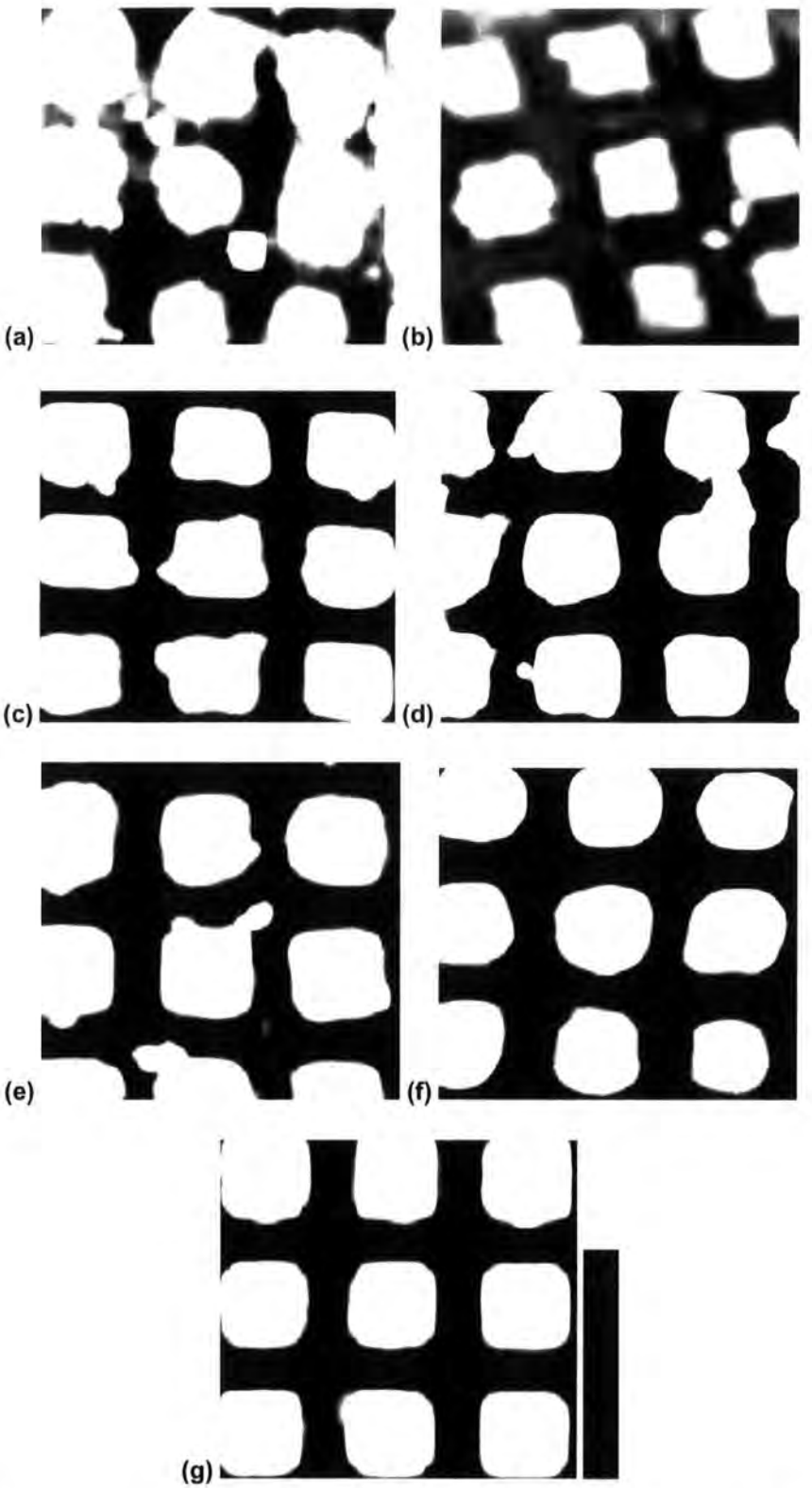

Figure 25: Fluorescence Micrographs showing the effect that embossing a grid (2000 Mesh, 7.5 µm Square, 5 µm Bar) into a polytetrafluoroethylene surface has on pattern definition

(a) 0 MPa, (b) 100 MPa, (c) 200 MPa, (d) 300 MPa, (e) 400 MPa, (f) 500 MPa, (g) 600 MPa. Scale bar is 20 µm.

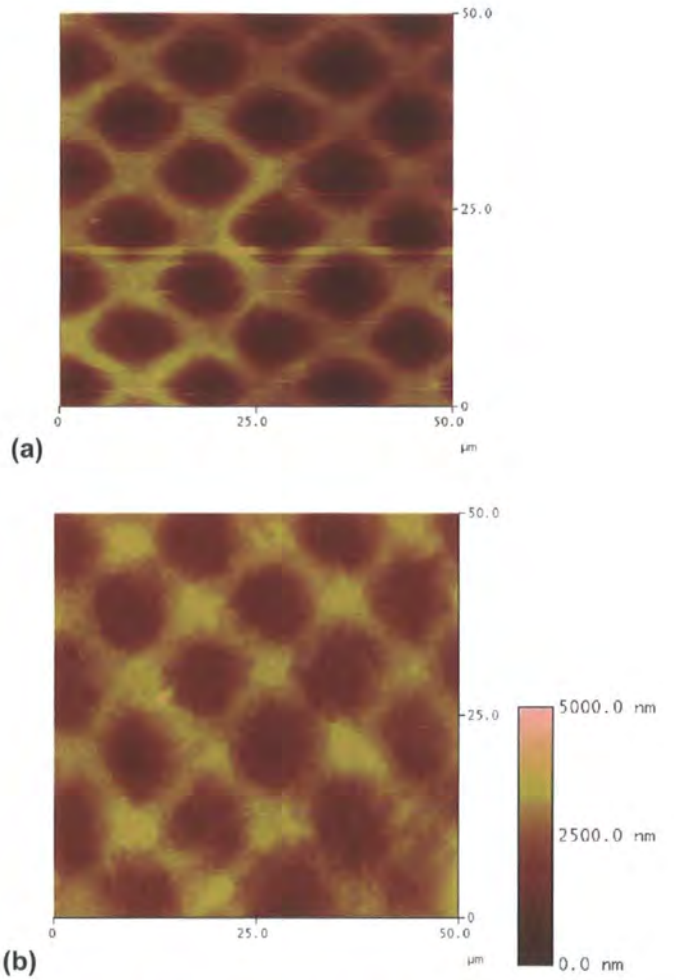

Figure 26: AFM images of wells created by Oxygen/Argon plasma etching a polytetrafluoroethylene film through a 2000 mesh grid (7.5 µm Square, 5 µm Bar). Using an embossed grid (200 MPA) prior to etching pattern, (a) and un-embossed grid, (b)

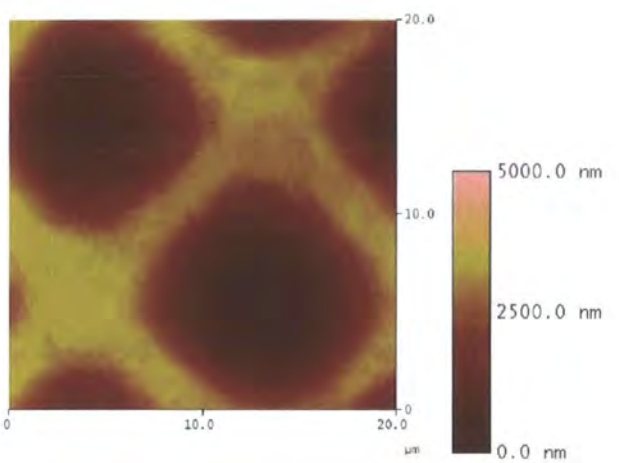

Figure 27: AFM image (20 µm by 20 µm) of a well created by oxygen/argon plasma etching a polytetrafluoroethylene film through an embossed 1000 Mesh Grid (15 µm square, 5 µm bar)

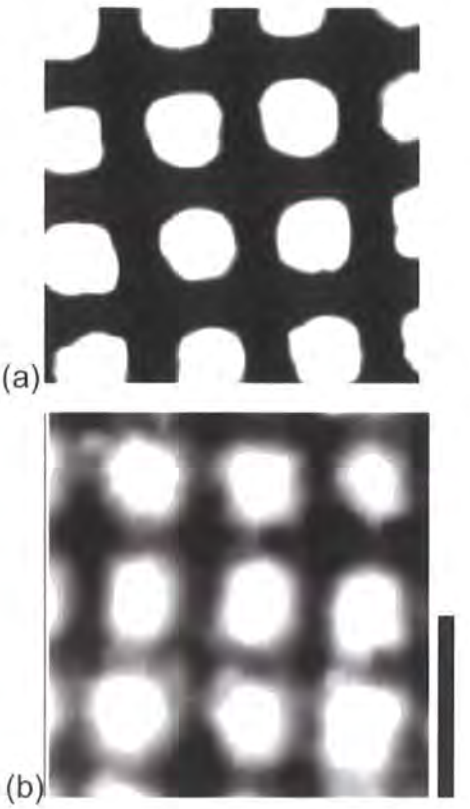

Figure 28: Fluorescence Map of Cresyl Violet Tagged Pulse Plasma Polymerised GMA Deposited into Oxygen/Argon Plasma Etched Wells (2000 Mesh, 7.5 µm Squares, 5 µm Bars) On A polytetrafluoroethylene Film. Using an Embossed Grid (200 MPa) Prior to Etching Pattern, (a) and Un-Embossed Grid, (b). (Scale bar is 20 µm)

2.2.4. Discussion

Conventional mask technology for chemically patterning solid surfaces is widely used for circuit board fabrication,[131] reactive ion etching (RIE),[113] and patterning photoactive polymers.[114] Plasma deposition through a mask is also a common process, and has in the past been successfully used to pattern carbon nanotubes,[118] conducting polymers[132] and cells.[119] However, these techniques rely solely on physical contact and therefore require flat substrates (*e.g.* silica or glass) to ensure close contact with the mask. Alternative approaches for plasma patterning include lift-off,[101] nanosphere lithography,[120] and photolithography.[98] The lift-off technique, i.e. the removal of an underlying resist pattern, can be susceptible to damage during lift-off. In the case of nanosphere lithography, it is difficult to extend the pattern over large areas, whereas photolithography critically depends upon the application of photo-resists and the vulnerability of the substrate towards radiation damage.

Although chemical patterns have been created before by plasma treatment through a grid, they have relied on close contact between the grid and the substrate. In this investigation it has been shown that pattern definition improves with increasing embossing pressure, Figure 24 and Figure 25. A pressure of 400 MPa is sufficient for the grid to be completely embossed into the surface, and higher pressures do not appear to alter the physical pattern definition. However, these higher pressures do seem to be necessary to achieve good pattern definition for etching and plasma polymer deposition. Functionalized microwells can be utilized by different chemical/biological moieties (*e.g.* biomolecules, catalysts, sensors, *etc.*) to act as sensors, high throughput screening devices *etc.*

Alternative ways of functionalizing through the open regions of the embossed template could include wet chemical methods, chemical vapour deposition, and physical vapour deposition. Also, there is considerable scope for employing a variety of different-shaped templates or pre-assembling objects on the substrate surface (*e.g.* micro/nanospheres) prior to embossing and plasmachemical deposition.

This technique has two main advantages, the use of plasma polymerisation allows for the generation of a wide variety of chemical functionalities and secondly the use of inexpensive disposable masks. Plasma polymerisation has been widely studied and its advantages well known but for patterning its ability to be applied to a variety of surfaces is one of its biggest advantages, there is also no limit caused by toxic reagents or resolution. The use of inexpensive masks limits the costs of production, however current mass production techniques only allow for simple 2 dimensional designs. This technique is capable to being expanded to both smaller patterns and 3 dimensional designs when suitable masks are available.

Chemically functionalized arrays and microwells can be prepared by mask embossing prior to plasmachemical etching and deposition. The pattern definition is shown to improve by increasing applied pressure during the embossing step.

2.3. Plasma Polymer Lift-Off Patterning

2.3.1. Introduction

Creating patterns of functionality on a surface has been an area of considerable research recently, the requirements of a wide range of industries from genomics and proteomics to microfluidics driving the dimensions of the patterns to ever smaller sizes. Current methodology has many limitations including volatile or toxic reagents, 2 dimensional patterns and surface suitability, these techniques include: photolithography, [98,99] laser ablation,[100] plasma patterning, [4,101] block co-polymers[102,103] and soft-lithography.[104,43]

In this work, a combination of widely available spotting technology has been combined with the versatility of plasma polymerisation to create a potential method for patterning surfaces. The concept has been expanded to work with a simple soft-lithographic approach to printing on a surface to allow lateral pattern dimensions below current spotting technology limitations. As the technology behind spotting improves this technique can be used to create smaller patterns.

Pulsed plasma polymerization has been selected as the surface functionalization technique of choice. Plasma polymerisation is amenable to a whole range of substrate materials and geometries, creates pin-hole free surfaces, requires only one quick step and can be employed to deposit a variety of chemical groups, *e.g.* hydroxyl,[121] perfluoroalkyl,[122] epoxide,[123] anhydride,[124] carboxylic acid,[125] cyano,[126] amine,[127] halide,[128] furfuryl,[129] and thiol[130]

2.3.2. Experimental

Microscope slides (18 x18 x 0.17 mm, BDH) were ultrasonically cleaned in a 50:50 cyclohexane/propan-2-ol (Aldrich) mixture for 10 minutes in order to remove surface contaminants and air dried. A solution of acrylic acid (Aldrich) in high purity water (BS 3978 Grade 1, 10% v/v) was spotted in a regular array using a mechanised spotter (Genetix Inc) equipped with 1 nL delivery micro-machined split pin as shown in Figure 29. Samples were allowed to dry in air overnight.

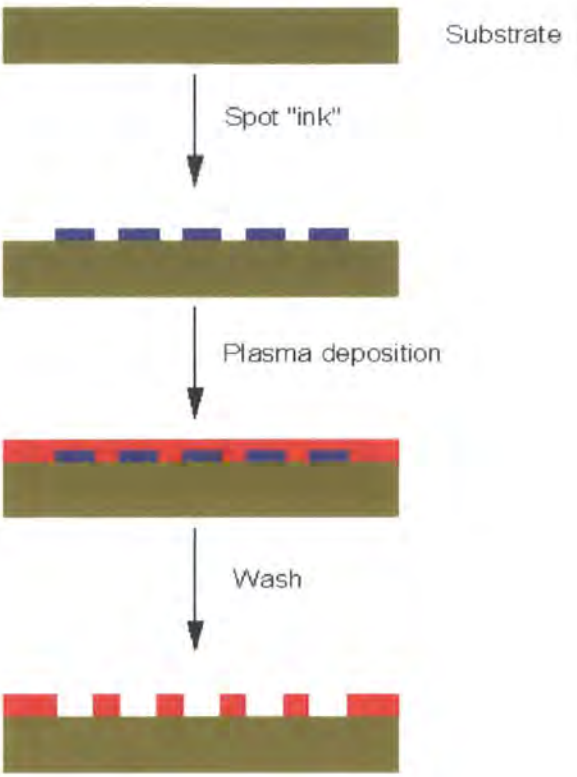

Figure 29: Schematic representation of the print and lift-off process used to pattern a plasma polymer

Plasma deposition was carried out as detailed previously (section 1.9.1) with glycidyl methacrylate (97%, Aldrich) used as the precursor and spotted microscope slides as the samples.

On completion of plasma polymerisation samples were immediately immersed in high purity water (BS 3978 Grade 1) and agitated for 1 week. The water was regularly replaced to encourage the acrylic acid to dissolve. Surface dye attachment to the epoxide centres entailed immersion of the patterned poly(glycidyl methacrylate) substrate into a 1% w/v solution of cresyl violet perchlorate (Aldrich) dissolved in high purity water for 1 hour. Afterwards, the surface was rinsed with high purity water for 2 hours and dried in air. A fluorescence map was obtained as described previously (section 1.9.2)

Plaques (10 mm x 10 mm) of polytetrafluoroethylene (Goodfellows, 0.1 mm thick film) were ultrasonically cleaned in a 50/50 cyclohexane/propan-2-ol mixture for 10 minutes in order to remove surface contaminants. Nickel grids (3.05 mm diameter, Agar Scientific) were embossed into the sheets of polytetrafluoroethylene by placing between two polished aluminium plates (75

mm diameter) in a hydraulic press (Moores Press) and applying a force between of 60 kN (an approximate pressure of 100–600 MPa). Prior to inking the nickel grid were carefully removed. Samples were inked with a 10% solution of acrylic acid (Aldrich) in water (v/v) spin coated onto polished (100) silicon wafers (MEMC Electronics Materials) using a photoresist spinner (Cammax Precima) operating at 2000 rpm. The acrylic acid coated silicon was inverted and attached to a small press to bring the stamp and substrate into parallel contact as shown in Figure 30. Plasma deposition, washing and fluorescent tagging were then completed as described previously.

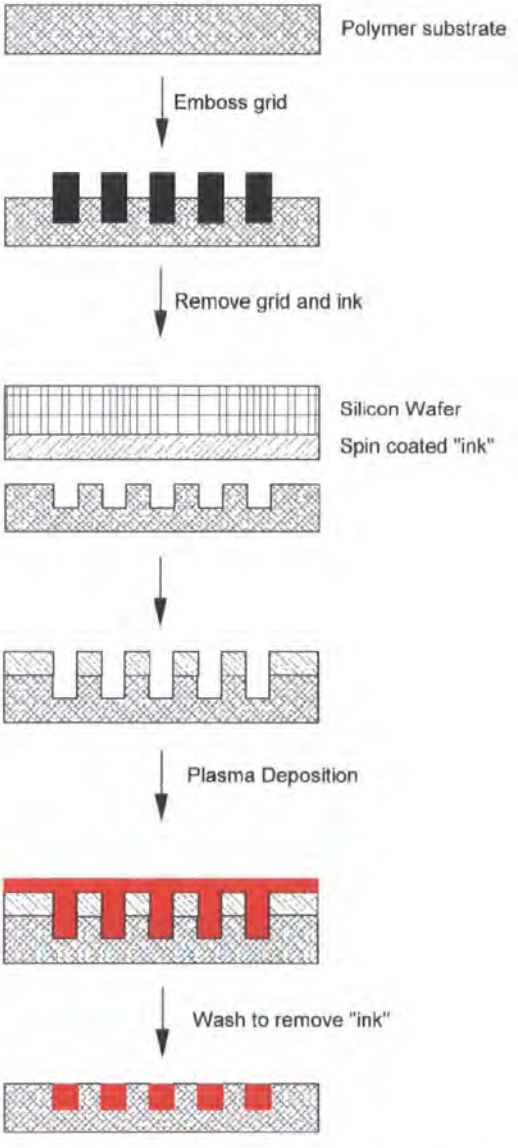

Figure 30: Schematic representation of the micro-contact printing and lift-off process used to pattern the plasma polymer

2.3.3. Results

The larger scale patterning samples are created by spotting with a soluble compound in the required pattern, followed by a plasma polymerisation step then the "lift-off" washing out of the soluble polymer pattern, the process is shown in Figure 29. Figure 31 shows the best image of the spotted lift-off patterning. It has the smallest features about 75 μm in diameter. The print pitch (centre to centre) is 180 μm. The pixilation is caused by the 10 μm resolution of the fluorescence microscope. At a larger scale pattern both the technique for creating the pattern and for analysing the sample are capable of showing the definition possible with this technique. Figure 32 shows the spots created at a larger pixel size. The spots are about 500 μm with a print pitch of 1000 μm.

It is possible to use the concept of lift-off patterning to create patterns at a smaller scale, Figure 30, this technique uses embossing prior to lift-off patterning. Here the pattern is created by inking an embossed polystyrene surface with a soluble compound, followed by plasma deposition and lift-off by washing in water.

XPS was used to characterise the surface at each stage of the lift-off process and the change in carbon spectra at each stage. Each step creates a layer thicker than XPS sampling depth. From a polystyrene chip the sample is inked with poly(acrylic acid) and then glycidyl methacrylate is plasma polymerised on top. The sample is then washed in water causing the acrylic acid to dissolve. The plasma polymer on top of the poly(acrylic acid) is washed away in this step to leave only the underlying polystyrene. When the sample is physically patterned prior to inking, the washing step removes the poly(acrylic acid), leaving the plasma polymer patterned on the substrate.

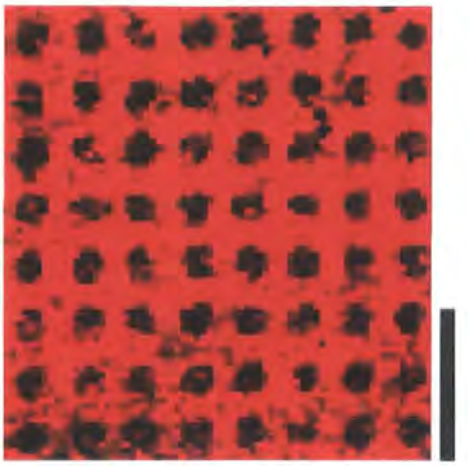

Figure 31: Fluorescence micrograph showing non-fluorescent spots of polybutadiene exposed after lift-off of an acrylic acid pattern and plasma polymerisation of glycidyl methacrylate

The whole surface has been washed in cresyl violet perchlorate in water, the dye attaching to the epoxide functionality. (Scale bar is 500 µm)

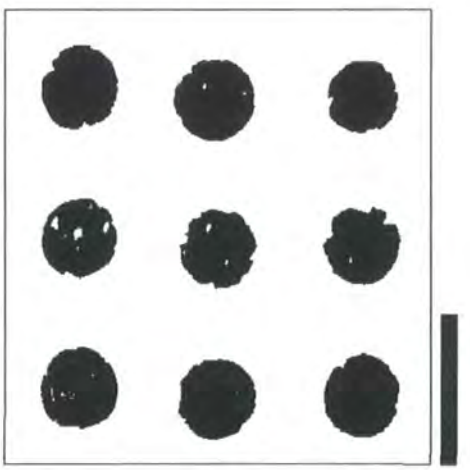

Figure 32: Fluorescence micrograph showing non-fluorescent spots of glass exposed after lift-off of an acrylic acid pattern and plasma polymerisation of glycidyl methacrylate

The whole surface has been washed in cresyl violet perchlorate in water, the dye attaching to the epoxide functionalization. (Scale bar is 1000 µm).

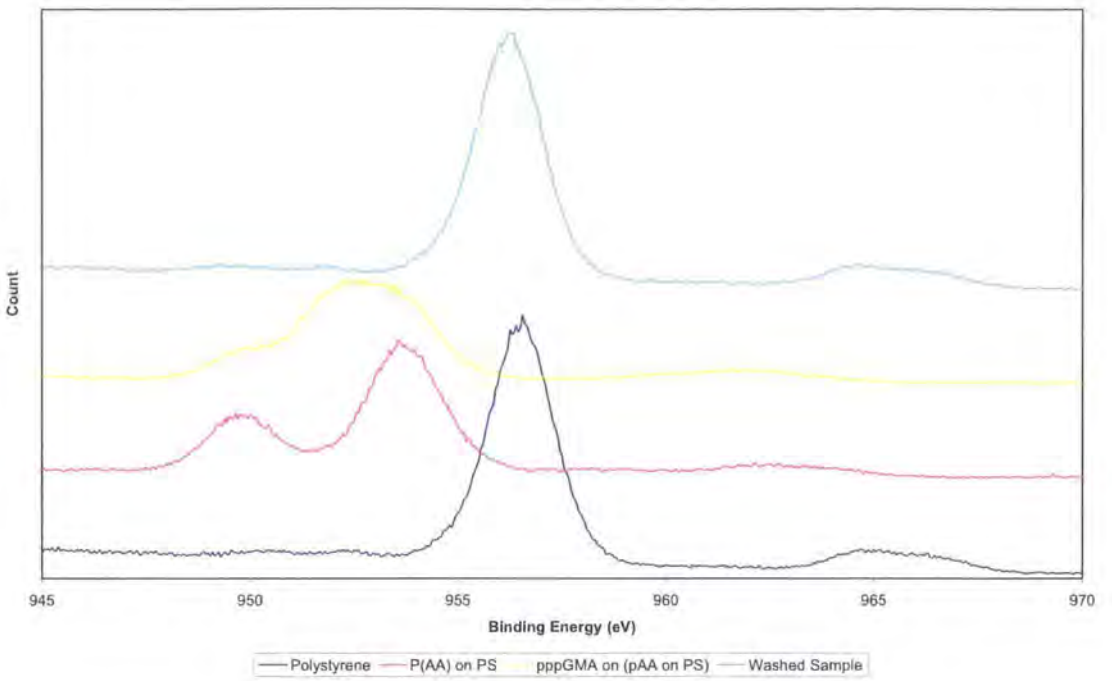

Figure 33: Carbon (1s) XPS Spectra showing the inking and washing process

AFM images shows the patterns created, Figure 34 shows a physical pattern. There is a small change in the phase image caused by the tip not tracking the polymer surface as the tip moves between high areas and low areas. This step is approximately 5 µm created by completely embossing the 5 µm thick grid into the polymer substrate. There may also be an effect caused by the compression on the polystyrene during the embossing at high pressure of the nickel grid. Figure 35 shows an AFM image following inking of the polymer stamp. Again a height difference but this time there is a more distinct phase change between the high squares inked with acrylic acid and the low untreated polystyrene areas. There is a small drift in the pattern of both phase and height images, this is caused by a slight slipping of the grid during the embossing process. Figure 36 shows the next step of the process, AFM images of the plasma polymer coating (GMA) on top of the inked substrate. There is no phase difference across the substrate, indicating a complete plasma polymer coating but the height image still shows the square pattern from the underlying embossed sample. After the final step an AFM image, Figure 37, shows the final washed sample. The plasma polymer remains in the channels but the raised squares are now exposed polystyrene. Figure 38 shows an AFM cross section and

equivalent height image of the final sample. Clearly showing the regular pattern created by the embossing and plasma patterning. This pattern is also shown as a fluorescence image in Figure 39, this is the pattern created by exposing the sample to cresyl violet perchlorate which selectively attaches to areas of poly(glycidyl methacrylate). The pattern is 7.5 µm squares and 5 µm bars.

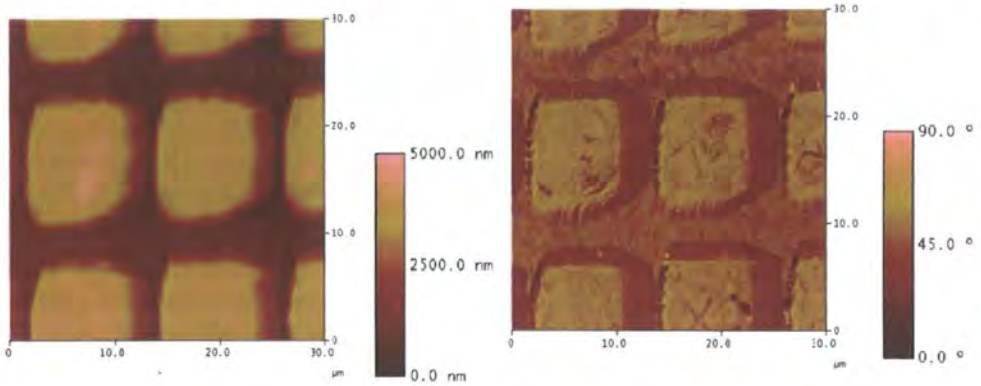

Figure 34: AFM height (top) and phase (bottom) of the embossed polymer stamp

The sample is polystyrene and the pattern is 7.5 µm squares and 5 µm bars. Z-axis scale between 0 – 5000nm, x/y scale bar is 10 microns

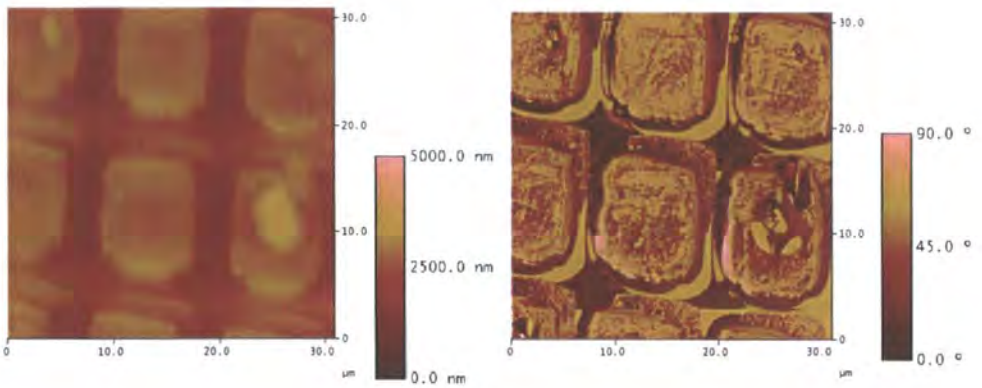

Figure 35: AFM height (top) and phase (bottom) of a poly(acrylic acid) inked polystyrene stamp

The pattern is 7.5 µm squares and 5 µm bars. Z-axis scale between 0 – 5000nm, x/y scale bar is 10 microns

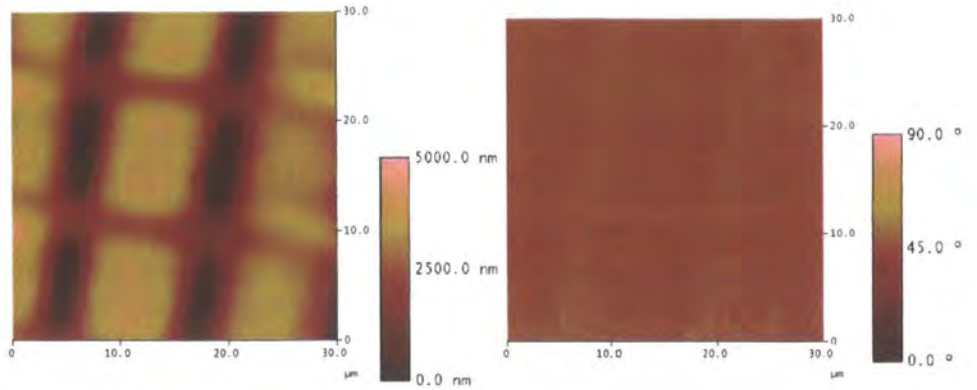

Figure 36: AFM height (top) and phase (bottom) images (30 μm x 30 μm) of poly(glycidyl methacrylate) plasma deposited on top of a poly(acrylic acid) inked polystyrene stamp

The pattern is 7.5 μm squares and 5 μm bars. Z-axis scale between 0 – 5000nm, x/y scale bar is 10 microns

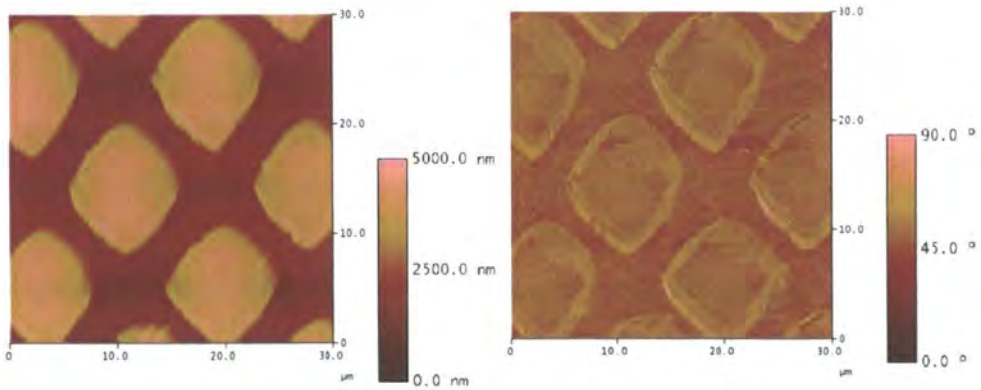

Figure 37: AFM height (top) and phase (bottom) images (30 μm x 30 μm) of the sample imaged in Figure 36 after washing in water to remove the poly(acrylic acid) "ink"

The pattern is 7.5 μm squares and 5 μm bars. Z-axis scale between 0 – 5000nm, x/y scale bar is 10 microns

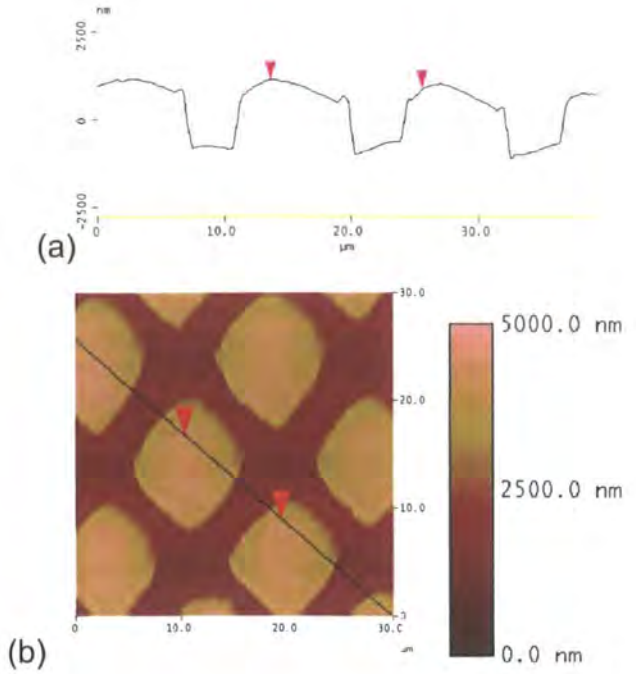

Figure 38: AFM Cross section (a) and height (b) images of a lift-off stamp

The pattern is 7.5 µm squares and 5 µm bars

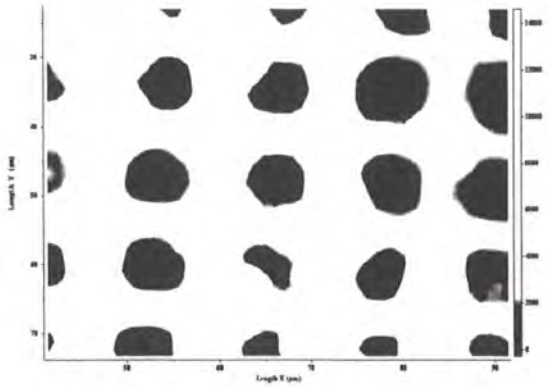

Figure 39: Fluorescence image (50 µm by 50 µm) of a cresyl violet tagged sample.

2.3.4. Discussion

Lift-off patterning has been used by research groups to pattern metals on a nano-scale but not using plasma polymers. Lift-off patterning is a valuable technology as the pattern is repeatable over large areas but retaining the small feature definition.

This work has developed two methods to create lift-off patterns from the millimetre scale to the micrometer scale. Both methods have advantages; the spotting pattern is reproducible over large scales in regular and definable patterns. The requirement for a spotting tool introduces costs which are not present with the embossed lift-off method. Here the need for cheap and readily available mesh grids limits costs.

Plasma polymerisation expands the technology to a range of applications. Plasma polymers can be created in a quick and relatively inexpensive manner across a range of substrates and structures; there is no requirement for toxic or hazardous chemicals.

2.4. Mimicking A Stenocara Beetle's Back For Microcondensation Using Plasmachemical Patterned Superhydrophobic-Superhydrophilic Surfaces

A simple two-step plasmachemical methodology is outlined for the fabrication of microcondensor surfaces. This comprises the creation of a superhydrophobic background followed by pulsed plasma deposition of a hydrophilic polymer array. Microcondensation efficiency has been explored in terms of the chemical nature of the hydrophilic pixels and the array dimensions.

2.4.1. Introduction

Hydrophobic-hydrophilic patterned surfaces offer a means for controlling the wetting behaviour of aqueous media. This is important for a whole host of technological applications including: cell growth,[133,134] protein manipulation,[135] the spotting of biomolecules,[136,137] micro-fluidics (to control the location and movement of liquids)[138,139,140,141] and the formation of anti-dew/frost-free protective exteriors.[142,143,144] Hydrophobic-hydrophilic patterned surfaces are also found in nature. One example is the Stenocara beetle; which lives in arid desert conditions where the only available source of water is fog droplets (these range between 1 and 40 μm in diameter, i.e. much smaller in size compared to normal rain droplets). Random arrays of smooth hydrophilic bumps are present on the Stenocara beetle's back (0.5 mm in size, and arranged 0.5-1.5 mm apart).[77] These hydrophilic regions are surrounded by waxy areas comprising physical features (approximately 10 μm in size), arranged in a hexagonal array. Water collection onto the non-waxy hydrophilic regions occurs by the beetle tilting its back wings into the fog. Any fog vapour incident upon the waxy hydrophobic regions is blown along the surface until it reaches a non-waxy hydrophilic region. The droplets grow until they cover the entire hydrophilic bump, and then, under their own weight, they detach and roll downwards into the beetle's mouth. This naturally-occurring microcondensation surface has been artificially duplicated in the laboratory using random and ordered arrays of 0.6 mm glass spheres on a waxy background.[77] It was found that an ordered

array of spheres gave rise to optimum microcondensation. However, the functionality of the surface was limited to only glass (contact angle of ~20°), and a waxy hydrophobic background (contact angle of 111°).[145] Additionally a manufactured equivalent of this superhydrophilic-superhydrophobic surface has been created by a micro-pipetting technique but this lacks the flexibility of functionality and control of lateral dimensions to allow further analysis of the microcondenser effect.[146]

In this section, we evaluate the microcondensation efficiency of a variety of hydrophobic-hydrophilic patterned substrates with respect to their surface functionality and dimensional parameters to establish whether the degree of hydrophobicity/hydrophilicity in the respective regions plays a role in determining the overall microcondensation efficiency. Two types of superhydrophobic background are employed, corresponding to plasma fluorinated polybutadiene (advancing/receding water contact angle = 154°/152°)[147] and plasma etched polytetrafluoroethylene (advancing/receding water contact angle = 152°/151°),[148,149,150] Figure 40. A range of hydrophilic plasma polymers have been patterned onto these superhydrophobic backgrounds and their water microcondensation performance compared.

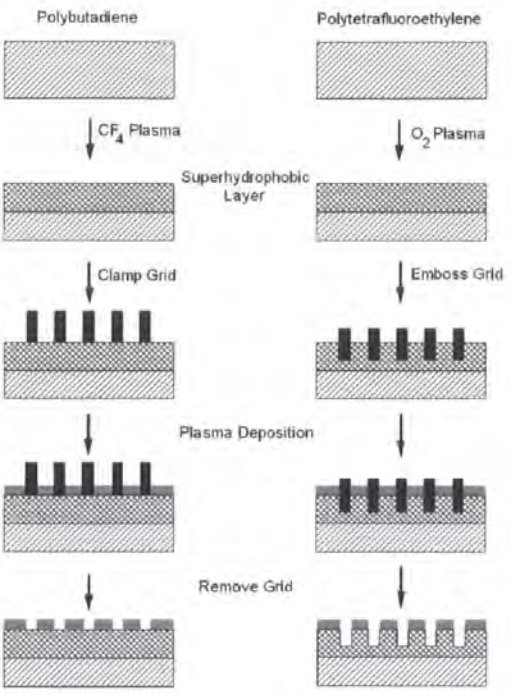

Figure 40: Micropatterning a hydrophilic plasma polymer onto a superhydrophobic background

Created by either CF4 plasma fluorination of polybutadiene film or oxygen plasma treatment of polytetrafluoroethylene polymer film.

2.4.2. Experimental

Plasmachemical modification and deposition was carried out as described previously (section 1.9.1). Two types of superhydrophobic surface were prepared, Figure 40. In one case, an 8% (w/v) solution of polybutadiene (Aldrich, MW = 420,000, cis 1,4 addition) in toluene (BDH, +99.5% purity) was spin-coated onto polished silicon wafers (MEMC Electronics Materials, 25 mm x 25 mm) using a photoresist spinner (Cammax Precima) operating at 2000 rpm for 60 s. These polymer films were subsequently vacuum annealed at 90 °C for 1 hour to remove entrapped solvent. Plasma treatment with CF_4 gas (99.7% purity, Air Products) at 50 W for 5 minutes yielded a superhydrophobic surface (advancing/receding water contact angle = 154°/152°).[147] The plasma fluorinated polybutadiene coated silicon wafers were then clamped screw-tight to a grid (0.1 mm thick brass sheet, machine-drilled with a regular square array of circular holes) mounted in an aluminium holder, Figure 41.

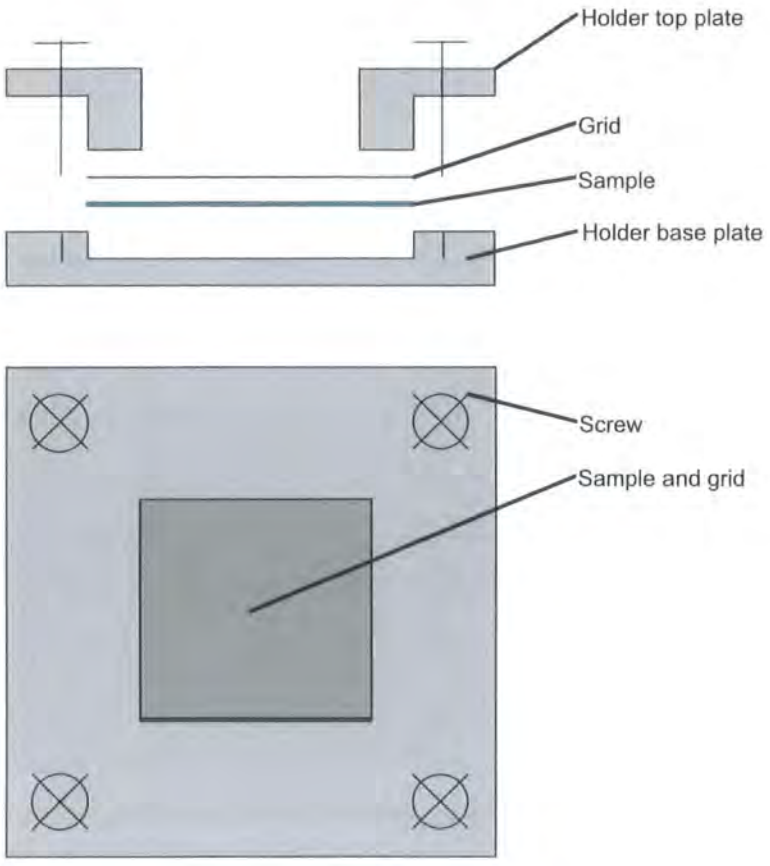

Figure 41: Side and top views of holder used to clamp the grid in position on top of the sample

The other approach for creating a superhydrophobic background consisted of ultrasonic cleaning of 25 mm x 25 mm plaques of polytetrafluoroethylene (Goodfellows, 0.1 mm thick film) for 10 minutes in propan-2-ol and cyclohexane (50/50 v/v) followed by O_2 gas (99% purity, Air Products) plasma treatment at 50 W for 60 minutes (advancing/receding water contact angle = 152°/151°).[151] These superhydrophobic substrates were then embossed with a grid (0.1 mm thick brass sheet, machine-drilled with a regular square array of circular holes) at a pressure of 400 MPa for 10 s using a mechanical press (Moores Press) and then mounted in the aluminium holder, Figure 41.

For both types of superhydrophobic substrate, the aluminium holder was then placed into the centre of the plasma chamber ready for hydrophilic functionalization through the exposed array holes. Evacuation to base pressure was followed by monomer vapour introduction into the system *via* a fine needle control valve at a pressure of 0.2 mbar for 5 minutes prior to electrical discharge ignition. In the case of pulsed plasma deposition, a signal generator was used

to trigger the RF power supply in combination with the respective monomer, Table 3.

Table 3: Optimum duty cycle and peak powers employed during pulsed plasma polymerization of various monomers

The thickness value corresponds to deposition onto a flat silicon wafer placed adjacent to the patterned sample.

Monomer	t_{on} (µs)	t_{off} (ms)	Peak Power (W)	Thickness (nm)(±5)
4-Vinyl pyridine	100	4	40	70
Maleic anhydride	20	1.2	4	63
Glycidyl methacrylate	20	20	40	104
Bromoethyl-acrylate	30	10	20	225
4-Vinyl aniline	100	4	40	62
Vinylbenzaldehyde	50	4	40	114

Water microcondensation onto the functionalized substrates entailed exposure to a mist of high purity water (BS 3978 Grade 1) generated by a nebuliser set to a gas flow rate of 11 l min^{-1} N_2 (99.7% purity, Air Products), Figure 42. The mass of water collected was measured in 30 minutes intervals over a period of 2 hours.

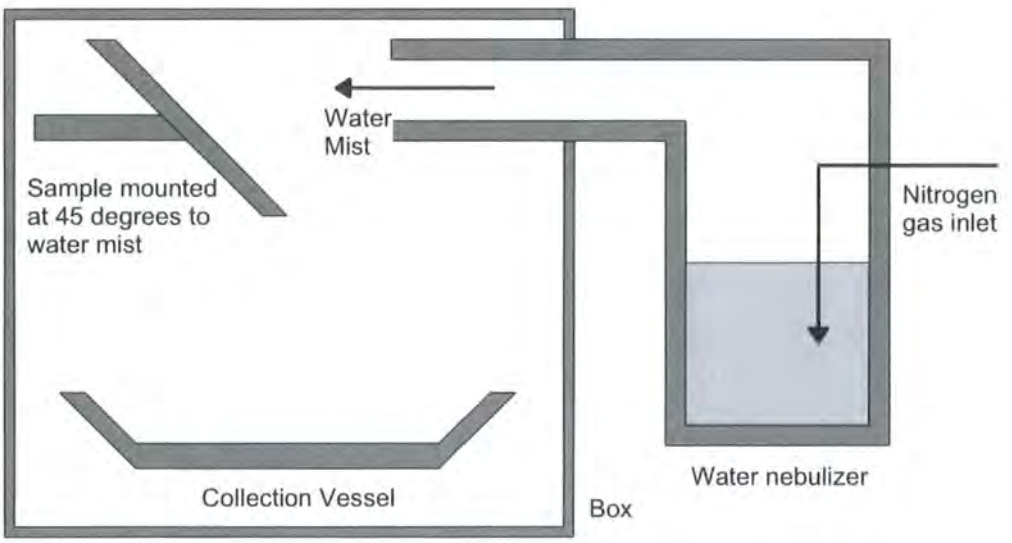

Figure 42: Apparatus for water microcondensation.

In order to demonstrate the practical potential of these hydrophobic-hydrophilic arrays for chemical immobilization, the patterned substrates were immersed in a

solution of water and drawn slowly out at an angle of 45°. This produced a uniform pattern of water droplets across the array of hydrophilic (poly(glycidyl methacrylate)) pixels. Aminomethyl polystyrene beads (~50 μm mean diameter, Biosearch Technologies) were sprinkled as a fine dust above the surface, mounted at 45°. The sample was then gently blown with air from a pipette, left overnight at 42 °C in a humidity chamber, and finally the surface was washed with high purity water.

Optical images of the patterned surfaces were taken with the mapping stage of an infrared microscope (Perkin-Elmer Spectrum One FTIR).

2.4.3. Results

The chemical compositions of the functionalized surfaces as measured by XPS are in good agreement with theoretically predicted values, Table 4. The efficiency of these surfaces to perform as microcondensers was investigated by collecting water from a fine mist over a 2 hours period, Figure 43. These studies clearly show that either non-patterned hydrophilic or superhydrophobic surfaces do not collect significant volumes of water. Large bulbous drops were evident around the bottom edge of the non-patterned hydrophilic surfaces (often they were insufficient in size to fall from the sample and be measured). The superhydrophobic surfaces were somewhat better at collecting water.

The patterned hydrophobic-hydrophilic surfaces were found to be the most efficient for water microcondensation. In this case, any small water droplets which formed on the hydrophobic areas were blown across the surface until they reached a hydrophilic region. Here, the droplets combined with droplets already present in the hydrophilic region. These droplets continued to expand until they reached a critical droplet size, and then fell (due to gravity) at a steady rate into the collection vessel. The combination of a superhydrophobic background and a superhydrophilic poly(4-vinyl pyridine) array was found to outperform all the other functional surfaces screened in this study, Figure 44. A similar trend was noted for both the plasma fluorinated polybutadiene and the O_2 plasma etched polytetrafluoroethylene superhydrophobic backgrounds, Scheme 1.

Beyond a threshold value of approximately 500 μm, water condensation was observed to decrease with increasing hydrophilic spot size, Figure 45. Above 1200 μm spot size, water collection became minimal. No variation in microcondensation behaviour due to the hydrophilic layer film thickness was observed.

These chemically patterned surfaces were also found to readily undergo derivatization reactions. For example, a poly(glycidyl methacrylate) micropatterned superhydrophobic polybutadiene surface selectively adsorbs amino-methyl-polystyrene beads via the microcondensation effect, Figure 46. These beads can then be chemically fixed into the regions of poly(glycidyl methacrylate) *via* the reaction between epoxide and amine groups[123] by heating to 42 °C. Following immobilization, these amine functionalised beads were found to be stable towards repeated washing in water.

Table 4: Surface chemical composition measured by XPS

Surface	% C (±1.0%)	% F (±1.0%)	% O (±1.0%)	% N (±1.0%)	% Br (±1.0%)
Polybutadiene	99	-	1	-	-
CF_4 plasma/polybutadiene	39	60	1	-	-
Poly(tetrafluoroethylene)	32	68	-	-	-
O_2 plasma/poly(tetrafluoroethylene)	31	67	2	-	-
Poly(4-vinyl pyridine) theoretical	88	-	-	13	-
Pulsed plasma poly(4-vinyl pyridine)	85	-	3	12	-
Poly(maleic anhydride) theoretical	57	-	43	-	-
Pulsed plasma poly(maleic anhydride)	66	-	34	-	-
Poly(glycidyl methacrylate) theoretical	70	-	30	-	-
Pulsed plasma poly(glycidyl methacrylate)	71	-	30	-	-
Poly(bromo ethyl-acrylate) theoretical	63	-	25	-	13
Pulsed plasma poly(bromo ethyl-acrylate)	64	-	24	-	12
Poly(4-vinyl aniline) theoretical	89	-	-	11.1	-
Pulsed plasma poly(4-vinyl aniline)	85	-	4	11.2	-
Poly(vinylbenzaldehyde) theoretical	90	-	10	-	-
Pulsed plasma poly(vinylbenzaldehyde)	92	-	8	-	-

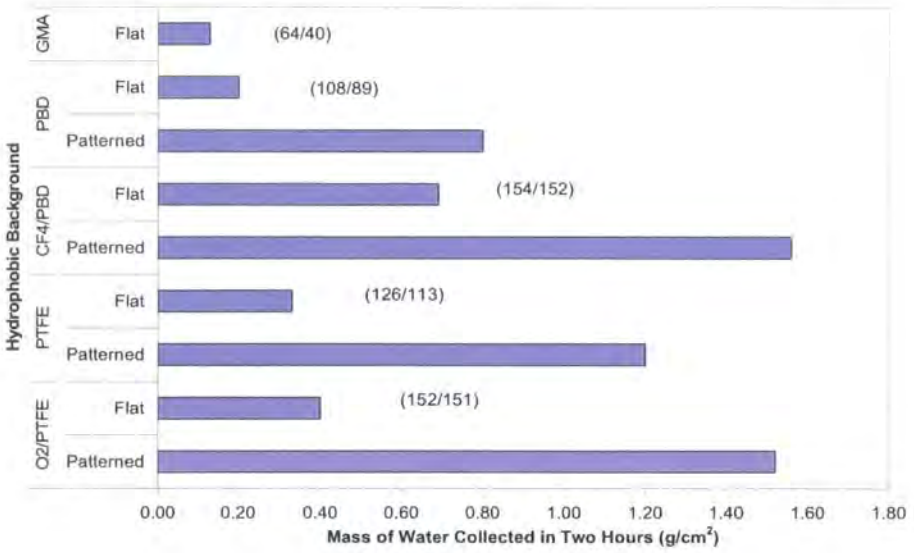

Figure 43: Water condensation study (mass of water collected over 2 hours) of a range of hydrophobic surfaces.

Flat samples of each superhydrophobic polymer are compared with superhydrophobic samples patterned with a regular array of 500 µm diameter spots of pulsed plasma deposited poly(glycidyl methacrylate) arranged 1 mm centre-to-centre. (The numbers in brackets correspond to advancing/receding water contact angle values).

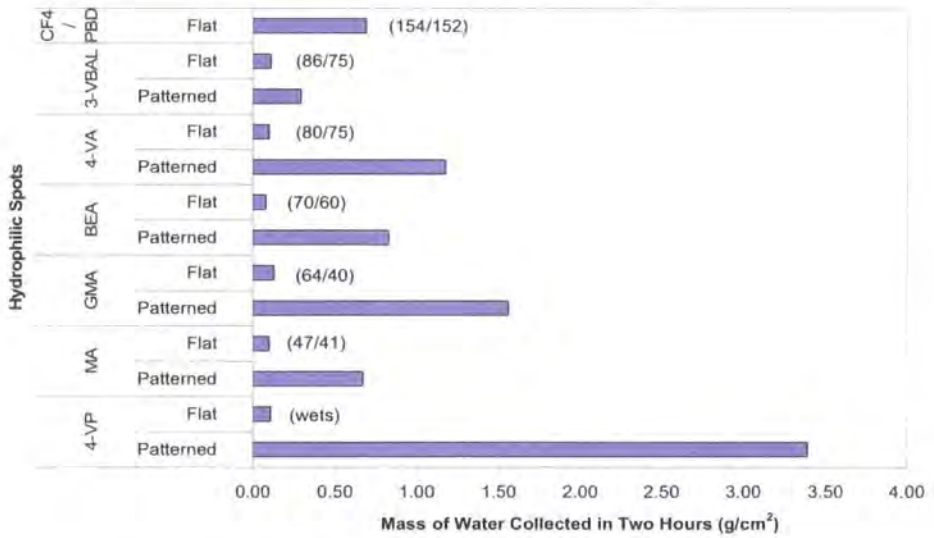

Figure 44: Water condensation study (mass of water collected over 2 hours) over a range of hydrophilic surfaces

Hydrophilic plasma polymer coatings are compared with a regular array of 500 µm diameter hydrophilic plasma polymer spots arranged, 1 mm centre-to-centre, on a superhydrophobic background (CF_4 plasma fluorinated polybutadiene). (The numbers in brackets correspond to advancing/receding water contact angle values).

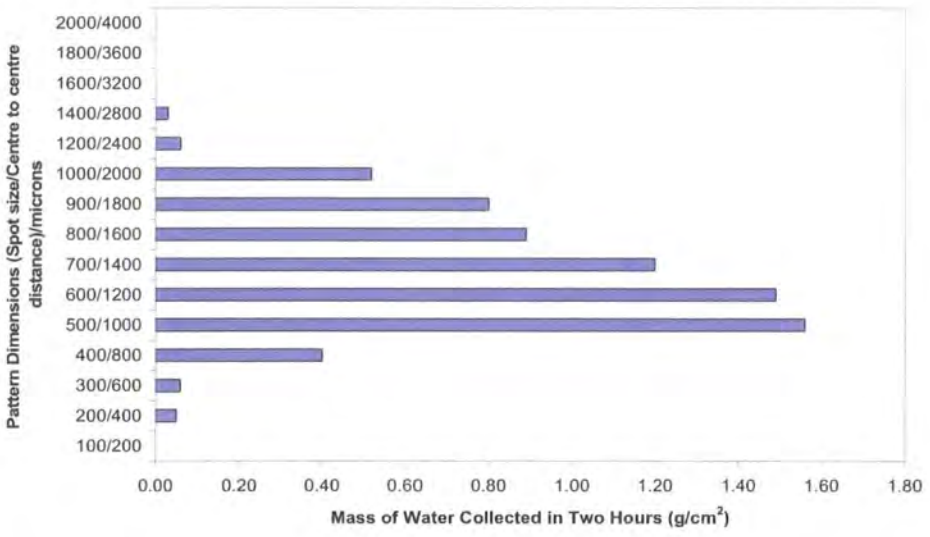

Figure 45: Water condensation study for different sized arrays of pulsed plasma deposited poly(glycidyl methacrylate) hydrophilic spots arranged in a regular array on a CF4 plasma fluorinated polybutadiene substrate.

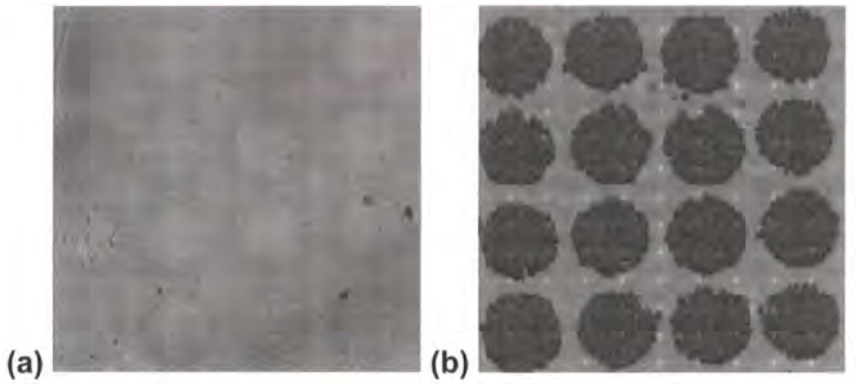

Figure 46: Optical micrographs showing: (a) pulsed plasma deposited poly(glycidyl methacrylate) array on a CF4 plasma fluorinated poly(butadiene) surface; and (b) the same pattern reacted with amino-polystyrene beads

The spots of pulsed plasma deposited poly(glycidyl methacrylate) are 500 µm in diameter and 1 mm centre-to-centre. Scale bar is 1mm.

2.4.4. Discussion

Microcondensation can be an effective means for fog-harvesting by utilizing vertically-mounted mesh sheets in the air to collect the dew from trees.[152] Steam condensation is another potential application.[153] There is also scope for

condensing organic vapours by combining oleophilic and oleophobic patterned surfaces.

In this study, pulsed plasma deposited poly(4-vinylpyridine) displays the lowest water contact angle of all the functional coatings screened. The contact angle is sufficiently low that the surface can be designated superhydrophilic, or completely wettable (water spreads out so rapidly that it becomes impossible to observe any meaningful contact angle).[154] When combined with a superhydrophobic background, the micropatterned superhydrophilic polymer outperforms the other hydrophilic surfaces. This is due to the wettability of the hydrophilic surface allowing the mist droplets to combine more readily and thus reaching the critical size for detachment sooner.

The critical size is depended on a number of factors; mass, size of the droplet are important. Also the absolute contact angle and the sliding angle, *a*, (the angle at which a droplet begins to move down a surface) play a significant role in detachment.

$$\frac{mg(\sin\alpha)}{w} = \beta_{LV}(\cos\theta_R - \cos\theta_A) \qquad (18)^{155}$$

$ß_{LV}$ is surface tension at the liquid - vapour interface, m is the mass of droplet, w is the width of the droplet (horizontal to the direction of drop movement), *g* is gravity, θ_R is the receding contact angle and θ_A is the advancing contact angle. Hence it is evident that the low contact angle hysteresis characteristic of the two superhydrophobic surfaces (oxygen treated polytetrafluoroethylene, and CF_4 plasma treated polybutadiene), can explain the enhancement in microcondensation. Such ease of movement of a droplet on a surface is beneficial to microcondensation in two ways: the fog droplets are more easily blown into the hydrophilic regions, and when the critical size of droplet is reached within the hydrophilic regions, the detached droplets can roll more readily down the hydrophobic surface.

It is also evident that the size of the hydrophilic spots has a large bearing on the surface's ability to collect water. Spots around 500 µm were found to be optimal in the present study, whereas spots exceeding 1200 µm showed little to no

condensation. In the latter case, it was observed that critical size for droplet detachment is never reached: namely, the rate of water loss through processes such as evaporation exceeds the rate of fog droplet condensation. Effectively, hydrophilic domains are so large that they act in a similar way to purely hydrophilic surfaces. In addition, there is also a minimum hydrophilic spot diameter required to facilitate microcondensation: below 400 μm droplets were seen to form and quickly reach critical size. However, they lacked sufficient mass to overcome the surface tension, and thus remained attached to the surface.

These results are consistent with the Stenocara beetle which has spots approximately 600 μm in diameter and 500 μm - 1.5 mm apart. Furthermore, such plasmachemical hydrophobic/hydrophilic patterned surfaces offer scope to control the wetting behaviour of aqueous media. This is potentially useful for the patterning of moieties dispersed within aqueous media (as exemplified by the amine functionalized polystyrene microspheres, Figure 46).

Microcondensor surfaces can be fabricated by the plasmachemical arraying of hydrophilic pixels onto a superhydrophobic background. CF_4 plasma fluorinated polybutadiene and O_2 plasma etched polytetrafluoroethylene provide appropriate superhydrophobicity, whilst superhydrophilic poly(4-vinyl pyridine) spots exhibit the greatest efficiency for microcondensation. The optimum hydrophilic pixel size/centre-to-centre distance of 500 μm/1000 μm compares favourably with the hydrophilic/hydrophobic patterned back of the Stenocara beetle used by the insect to collect water in the desert.

3. Bioactive Plasma Polymer Surfaces

3.1. Introduction

Biocompatible surfaces are important in a number of applications such as artificial tissue,[156] vascular grafts[157] and bone prosthesis.[158] The ideal surface will be cost effective, applicable to a whole host of surfaces and apply to sustain cell adhesion and proliferation without altering the function of the cell.

Numerous studies have discussed cell culture and each draws its own conclusion on the variety of substrate properties that may affect growth including surface energy,[159] surface functionality,[160] immobilized adhesive proteins,[161] topography[160] and charge.[162]

It is generally accepted that the cell/substrate adhesion process is controlled by a specific process of binding between the surface and proteins belonging to the extra-cellular matrix (ECM).[163,164] Polar and electrostatic interactions may occur between a cell and a substrate but these are replaced in the long term by protein linkages.[165] Several studies have shown that preventing ECM production by using cycloheximide slows[166] or actually inhibits cell attachment.[167]

3.1.1. Mechanism for cell adhesion

Adhesion of a cell to a substrate is a multi-step process. First attachment factors, such as glycoproteins, are adsorbed to the surface followed by cell attachment to this coating layer.[168] The attached cells spread on the surface by distorting their shapes and start proliferating after the end of the spreading step.

The rate of cell attachment is controlled by two main variables, the quantity of cells and the quantity of sites on the surface that are suitable for cell adhesion. The number of sites is limited by the adhesion of the attachment factors which is limited by the amount of the relevant factors and the conformation of their attachment. An incorrectly adhered protein in the wrong conformation can affect the process in two ways, it directly blocks that particular site from immediate cell attachment and there

is also an energy barrier to replacement of the protein with one suitable for cell attachment. As cells require several attachment points in the same location, poor conformation at a particular site may affect the sites in close proximity.

3.1.2. Coating with proteins

Proteins have been extensively adhered to substrates to evaluate their effect on the process of cell adhesion. Adhesion of a protein layer prior to evaluating cell growth was shown to prevent competitive adsorption of other proteins, eliminating the effect of substrate effects such as hydrophobicity and surface charge (either positive or negative).[160] fibronectin adsorption to hydrophilic and hydrophobic surfaces has been examined and the protein adsorbed well on both types of surfaces but only the conformation on hydrophilic surfaces was biologically active.[169] In general a pre-coating of a cell adhesive protein was enough to enhance the adhesion and spreading of cells.

3.1.3. Proteins involved in cell adhesion

Many studies have been carried out to determine the effect of certain proteins on the adhesion of cells; mostly these involve either the removal of the required protein from serum or the deposition of a layer of the required protein and culture in serum-free environments.

These studies can lead to useful results and there now appears to be a group of proteins that are useful in cell adhesion: fibronectin, vitronectin and Fibrinogen.[170] There are also a number of proteins: albumin, IgG and HDL, which limit or block cell adhesion.[171] These are not fixed rules and each cell responds in different ways (hence disagreement in the literature about which proteins are important) but the absence of one or more of the cell adhesive proteins limits the cell adhesion and growth.[172]

Covering the surface in "blocking" proteins is also not a way of preventing cell adhesion as most proteins can be displaced.[173] The nature of adhesion of any protein is crucial. Simply measuring the absolute amount of attached protein is not

valid. Surfaces bind proteins in different ways and this affects biological activity, depending on the conformation or orientation. One method of determining the activity is by determining the strength of adhesion of the protein to the surface. The elution of proteins by sodium dodecyl sulphate (SDS) has been used as a valid method of determining the strength of protein-surface interactions.[174] However the strength of the binding of proteins to a surface can have differing effects: tightly bound proteins may prevent displacement by other proteins and strong adhesion may also slightly denature the protein and prevent biological activity.

Therefore it has been suggested that to be biologically active a surface must adsorbed adhesive proteins to allow cell adhesion and growth but allow the non-adhesive blocking proteins to be loosely bound and easily displaced.[174]

3.1.4. Proteins in serum and blood

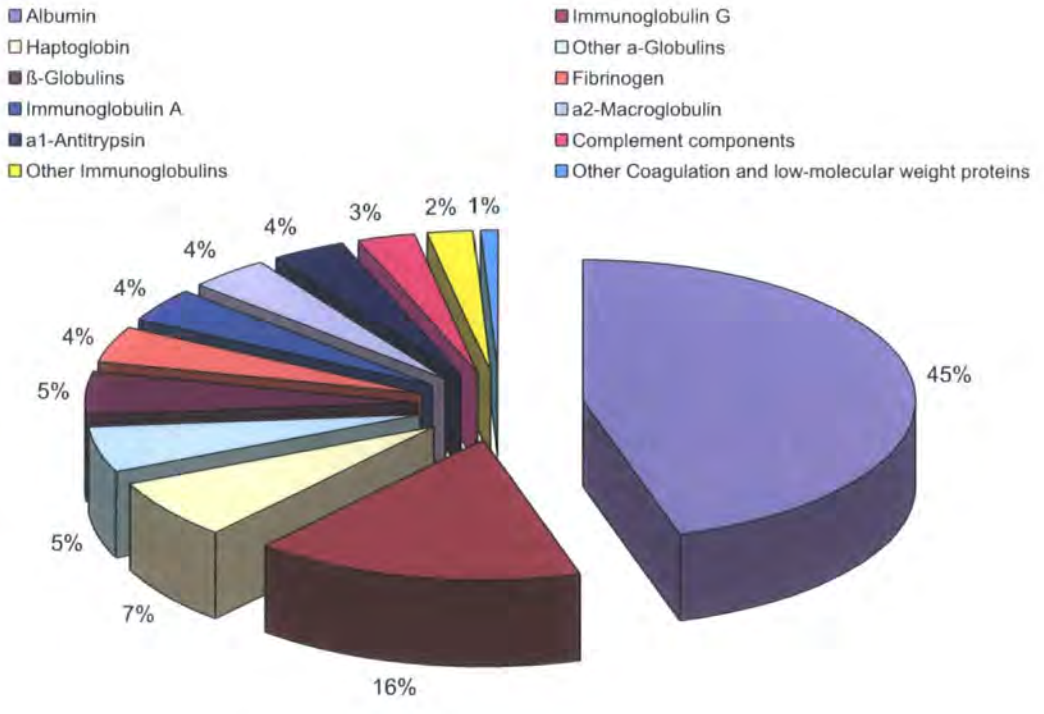

Figure 47: Pie chart of the proteins present in blood[g]

[g] Data from SigmaAldrich.com

Figure 47 shows the relative amounts of the various proteins present in blood, this is approximately matched in serum. Protein attachment onto a surface occurs on timescales much shorter than those typical for cell adhesion. The proteins that adsorb onto the surface depend on the size and abundance of each protein and also the chemical nature of the surface. Different protein layers will form on different surfaces in the same environment. The surfaces will have different concentrations of proteins and different conformations of these proteins. This in turn determines the adhesion and proliferation of cells that attempt to adhere to these surfaces. The adhered protein layer can undergo conformation and orientation changes with time; the extent of exchange of proteins is usually greater for hydrophilic than for hydrophobic surfaces.[173]

3.1.5. Serum-free/serum-containing Media

The mechanism of attachment does not differ between serum-free and serum-containing media, both being controlled by the Arg-Gly-Asp (RGD) sequence containing proteins. In serum-free media the proteins are directly produced by cells whereas serum-containing media contains a whole host of proteins. This plentiful supply of proteins causes problem with cell adhesion and non cell adhesive proteins such as albumin (the most common protein in serum) must be easily removed and replaced with cell-adhesive proteins such as vitronectin and fibronectin if cell adhesion and growth is to occur. If a surface tightly binds albumin then it is usually prevented from rapid cell culture. In serum-free media there is no competitive adsorption of proteins and the cell will secrete proteins it needs for adhesion and growth.

3.1.6. Protein Resistance

There is a group of surfaces at the middle of the hydrophilicity range (between a 30-50 degree contact angle with water) such as poly(ethylene glycol) and poly(N-acryloylsarcosine methyl ester). This family has been given a set of parameters by Whitesides[175] defined by electrostatic, hydrophilic and hydrogen bonding factors.

These parameters are not complete and serve only as a guide. The mechanism of protein resistance is not completely understood but appears to centre on the ability of a surface to hydrogen bond to water.

3.1.7. Methods of surface modification for bioactivity

Biomedical applications commonly use polymers with useful bulk properties such as PTFE, polyolefins and silicones *etc.* but these do not have surface biocompatibility and do not encourage cell growth. A number of methods have been used to deposit or modify surfaces to create bioactivity.

The standard surface used in research is polystyrene, a relatively hydrophobic substrate which has been modified by hydroxylation[176] and carbonylation[177] to encourage cell adhesion. Modification has been achieved by acetone, air, ethylene oxide, methanol and water plasma treatments.[178]

Self-assembled monolayers are useful for creating *in vitro* experiments to determine the effect of different functionalities[179] on cell growth[180] or protein attachment.[181] Self-assembled monolayers can be applied to more systems than just alkanethiols onto gold (*e.g.* alkanesiloxanes onto glass or polymers) but this limits their main advantages, namely their well ordered nature and ease of production. Self-assembled monolayers also have limited stability and cannot be expected to survive exposure to *in vivo* environments.

UV-modification[182] or ion-beam treatments[183] of polymer surfaces have also shown improved cell adhesion. L-lactide has been plasma grafted onto polymer films to increase the attachment of fibroblast cells. L-lactide surfaces had a lower contact angle compared with the host polyurethane substrate and have the added advantage of being biodegradable.[184] Lysine (an amino acid with a $CH_2CH_2CH_2CH_2NH_2$ side chain) and poly(lysine) have been both adhered[185] and polymerized by plasma deposition[186] to produce hydrophilic surfaces for cell adhesion, in particular the adhesion of human nerve cells.

3.1.8. Parameters currently studied for cell adhesion

3.1.8.1. Wettability

There has been a considerable amount of research on the effect of wettability on the adhesion of cells onto surfaces with differing conclusions on its affect. Poor growth on hydrophobic surfaces and extensive growth on hydrophilic surfaces has been reported[187] however other studies have concluded that moderate wettability is ideal.[188,189] Cells also attached more strongly with increasing wettability although tissue culture polystyrene was noted as a particularly strong adhesion out of sink with its wettability.[190] However these studies suffer from a lack of availability of substrates over the complete wettability scale[189] or from using non-polymeric species as super-hydrophilic substrates.[190]

Several studies have shown that whilst wettability is a general macroscopic factor there are often quite large differences in cell adhesion between polymers of similar wettability.[191] Wettability is a consequence of surface functionality; different functionalities may form surfaces of similar wettability. It is important to consider wettability as part of the overall surface properties rather than independent of surface functionality.

Self-assembled monolayers have been produced with a contact angle of approximately 10° from alkanes terminated in COOH functionality.[165] Here it is important to distinguish the differences between Self-assembled monolayers and polymers. Self-assembled monolayers produce a functional surface with excellent structural integrity and organization. Cells have shown the ability to differentiate substrates through a layer of pre-adsorbed proteins and an extension of this is the ability to differentiate between a monolayer of atomic functionality and a thicker layer of functionality. Polymers also have the ability to adsorb large quantities of water due to their bulk properties, whereas the "bulk" properties of Self-assembled monolayers are the straight chain of the alkane. This in some respects should explain the apparent lack of differentiation of some cell lines to self-assembled monolayer functionalities.[165]

3.1.8.2. Hydrophilicity

Hydrophilicity arises from the ability of a surface to form hydrogen bonds with water; this bonding having several defined stages with interesting properties. Low hydrophilicity and even weakly hydrophobic surfaces act in similar manners to macromolecules such as proteins and cells. Intermediate wettability (contact angle around 35-50°) has been shown[192] to be a region of protein resistance caused by the nature of packing of the water molecules on the surface. This packing of water molecules can become too efficient and this results in a super-hydrophilic surface (contact angle less than 20°) which is truly wettable.

The two main wettable polymers that have been covered extensively in the literature are polymers of acrylic acid and 2-hydroxyethylmethacrylate. The direct production of insoluble super-hydrophilic surfaces has yet to be achieved, one of the best methods is a continuous wave plasma deposition of acrylic acid containing less than 10% acid functionality.[193] Higher functionality concentration is possible but the film lacks long term stability.[157] Both 2-hydroxyethylmethacrylate and acrylic acid polymers have long been seen as good cell adhesive surfaces but suffer from a lack of stability in aqueous media[194,195] and mechanical problems.[196] A variety of methods of solving these problems have been used including plasma co-polymerization[197] and grafting onto substrates by plasma[163] or UV irradiation pre-treatment.[198] Co-polymerization is limited by the amount of cell adhesive functionality retained[195] and graft-polymers can be expensive and time-consuming to produce.

3.1.8.3. Surface functionality

The introduction of oxygen functionality has been explored by self-assembled monolayers. Cell growth increased with increasing oxygen content[199] but the oxygen-containing functionality; carbonyl rather than hydroxyl or carboxyl, was deemed more important.[177] Contrasting results have been produced using different cell strains or different testing methods. Further experiments have screened a range of oxygen surface functionalities (CH_3, CH_2OH, CO_2CH_3, COOH) for cell

growth and shown the acidic functionality to be superior.[174] Nitrogen-containing Self-assembled monolayers have also been explored and shown good adhesion and growth.[200] This incorporation of nitrogen has been shown to influence the adhesion of corneal epithelial cells;[165] with a NH_2 terminated self-assembled monolayer showing greater cell adhesion in serum than tissue culture polystyrene and COOH terminated Self-assembled monolayers. UV irradiation of PTFE was shown to introduce C=O, C-OH, C-OOH, C-NH_2 functionality[182] and these polar groups created a higher surface energy and increased cell growth.

3.1.8.4. Ion implantation and charged surfaces

Cell adhesion can be improved in polymers by implantation of ions such as Na^+, O_2^+, N_2^+ and Kr^+, this increase occurs above a threshold level of ion bombardment[201] and occurs because of the formation of a hydrogenated amorphous carbon phase which leads to a higher surface energy. Carbon deposition can also be achieved by vacuum evaporation and this yielded improved cell adhesion.[170]

The presence of electrical charges at the surface has also played a role in the adhesion of cells.[202] Cells can adhere onto surfaces with both positive and negative charge but the shape of the attached cells varies.

3.1.8.5. Surface topography

Topography of the substrate is an area concerning several research groups. A variety of methods of creating surface topography have been examined including photolithography,[203] electron-beam lithography and polymer de-mixing.[204] These techniques are used to control the features in the nanometer to micrometer scale. Random roughness created by sandblasting PMMA has also been explored and found to improve the cell adhesion.[205] Cells are also known to align to steps and grooves in the surface.[203]

3.1.9. Cell types

There are five main groups of cells found in the tissue of animals: Epithelial, Connective, Muscle, Nervous and Blood/Lymph. Epithelial cells are those which form the coatings of organs and cavities. Connective cells are those whose function is structural, such as bone or cartilage. Muscle tissue is made up of ordinary skeletal muscle cells. Nervous tissue includes the brain, spinal cord and nerve cells. Blood cells include all the cells found in blood, such as red blood cells.

3.2. MCF7 Cancer Cell Growth on Plasma Polymer Surfaces

3.2.1. Introduction

Plasma polymers have been reviewed as bio-active surfaces and the surface characteristics that are most important in designing a good bio-active polymer have been established. Plasma chemistry offers a whole host of benefits to the production of cell culture surfaces; namely the ability to produce sterile surfaces, be directly coated onto any substrate and the ease of control of the surface functionality.

Pulsed plasma polymerization has been shown to be the most reliable polymerization method with excellent structural retention; it has been used to create a wide variety of surface functionality including hydroxyl,[206] perfluoroalkyl,[207] epoxide,[208] alcohol,[206] anhydride,[209] carboxylic acid[210] and cyano.[211] Plasma modification of surfaces for cell growth has also been extensively covered using air,[189] acetone,[212] ethylene oxide,[178] methanol, [177] water,[191] nitrogen, ammonia[160] and oxygen[213] plasma treatments.

3.2.2. Experimental

Protein adhesion was measured on a Surface Plasmon Resonance machine (BIACore 1000/upgrade). Values quoted are in response units which are approximately equivalent to 1 pg protein/mm^2.[214] Using the conditions and deposition rate for each monomer as described in Table 6 and process described previously (section 1.9.1), polymer films of less than 20 nm were created on gold SPR chips (SIA Kit Au chips, Biacore). For each flow cell, the cross sectional area is 0.05 x 0.5 mm and the length is 2.4 mm, giving a volume of about 60 nL; and the total sensor chip area in each flow cell is 1.2 mm^2. The surface plasmon resonance protocol for measuring protein adsorption entailed first cleaning the surface by flowing a 40 mM sodium dodecyl sulfate (+99% Sigma) in phosphate buffered

saline solution over the surface for 3 min, followed by flushing with phosphate buffered saline (pH 7.4) for 10 min. Next, protein solution (1 mg mL^{-1} in phosphate buffered saline, pH 7.4) was passed over the surface for 30 min. Finally, phosphate buffered saline was purged through the system for 10 min in order to remove loosely bound protein. Throughout, the flow rate was kept constant at 10 µL min^{-1} and identical baselines re-established before each SPR measurement. This was repeated twice using fibronectin (Sigma) and twice using albumin (Sigma). Results are quoted for a minimum of three plasma polymer samples.

MCF7 cells were purchased from ATCC (Manassas, VA). The cells were routinely maintained in Dulbecco's modified eagle's medium (BioWhittaker, Walkersville, MD) supplemented with 10 % foetal bovine serum (Gibco, Grand Island, NY), 2 mM glutamine, penicillin (100 Units/mL), and streptomycin (100 mg/mL) in a humidified chamber at 37 °C in 5% CO_2/95% O_2. Cells were grown in T-25 flasks (Gibco) to confluence. Cells were trypsinized, washed with phosphate buffered saline (pH 7.4) and re-suspended in Dulbecco's modified eagle's medium. Plasma polymers were deposited onto 1 cm diameter circular glass discs (Agar Scientific) and autoclaved at 110 °C. Samples were then seeded with 500 cells at a concentration of 1000 cells/ml. Samples were cultured in 24 well plates in a humidified chamber at 37 °C in 5% CO_2/95% O_2. At the required time the samples were removed, washed with phosphate buffered saline (pH 7.4), stained with Hemoxyclin (Aldrich) for 1 minute and washed with high purity water (BS 3978 Grade 1). Samples were mounted onto glass microscope slides, covered with glass cover slips and cell counts were performed using an inverted optical microscope.

3.2.3. Results

A variety of different compounds were created using plasma deposition to compare previously analysed properties such as oxygen, nitrogen and halogen content as well as hydrophilic and hydrophobic surfaces. All the species are shown in Table 5.

Table 5: Table of the species polymerized to create cell adhesive surfaces

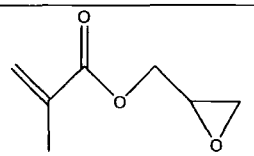 Glycidyl methacrylate	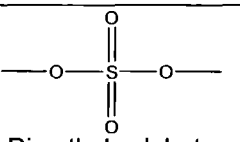 Dimethyl sulphate	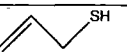 Allyl mecaptan
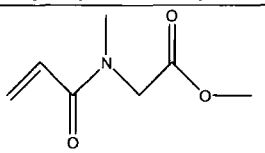 N-acryloylsarcosine methyl ester	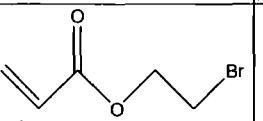 2-bromoethyl acrylate	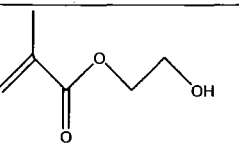 2-hydroxyethyl methacrylate
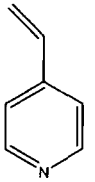 4-vinyl pyridine	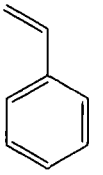 Styrene	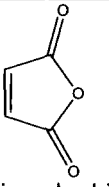 Maleic anhydride
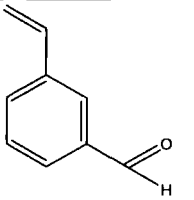 3-vinylbenzaldehyde	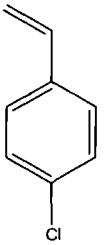 4-vinylbenzyl chloride	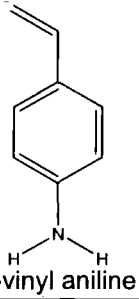 4-vinyl aniline
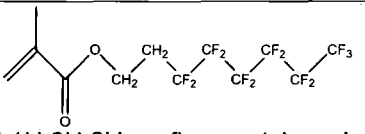 1H,1H,2H,2H-perfluorooctyl acrylate	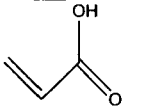 acrylic acid	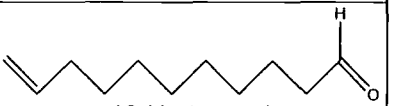 10-Undecenal

Each polymer was created using a range of plasma conditions as shown in Table 6 for pulsed plasma deposition and Table 7 for continuous wave plasma deposition. Both tables also show the resulting contact angle and the thickness of polymer created. Conditions are as referenced in earlier work, using standard conditions known to ensure structural retention whilst maintaining insolubility.

Table 6: Pulsed plasma polymer conditions and resulting thickness and contact angle

Monomer	Label	Time on (μs)	Time off (ms)	Peak Power (W)	Duration (min)	Thickness (nm)	Contact Angle (deg)	Contact Angle - Autoclaved (deg)	Ref.
4-vinyl pyridine (4-VP)	A	100	4	40	30	240	Wets (5 ± 1)	Wets (5 ± 1)	[215]
Dimethyl sulphate (DMS)	C	40	30	40	30	156	13 ± 1	13 ± 1	[216]
Maleic anhydride (MA)	F	20	1.2	4	30	80	47 ± 1	48 ± 1	[217]
N-acryloylsarcosine methyl ester (NASME)	G	20	5	30	3	34	47 ± 2	49 ± 1	[218]
Allyl mecaptan (AM)	K	100	4	40	10	85	80 ± 1	65 ± 1	[219]
Glycidyl methacrylate (GMA)	L	20	20	40	20	350	65 ± 1	73 ± 1	[208]
4-vinyl aniline (4-VA)	M	100	4	40	30	889	87 ± 2	78 ± 2	
10-Undecenal (UA)	N	15	20	40	180	210	86 ± 2	81 ± 1	
2-bromoethyl acrylate (BEA)	O	30	10	20	10	690	70 ± 1	83 ± 1	[220]
4-vinylbenzyl chloride (VBC)	P	100	4	40	5	440	81 ± 1	83 ± 1	[220]
3-vinylbenzaldehyde (3-VBAL)	Q	50	4	40	3	70	73 ± 1	84 ± 1	[221]
Styrene (PS)	R	100	4	40	45	300	80 ± 1	95 ± 1	
1H,1H,2H,2H-perfluorooctyl acrylate (PFAC-6)	S	20	20	40	10	150	135 ± 1	138 ± 2	[222]

Table 7: Continuous wave plasma polymer conditions and resulting thickness and contact angle

Monomer	Label	Peak Power (W)	Duration (min)	Thickness (nm)	Contact Angle (deg)	Contact Angle - Autoclaved (deg)	Ref.
CW Dimethyl sulphate (CW DMS)	B	3.0	20	100	14 ± 1	13 ± 1	[216]
CW acrylic acid (CW AA)	D	3.0	10	241	Wets (5 ± 1)	Wets (5 ± 1)	[210]
CW 4-vinyl pyridine (CW 4-VP)	E	3.0	3	198	38 ± 1	30 ± 2	[215]
CW 2-hydroxyethyl methacrylate (CW HEMA)	I	3.0	10	137	59 ± 1	63 ± 1	[223]

Structural retention was monitored by XPS (Table 8 and Table 9) and IR spectroscopy. As previously noted the longer the off-time and shorter the on-time the greater the structural retention. Longer on-times are used to guarantee insolubility.

Table 8: Elemental composition of continuous wave plasma samples measured by XPS

Monomer		% C (±1.0%)	% O (±1.0%)	% N (±1.0%)	% S (±1.0%)	% Halogen (±1.0%)
Acrylic Acid	Theoretical	60.0	40.0	0	0	0
	Experimental	66.8	33.2	-	-	-
	Autoclaved	71.6	28.4	-	-	-
2-hydroxyethyl methacrylate	Theoretical	66.7	33.3	0	0	0
	Experimental	72.5	27.5	-	-	-
	Autoclaved	73.4	26.6	-	-	-
Dimethyl sulphate	Theoretical	28.6	57.1	0	14.3	0
	Experimental	38.8	37.6	-	23.6	-
	Autoclaved	39.4	36.3	-	24.2	-
4-vinyl pyridine	Theoretical	87.5	0	12.5	0	0
	Experimental	86.5	2.2	11.3	-	-
	Autoclaved	74.6	15.2	10.2	-	-

Table 9: Elemental composition of pulse plasma samples measured by XPS

Monomer		% C (±1.0%)	% O (±1.0%)	% N (±1.0%)	% S (±1.0%)	% Halogen (±1.0%)
4-vinyl pyridine	Theoretical	87.5	0	12.5	0	0
	Experimental	86.0	1.5	12.5	-	-
	Autoclaved	79.1	8.2	12.6	-	-
Dimethyl sulphate	Theoretical	28.6	57.1	0	14.3	0
	Experimental	18.7	72.5	-	8.8	-
	Autoclaved	20.4	69.8	-	9.8	-
N-acryloylsarcosine methyl ester	Theoretical	63.6	27.3	9.1	0	0
	Experimental	64.2	26.5	9.3	-	-
	Autoclaved	62.7	29.1	8.2	-	-
Maleic anhydride	Theoretical	57.1	42.9	0	0	0
	Experimental	63.6	36.4	-	-	-
	Autoclaved	65.3	34.7	-	-	-
Glycidyl methacrylate	Theoretical	70.0	30.0	0	0	0
	Experimental	66.6	33.4	-	-	-
	Autoclaved	72.4	27.6	-	-	-
2-bromoethyl acrylate	Theoretical	62.5	25.0	0	0	12.5
	Experimental	63.9	24.1	-	-	12.0
	Autoclaved	63.5	25.2	-	-	11.3
3-Vinylbenzaldehyde	Theoretical	88.9	11.1	0	0	0
	Experimental	89.9	10.1	-	-	-
	Autoclaved	85.4	14.6	-	-	-
Allyl mecaptan	Theoretical	75.0	0	0	25.0	0
	Experimental	70.4	-	-	29.6	-
	Autoclaved	68.3	10.5	-	21.2	-
Styrene	Experimental	95.4	4.6	-	-	-
	Theoretical	100.0	0	0	0	0
	Autoclaved	93.5	6.5	-	-	-
4-vinylbenzyl chloride	Theoretical	88.9	0	0	0	10.9
	Experimental	96.4	-	-	-	3.6
	Autoclaved	92.8	4.0	-	-	3.1
10-Undecenal	Theoretical	91.7	8.3	0	0	0
	Experimental	92.5	7.5	-	-	-
	Autoclaved	86.1	13.9	-	-	-
4-vinyl aniline	Theoretical	88.9	0	11.1	0	0
	Experimental	85.3	6.5	8.2	-	-
	Autoclaved	82.1	10.0	7.9	-	-
1H,1H,2H,2H-perfluorooctyl acrylate	Theoretical	42.3	7.7	0	0	50
	Experimental	50.5	3.5	-	-	45.9
	Autoclaved	40.1	5.2	-	-	54.7

Infrared spectra are shown; Figure 48, Figure 49 and Figure 50, for polymers not previously published by this laboratory. Each graph is stacked from bottom to top with the IR of the monomer, plasma polymer (either pulsed or continuous wave) and the autoclaved polymer. The autoclaved polymer as expected shows a large absorption from O-H at 3200 cm^{-1}.

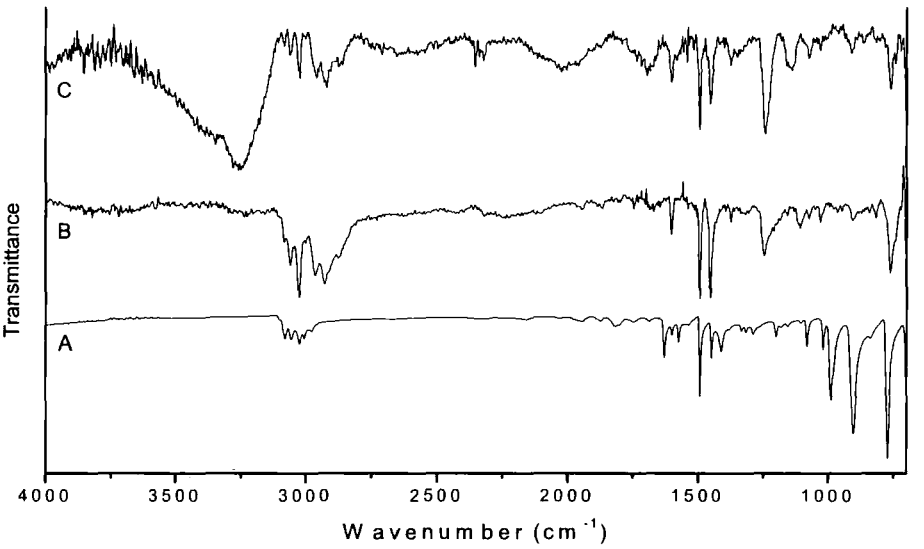

Figure 48: Infrared spectra of styrene: monomer (bottom, A), pulsed plasma polymer (middle, B), autoclaved pulsed plasma polymer (top, C)

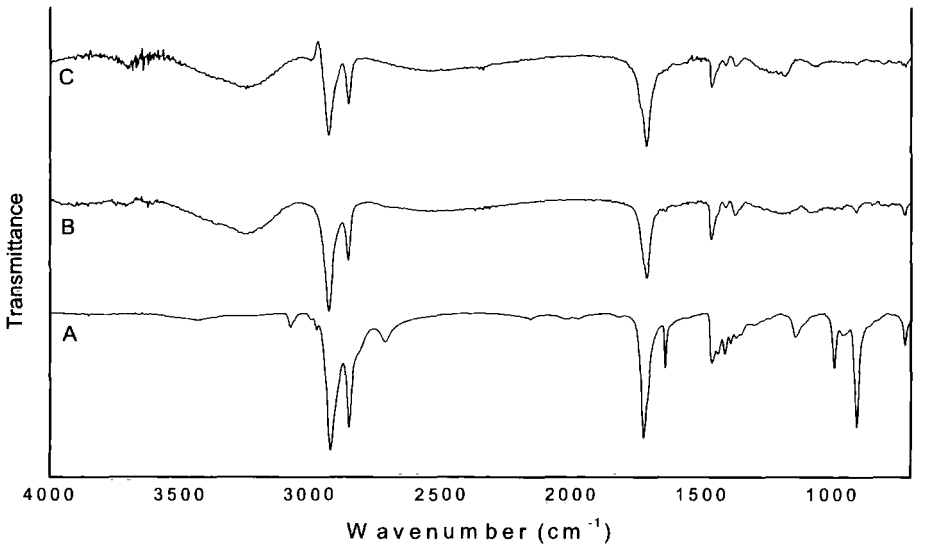

Figure 49: Infrared spectra of 10-Undecenal: monomer (bottom, A), pulsed plasma polymer (middle, B), autoclaved pulsed plasma polymer (top, C)

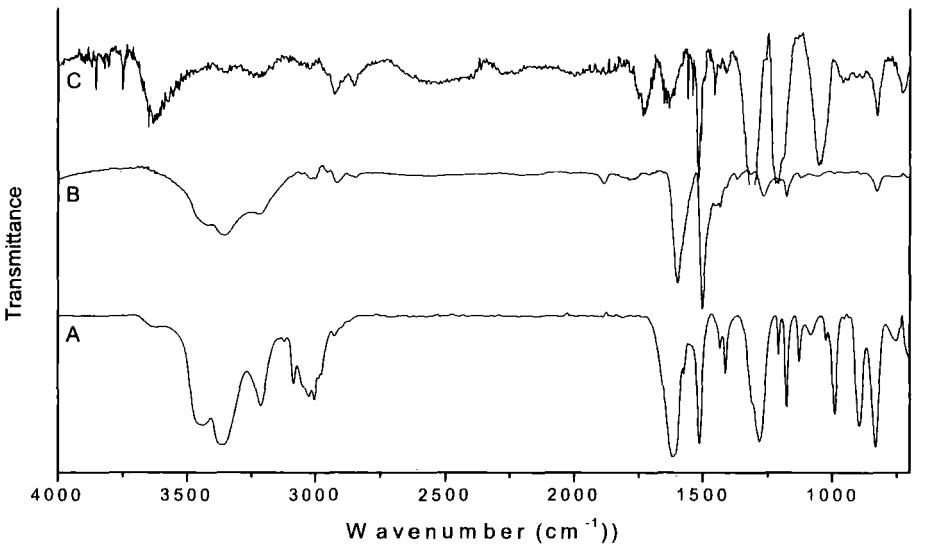

Figure 50: Infrared spectra of 4-vinyl aniline: monomer (bottom), pulsed plasma polymer (middle), autoclaved pulsed plasma polymer (top)

There are three broad types of protein adhering polymers that correlate strongly to their hydrophilicity. At moderate hydrophilicity, around 30 - 50° contact angle, there appears to be little or no protein absorption. At lower and higher hydrophilicity there

are polymers that show high attachment of loosely bound protein. The correlation between loosely bound protein adhesion and hydrophilicity seems apparent for both albumin, Figure 51 and fibronectin, Figure 52. Only the continuous wave plasma polymer of 2-hydroxyethylmethacrylate shows lower levels of protein absorption than the contact angle might suggest.

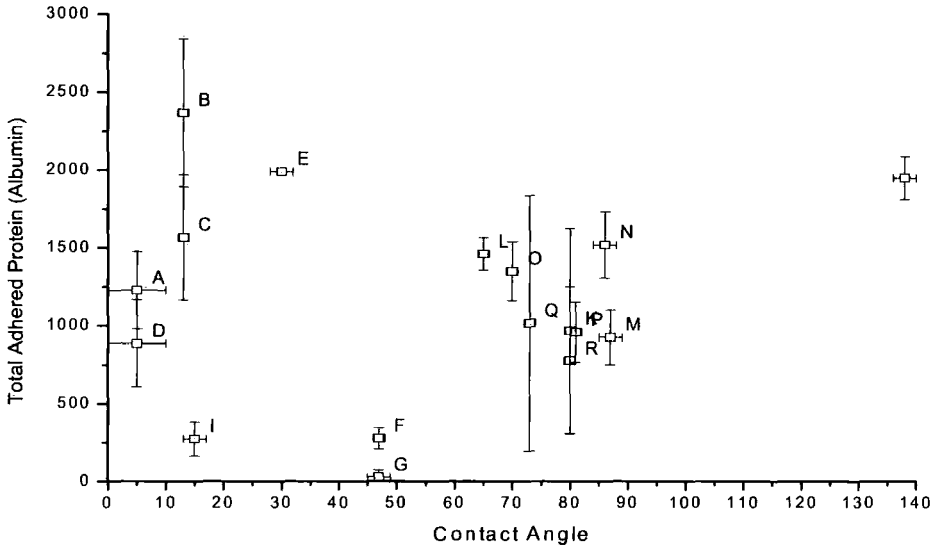

Figure 51: Total adhered albumin versus contact angle for a range of plasma polymer surfaces. Label's refer to Table 6 and Table 7

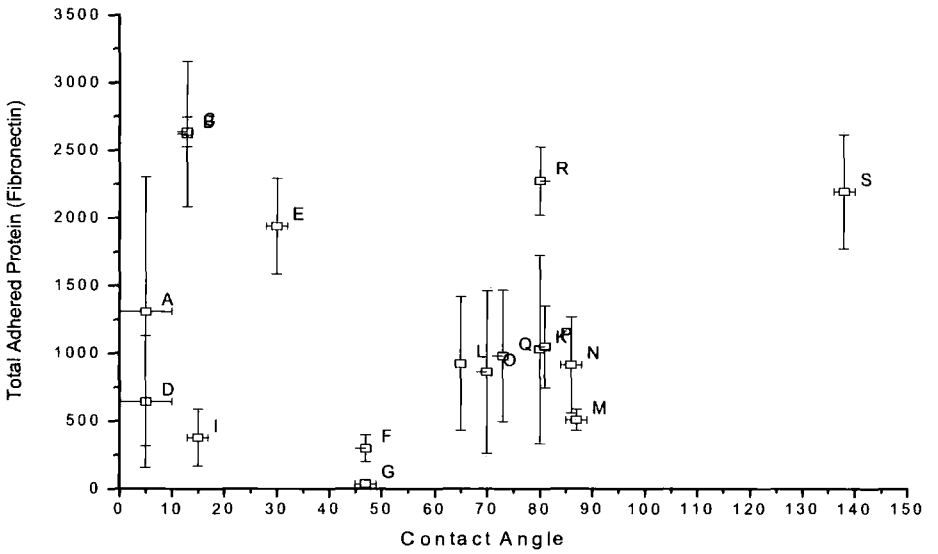

Figure 52: Total adhered fibronectin versus contact angle for a range of plasma polymer surfaces. Label's refer to Table 6 and Table 7

The process of testing for protein absorption requires continually washing with aqueous solutions and 2-hydroxyethylmethacrylate is well known as a difficult compound to polymerise, often with solubility issues causing problems, especially with thin films. The amount of protein that is more strongly bound drops substantially more for albumin, Figure 53 than fibronectin, Figure 54, at lower contact angles. Albumin is known to inhibit cell adhesion with fibronectin aiding cell adhesion and this correlates with the cell adhesion results at low contact angles.

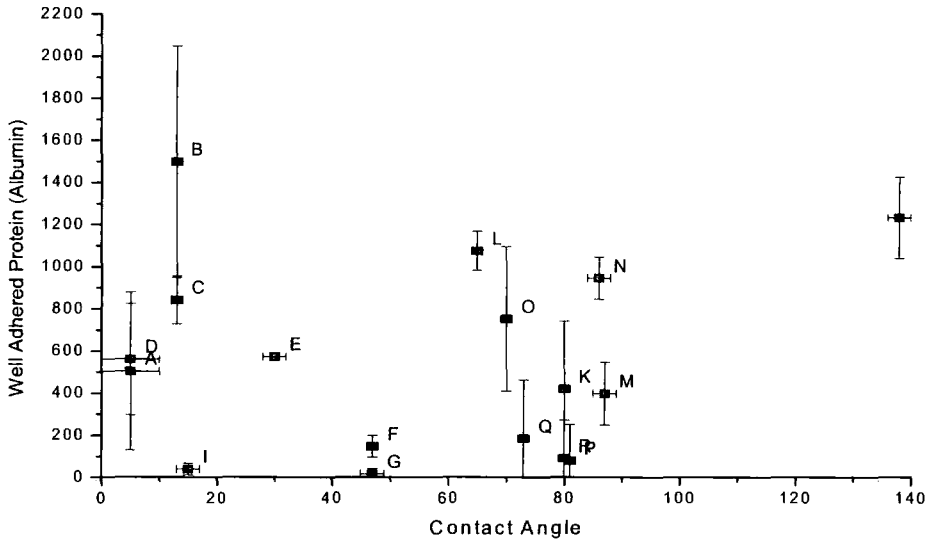

Figure 53: Well adhered albumin versus contact angle for a range of plasma polymer surfaces. Label's refer to Table 6 and Table 7

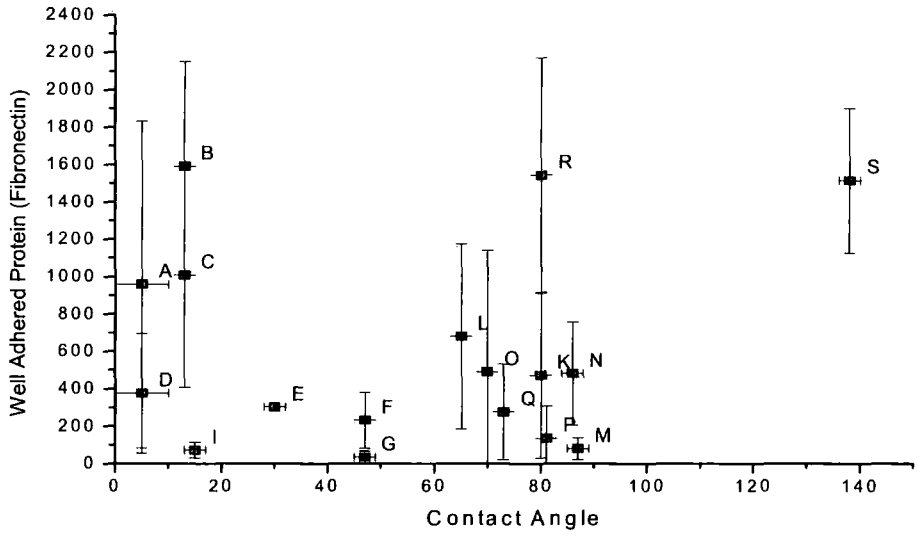

Figure 54: Well adhered fibronectin versus contact angle for a range of plasma polymer surfaces. Label's refer to Table 6 and Table 7

A plot of the cell growth versus protein absorption shows the good cell adhering surfaces have low absorption of well adhered albumin, Figure 55, but high levels of loosely bound fibronectin, Figure 56. High absorption of albumin generally prevents

good cell adhesion unless coupled with high levels of fibronectin adhesion. As in previous studies the conformation of the protein appears to be more important than the rate of protein absorption.

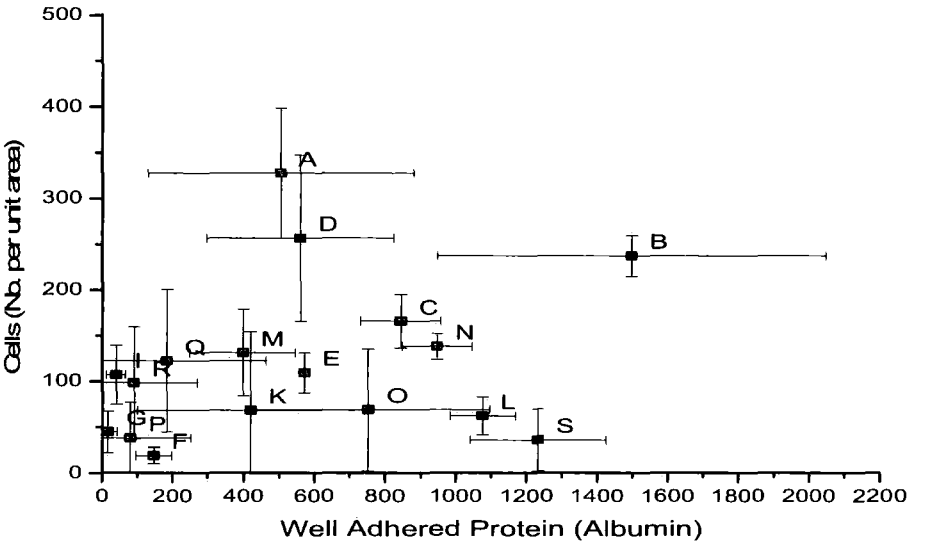

Figure 55: Cell adhesion versus well adhered albumin for a range of plasma polymer surfaces

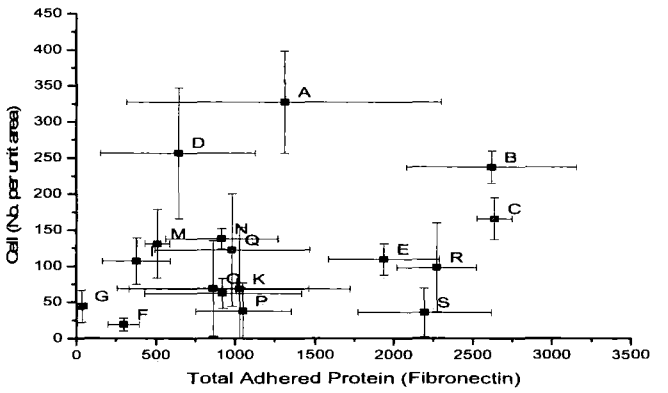

Figure 56: Cell adhesion versus total absorbed fibronectin for a range of plamsa polymer surfaces

The absorption of protein does not appear to be affected by the concentration of oxygen in the surface layer. This is confirmed by the analysis of both loosely and well adhered albumin, Figure 57 and Figure 58 respectively.

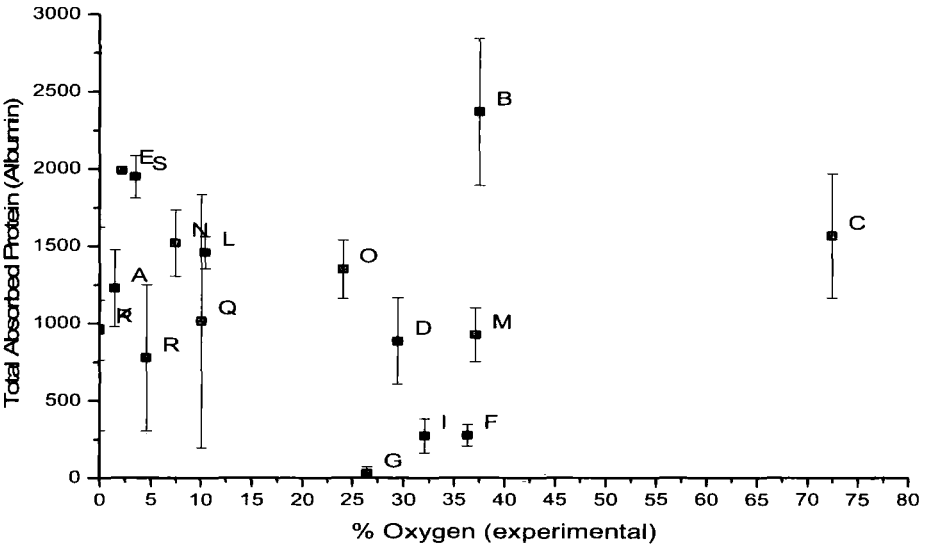

Figure 57: Level of albumin loosely adhered relative to the experimentally observed level of surface oxygen in a range of plasma polymers. Labels refer to Table 6 and Table 7

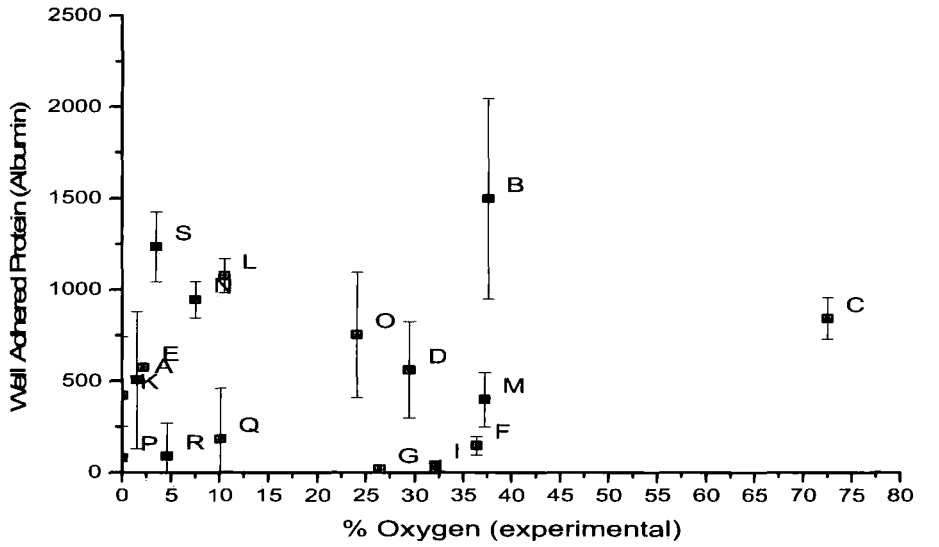

Figure 58: Level of albumin well adhered relative to the experimentally observed concentration of oxygen in the surface of a range of plasma polymer surfaces. Labels refer to Table 6 and Table 7

The amount of fibronectin absorbed on to the plasma polymer surface does show some tendency to be inverse to the amount of oxygen in the surface layer. Minimal

amounts of oxygen appear to encourage adhesion, Figure 59. This is confirmed by the analysis of the well adhered protein, Figure 60. This suggests that polymers with low levels of surface oxygen should encourage cell adhesion as fibronectin is well known as an important factor in the attachment process. However dimethyl sulphate polymerised by pulsed and continuous wave plasma shows excellent protein adhesion with very high levels of surface oxygen.

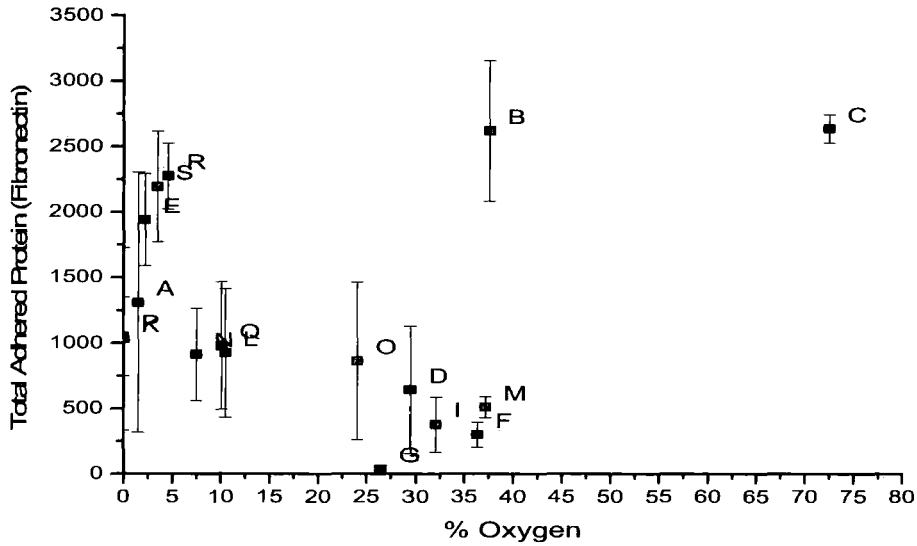

Figure 59: Level of fibronectin loosely adhered relative to the experimentally observed level of surface oxygen in a range of plasma polymers. Labels refer to Table 6 and Table 7

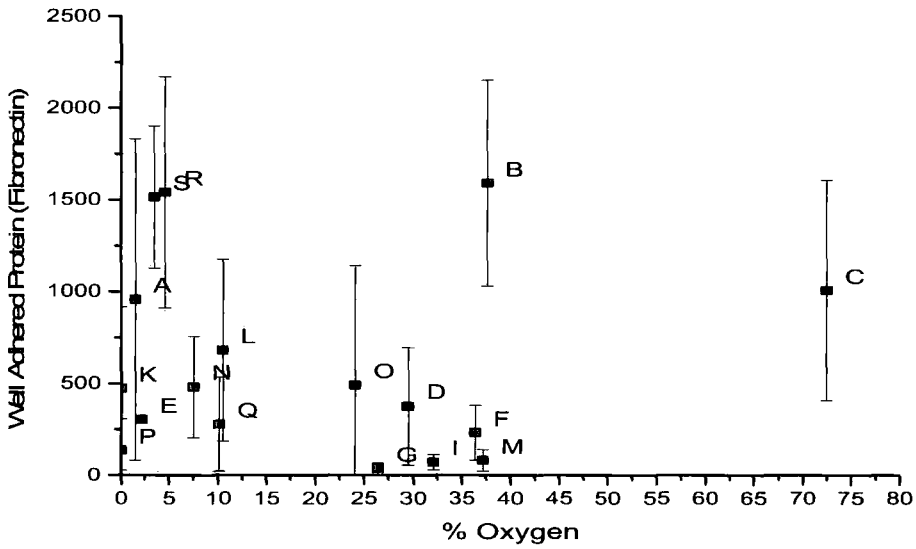

Figure 60: Level of fibronectin well adhered relative to the experimentally observed concentration of oxygen in the surface of a range of plasma polymer surfaces. Labels refer to Table 6 and Table 7

Figure 61 shows the number of cells per unit area (field of view on microscope) after 24 hours for a range of plasma polymers plotted as a function of the contact angle. Error bars are the standard deviation from at least three samples.

Figure 62 shows the pattern of cell adhesion and growth after 24 hours when 4-vinyl pyridine is pulse plasma deposited onto a protein resistance background of pulse plasma polymerized N-acryloylsarcosine methyl ester. The pattern was produced by depositing through a grid. The grid dimensions are 100 μm diameter but the pattern of 4-vinyl pyridine is obviously larger than this due to creep during deposition.

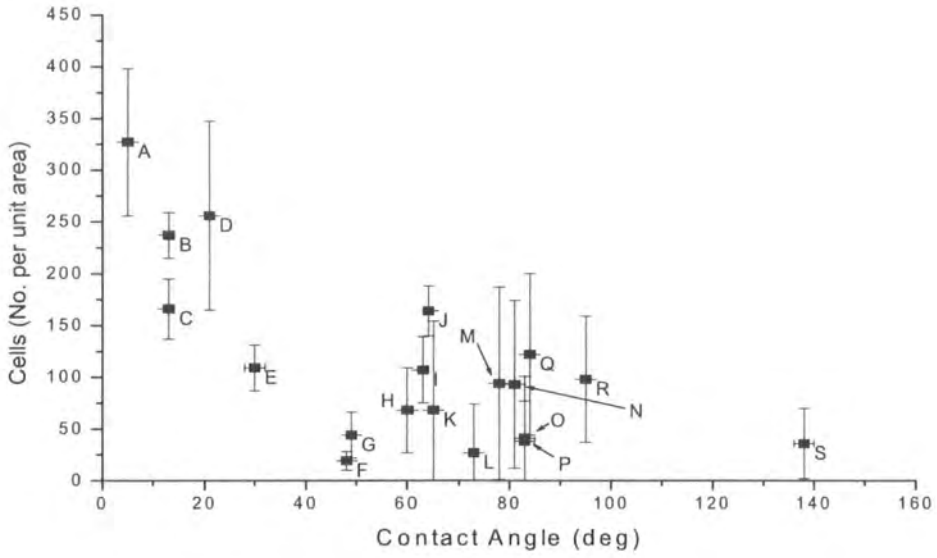

Figure 61: Cell growth versus Contact Angle for a range of hydrophilic plasma polymers 24 hours after seeding.

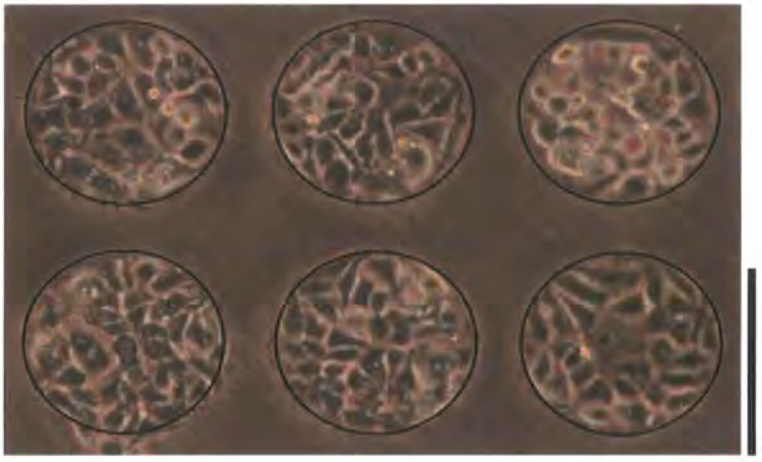

Figure 62: MCF7 cell growth after 24 hours on a pattern of 4-vinyl pyridine pulse plasma polymer spots on a background of N-acryloylsarcosine methyl ester pulse plasma polymer

The pattern was created by depositing the 4-vinyl pyridine through a grid held in close contact with the substrate, the grid dimensions were: diameter 100µm, centre to centre 200 µm. The black circles are 145 µm in diameter showing that the pattern transfer has not been perfect. The scale bar is 200 µm

Figure 63 shows how eventually the cells cross over areas of protein resistance but this image does not prove that they are adhered to the substrate. The cells are merging across the shortest gap, Figure 64 shows how the cells are seeing each

other, using protrusions that they send out over the protein resistant background looking for areas to proliferate into. When they meet other cells also looking to expand the colonies grow out towards each other.

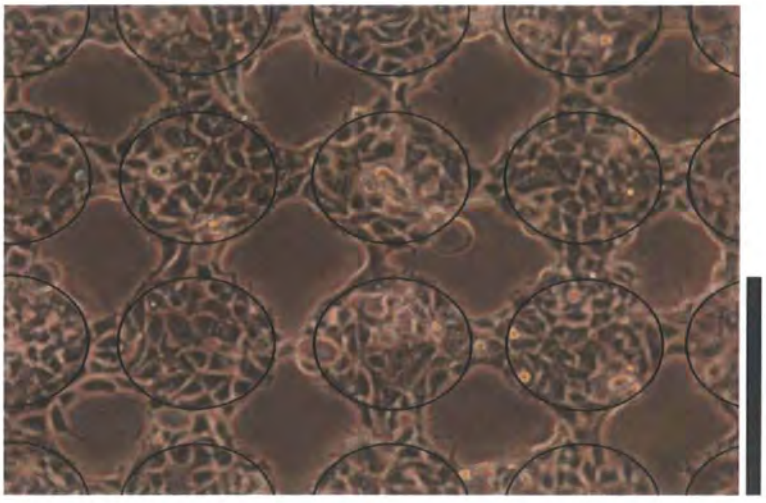

Figure 63: MCF7 cell growth after 48 hours on a pattern of 4-vinyl pyridine pulse plasma polymer spots on a background of N-acryloylsarcosine methyl ester pulse plasma polymer

The scale bar is 200 µm and the circles are 145 µm in diameter.

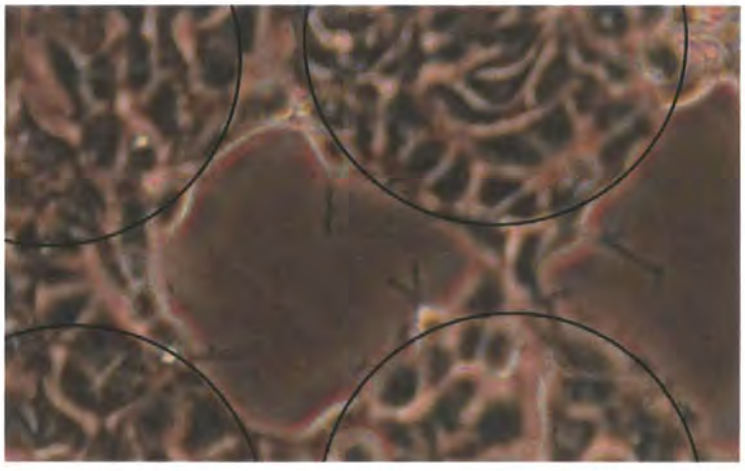

Figure 64: Close up image showing the protrusions extending onto the protein resistant background

3.2.4. Discussion

There are three distinct regions of wettability that control adhesion of cells to substrates. The boundaries of which will vary slightly with potentially some overlap between the three regions:

- Super-hydrophilicity. Below 30° the surface is highly cell adhesive, with the highest cell adhesion occurring below 10°.
- Mid-range wettability or protein resistance. This region occurs between 30 - 50° and occurs when the packing of the water molecules reaches a critical point to prevent protein adhesion.
- Mild-wettability. Above 50° there appears to be a general cell adhesive bulk of polymers, with a peak adhesion around 60° depending on the levels of various nitrogen and oxygen (usually carbonyl) functionality.

A number of the polymers tested in this work have been studied by other groups. 1-vinyl 2-pyrrolidone is an example which has been pulse plasma deposited by Han and Timmons[224] but their lack of any subsequent study on its cell adhesion suggests, as we found, that the pulse plasma polymer was not stable under aqueous media. The continuous wave polymer has been covered quite extensively by various groups[225] but is not super-wettable, having a quoted contact angle between 33° and 50°. The lower contact surfaces did however show good cell adhesion compared to other less hydrophilic surfaces.

The use of thermo-responsive protein resistant surfaces indicates the change between polymers with mid-range wettability and mild wettability. Poly(N-isopropylacrylamide) is protein resistant at 20 °C when the contact angle is around 45-55°.[192] When raised to body temperature (37 °C) it passes a lower critical solution temperature of 31-32 °C and becomes protein adhesive with a contact angle of approximately 90°. The protein adhesive nature allows cell adhesion whilst the protein resistance at lower temperatures inhibits cell adhesion.[226] These results stem from a change in physical conformation of the surface from hydrogen-bond forming secondary amides and carbonyls to hydrophobic propyl groups. When proteins exist in aqueous solution their outmost surface is covered in hydrophilic

groups surrounded by a layer of water molecules in a structured and well packed manner.[227] A similar layer of water molecules will exist at the surface of a hydrophilic substance.[228,229] These two boundary layers create a steric repulsion when the two entities try to interact due to substrate/protein attraction, however additional factors must come into effect at very low contact angles. At low-mid wettability the packing of water molecules on the surface is known to mimic the density of bulk water,[230] below about 15° the density and packing of molecules increases and a layer of water around 3 Å thick forms.[231] Studies done on Self-assembled monolayers also show high protein absorption for low contact angle surfaces such as COOH terminated structures.[174]

As surfaces become increasingly more hydrophobic the general trend is to absorb more protein but factors such as hydrogen bonding and dipole moments of functional groups at the surface cause anomalies to this general rule.[172] Polystyrene and poly(1H,1H,2H,2H-perfluorooctyl acrylate) are examples of hydrophobic surfaces with strong absorption of fibronectin but polystyrene shows low levels of absorption of albumin. The hydrogen bonding abilities of poly(glycidyl methacrylate), poly(10-undecenal), poly(2-bromoethyl acrylate) may explain their ability to absorb large amounts of albumin but also the strength of adhesion to fibronectin. The lower electronegativity of sulfur and nitrogen compared to oxygen and the lack of hydrogen bonding ability of poly(allyl mecaptan), poly(4-vinylbenzyl chloride) and poly(4-vinyl aniline), coupled with moderate hydrophobicity account for their low levels of protein adsorption. The dipole moment of molecules like poly(4-vinyl pyridine) and poly(acrylic acid) should help explain their high protein absorptions.

3.3. Stem cell attachment and proliferation on 4-vinyl pyridine

3.3.1. Introduction

Cell adhesion is of interest for many applications including wound dressings, implants and biological arrays. A variety of cell types have been studied and

different theories presented as to why cells adhere to surfaces. A number of surface functionalities have been suggested as important including wettability, protein adhesion and surface functionality. In the previous chapter MCF7 breast cancer cells were studied and the cell adhesion measured across a range of plasma polymers and contrasting functionalities. Cell adhesion varied according to the wettability with three distinct characteristic zones:

- Super-hydrophilicity. Below 30° the surface is highly cell adhesive, with the highest cell adhesion occurring below 10°.
- Mid-range wettability or protein resistance. This region occurs between 30 - 50° and occurs when the packing of the water molecules reaches a critical point to prevent protein adhesion.
- Mild-wettability. Above 50° there appears to be a general cell adhesive bulk of polymers, with a peak adhesion around 60° depending on the levels of various nitrogen and oxygen (usually carbonyl) functionality.

Many previous studies have concluded from a series of tests on a certain cell line with assumptions that findings for a particular cell type can be applied across other types of cell. We have taken the best performing plasma polymer from the previous chapter on MCF7 adhesion, created from the monomer 4-vinyl pyridine, and compared its performance against two industry standards, polystyrene and tissue-culture polystyrene.

We tested these three surfaces using a human embryonic carcinoma (EC) stem cell (named TERA2.SP12). Stem cells are a particular type of cell; they have no defined function and are known as uncommitted cells. They can be encouraged to differentiate into different types of cell such as neurons and glial cells in response to retinoic acid. TERA2.SP12 cells were chosen for this study as they show a characteristic behavior on each of the two standard materials. TERA2.SP12 adheres and grows well on tissue-culture polystyrene but on polystyrene it fails to adhere and forms large disorganized aggregates in the solution.[232]

3.3.2. Experimental

Stem cell adhesion samples were prepared as follows: Square of tissue culture polystyrene and polystyrene petri dishes (90 mm diameter, VWR international) were hand cut into 50 mm by 50 mm squares and kept in a sterile environment at all times. Squares of polystyrene were used as the substrate for the plasma polymer to ensure a negative background. Plasma deposition of 4-vinyl pyridine was performed as described previously (1.9.1). Plasma polymer samples were stored in sealed sterile polystyrene petri dishes and prior to treatment with stem cells were washed in ethanol. Cell adhesion samples were each fixed into the base of a polystyrene petri dish using sterile silicon high-vacuum grease (Rhodia Siliconi).

TERA2.SP12 stem cells were grown and maintained in Dulbecco's modified eagle's medium (DMEM, Life technologies) supplemented with 10% foetal bovine serum and 2 mM L-glutamine at 37 °C in 5% CO_2. When confluence was reached, cells were harvested using 2 ml 0.25% trypsin in Dulbecco's phosphate-buffered saline (PBS) for 2 min at 37 °C in 5% CO_2. 8 ml of medium was added and aliquots of $1x10^6$ cells were pelleted in a centrifuge (800 rpm for 2 min). Pellets of cells were re-suspended in 20 ml medium and seeded in each petri dish. Optical images were taken immediately after seeding and every 24 hours for four days.

A 1 cm^2 polystyrene sample was coated with the plasma polymer of N-acryloylsarcosine methyl ester using conditions described previously. The sample was embossed with a 400 mesh grid using a force of 40 kN; this was followed by plasma polymerization of 4-vinyl pyridine prior to removal of the grid. The sample was then seeded with Stem cells as above and grown to confluence on the super-hydrophilic polymer squares.

Small 1 cm^2 test samples of tissue culture polystyrene, polystyrene and plasma polymer coated polystyrene petri dish were tested using a video contact angle machine, XPS machine and IR spectrometer as detailed previously(1.9).

3.3.3. Results

Tissue culture polystyrene is widely used for culturing cells due to its relatively hydrophilic nature and suitability for culturing stem cells. Conversely polystyrene is known for being poorly adhesive for stem cells. The hypothesis that super-hydrophilicity is important for cell adhesion was discussed in the previous chapter and has been further explored here. Polystyrene is hydrophobic, Tissue culture polystyrene moderately hydrophilic and 4-vinyl pyridine is super-hydrophilic, Table 10.

Table 10: Contact angles of polymers.

Monomer	Contact Angle (degrees)
4-vinyl pyridine	Wets
N-acryloylsarcosine methyl ester	47 ± 2
Polystyrene	100 ± 2
Tissue Culture Polystyrene	56 ± 1

XPS and IR Spectroscopy were used to confirm the consistency of the polymers used in this study. The elemental composition of the polymers shows the consistency of the polymers used, Table 11. Figure 65 shows IR spectra of the samples tested and highlights that IR spectroscopy studies more of the bulk properties of the polymers so the thin layer of 4-vinyl pyridine is only evident by the strength of absorbance at 1700 cm^{-1}.

Table 11: Elemental composition of pulse plasma samples measured by XPS

Monomer		% C (±1.0%)	% O (±1.0%)	% N (±1.0%)
4-vinyl pyridine	Theoretical	87.5	0	12.5
	Experimental	80.9	5.6	13.5
N-acryloylsarcosine methyl ester	Theoretical	63.6	27.3	9.1
	Experimental	62.7	29.1	8.2
Polystyrene	Theoretical	100	0	0
	Experimental	98.9	1.1	-
Tissue Culture Polystyrene	Theoretical	-	-	-
	Experimental	86.1	13.9	-

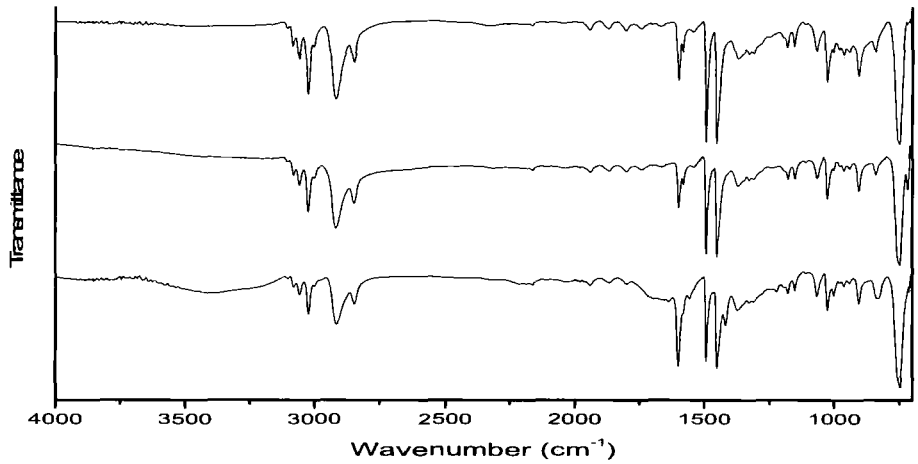

Figure 65: Infrared spectra of polymer surfaces tested for stem cell adhesion: 4-vinyl pyridine on polystyrene (bottom), polystyrene (middle), tissue culture polystyrene (top)

Cells were seeded at the same concentration but on polystyrene, the cells do not adhere to the surface of the polymer. Instead, they form aggregations of cells in the solution, floating above the surface. Occasionally these tether to imperfections in the surface. Figure 66 shows optical images from seeding every day for three days. At no stage is attachment evident with large clumps of cells floating above the surface, however with the more hydrophilic tissue-culture polystyrene, shown in the optical images in Figure 67, stem cells grow on tissue-culture polystyrene after the first day. Attachment is clearly evident and after 4 days confluence is virtually

reached. Plasma polymerization was used to deposit a thin surface coating of polymer from a 4-vinyl pyridine monomer onto a polystyrene chip. Optical images were again taken at seeding and after each day, Figure 68. Attachment is clearly evident and is proceeding at a quicker rate than the tissue culture polystyrene sample. Confluence is almost reached after three days and has been reached by 4 full days.

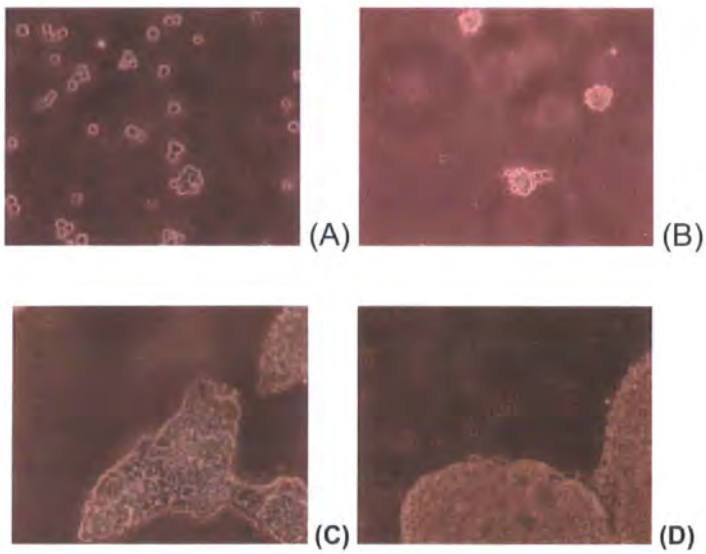

Figure 66: Stem cell growth on styrene: A 0 hrs, B 24 hrs, C 48 hrs, D, 72 hrs

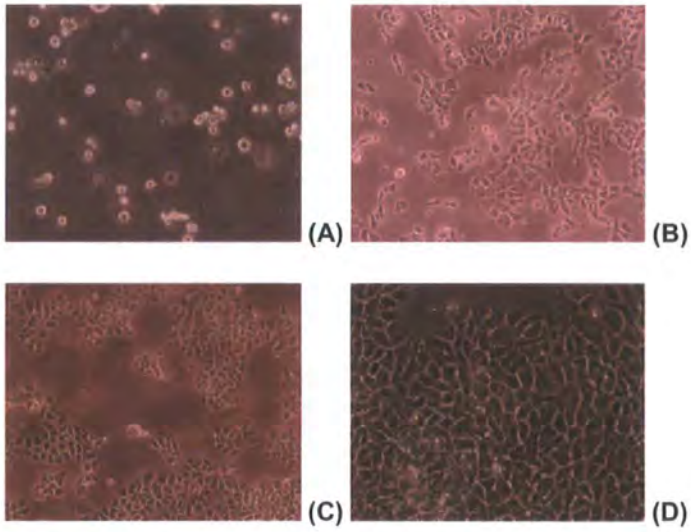

Figure 67: Stem cell growth on tissue culture polystyrene: A 0 hrs, B 24 hrs, C 48 hrs, D, 72 hrs

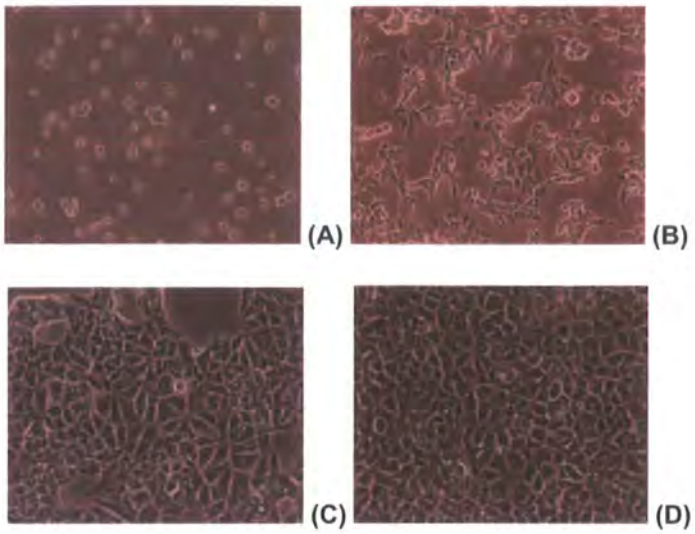

Figure 68: Stem cell growth on 4-vinyl pyridine: A 0 hrs, B 24 hrs, C 48 hrs, D, 72 hrs

Figure 69 shows the IR spectra of a layer of 4-vinyl pyridine on gold relative to a background of pure gold. Here the finer details of the structure can be seen in the spectra. N-acryloylsarcosine methyl ester was used as a protein resistant and low cell-growth polymer to pattern the surface as a non-adhesive plasma polymer, Figure 70.

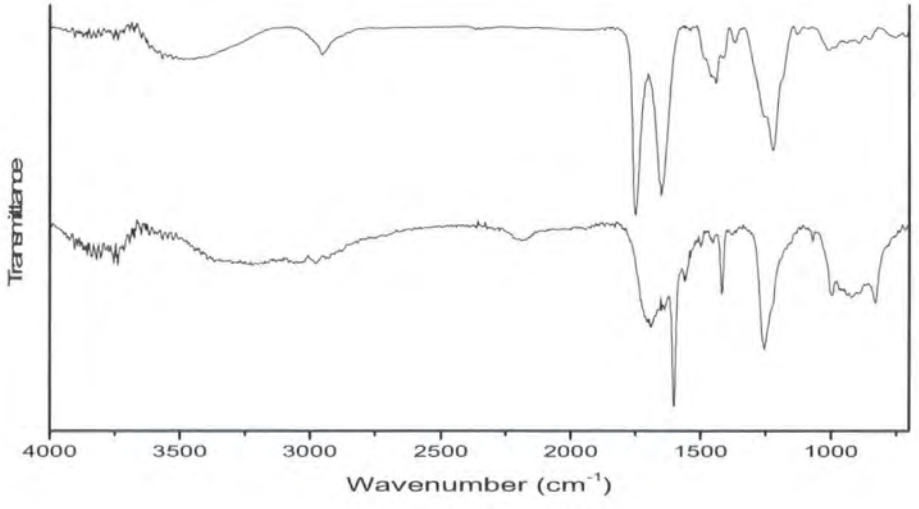

Figure 69: Infrared spectra of 4-vinyl pyridine (bottom) and N-acryloylsarcosine methyl ester (top) on gold

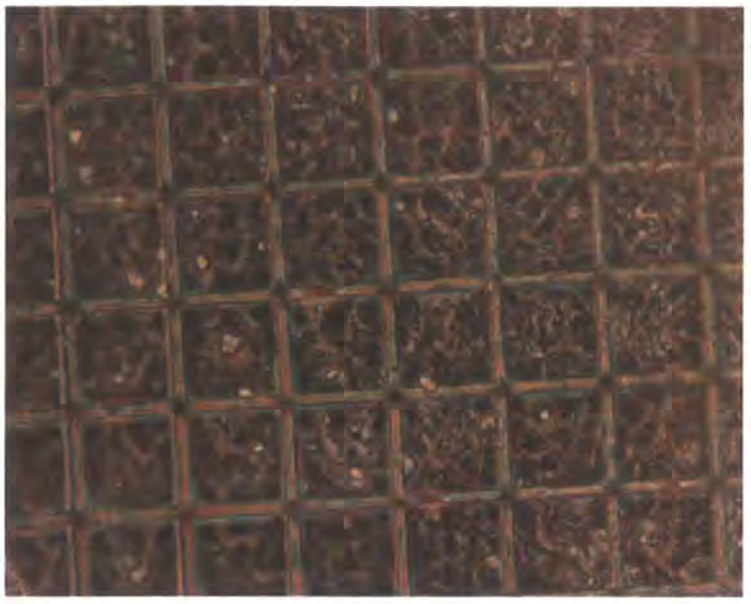

Figure 70: Stem cell pattern on 4-vinyl pyridine squares on a background of N-acryloylsarcosine methyl ester using an embossed polystyrene substrate

3.3.4. Discussion

As discussed in the previous chapter, hydrophilicity has been widely explored as an important factor in cell adhesion. The conclusions of the previous chapter were that it was the most important factor examined and that surfaces with greater hydrophilicity would encourage greater adhesion and growth. The previous work was limited to one cell type, a simple breast cancer cell; in this chapter a different cell type was examined. Stem cells have a very contrasting response to polystyrene and tissue-culture polystyrene with the more hydrophobic polystyrene preventing cell adhesion and growth. The hydrophilic tissue-culture polystyrene adheres stem cells very well and they grow at a reasonable rate. However when compared to the super-hydrophilic polymer of 4-vinyl pyridine the rate of adhesion is significantly slower on tissue-culture polystyrene.

Also created was a micro-patterned sample with squares of 4-vinyl pyridine on a background of N-acryloylsarcosine methyl ester. N-acryloylsarcosine methyl ester has been reported as protein resistant and as shown in the previous chapter this prevents cell adhesion. An optical image of this sample was taken after 3 days, Figure 70 and shows that the cells are adhering to the squares of the super-

hydrophilic polymer but not to the protein resistant N-acryloylsarcosine methyl ester.

Stem cells are regularly grown on both polystyrene and tissue-culture polystyrene. The hydrophobic polystyrene prevents good adhesion and aggregation occurs in suspension. On the hydrophilic tissue-culture polystyrene the cells adhere easily and confluence is achieved within days (depending on initial concentration).[232] Poly-D-lysine and laminin coated glass have also been used by the same group; these coatings providing a cheaper and more efficient method of differentiating the cells into neurospheres than the conventional retinoic acid methodology.

Stem cells have also been grown successfully onto poly(acrylic acid), poly(allyl amine), phospholipids and gelatin[233] with the surface properties important in determining the cell response. Less adhesive surfaces showing strong ability to induce cell differentiation, phospholipids[234] and polypropylene[235] in particular encouraged differentiation rapidly, with gelatin and acrylic acid promoting cell adhesion and growth in preference to differentiation. Hydrogels, including cross linked poly(2-hydroxyethylmethacrylate),[236] have also shown excellent ability to encourage cell growth without initiating cell differentiation. Polymerization with a co-polymer was required to ensure insolubility of the hydrogel but increasing levels of co-polymer increased the hydrophobicity and reduced the cell growth potential.

---

[1] Yasuda, H. *Plasma Polymerisation* Academic Press, Pg. 19, **1985,** Florida,

[2] Langmuir, I. *Phys. Rev.,* **1929,** *33*, 954

[3] Dresvin, S.V.; Donskoi, A.V.; Goldfarb, V.M.; Klubnikin, V.S. *Physics and Technology of Low Temperature Plasmas*, Iowa University Press, **1977**, Ames

[4] Dai, L.; Grieseer, H.J.; Mau, A.W.H. *J. Phys. Chem. B* **1997**, *101*, 9548

[5] Chen, Q.; Dai, L. *Appl. Phys. Lett.* **2000,** *76*, 2719

[6] Tarducci, C.; Kinmond, E.J.; Brewer, S. A.; Willis, C.; Badyal, J. P. S. *Chem. Mater.* **2000**, *12*, 1884

[7] Badyal, J.P.S.; Schofield, W.C.E. European Patent 1,492,630

[8] Morra, M.; Occhiello, E.; Garbassi, F. *Langmuir*, **1989**, *5*, 872.

[9] Tarducci, C.; Brewer, S. A.; Willis, C.; Badyal, J.P.S. *Chem. Mater.* **2000**, *12*, 1884.

[10] *Practical Surface Analysis by Auger and X-ray Photoelectron Spectroscopy*, 2nd edition, Seah, M.P.; Briggs, Ed.; D., Wiley & Sons, **1992**, UK

[11] Christie, A. B. *Method of Surface Analysis*, Walls, J. M., Ed.; Cambridge University Press, **1989**,

Cambridge

[12] Behrning, S.; Bley, H.; Braun, P. *Proceedings of the 10th International Colloquium on Surfaces*, **2000,** Chemnitz, Germany, p.230

[13] Adam, N.K. *The Physics and Chemistry of Surfaces*, 3rd Edition. **1941**, Oxford, p.179

[14] Wenzel, R.N. *Ind. Eng. Chem.*, **1936**, *28*, 988

[15] Wenzel, R.N. *J Phys. Colloid Chem.*, **1949**, *53*, 1466

[16] Cassie, A.B.D.; Baxter, S. *Trans. Faraday Soc.*, **1944**, *40*, 546

[17] Shuttleworth, R.; Bailey, G.L.J. *Diss. Faraday Soc.*, **1948**, *3*, 16

[18] Bartell, F.E.; Wooley, J. *J. Amer. Chem. Soc.*, **1936**, *55*, 3515

[19] Cassie, A.B.D. *Diss. Faraday Soc.*, **1948**, *3*, 11

[20] Gao, L.; McCarthy, T.J. *Langmuir*, **2006,** *22*, 6234

[21] Bartell, F.E.; Shepard, J.W. *J. Phys. Chem. Soc.*, **1953**, *57*, 211

[22] Bartell, F.E.; Shepard, J.W. *J. Phys. Chem. Soc.*, **1953**, *57*, 455

[23] Bartell, F.E.; Shepard, J.W. *J. Phys. Chem. Soc.*, **1953**, *57*, 458

[24] Johnson, R.E. Jnr.; Dettre, R.H. *Contact Angle, Wettability, and Adhesion*; Fowkes, F.M., Ed.; Adv. Chem. Ser. 43, A.C.S., **1963**, Washington D.C., p.112

[25] Binnig, G.; Roher, H.; Gerber, C.; Weibel, E. *Phys. Rev. Lett.* **1982**, *49*, 57

[26] Binnig, G.B.; Quate, C.F.; Gerber, C.H.; *Phys. Rev. Lett.* **1986**, *56*, 930

[27] Briggs, D.; Seah, M. P. *Practical Surface Analysis. Vol 1 – Auger and X-Ray Phtoelectron Spectroscopy*; John Wiley, **1990,** Chichester, UK

[28] Johnson, R. E.; Dettre, R. H. *Wettability*; Berg, J. C., Ed.; Marcel Dekker, Inc. **1993**, New York, p13

[29] Lovering, D., NKD-6000 *Technical Manual: Aquila Instruments*, **1999,** Cambridge, UK

[30] Craighead, H.G.; James, C.D.; Turner, A.M.P. *Curr. Opin. Solid State Mat. Sci.* **2001**, *5*, 177

[31] Kam, L.; Shain, W.; Turner, J.N.; Bizios, R. *Biomaterials* **2001**, *22*, 1049

[32] Fay, B. *Microelec. Eng.* **2002**, *61*, 11

[33] Chang, T.H.P.; Thomson, M.G.R.; Yu, M.L.; Kratschmer, E.; Kim, H.S.; Lee, K.Y.; Rishton, S.A.; Zolgharnain, S. *Microelec. Eng.* **1996**, *32*, 113

[34] He, W.; Poker, D.B.; Gonsalves, K.E.; Batina, N. *Microelec. Eng.* **2003**, *65*, 153

[35] Masuda, T.; Sugiyama, T.; Lin, H.; Seo, W.S.; Kumoto, K. *Thin Solid Films* **2001**, *382*, 153

[36] Falconneta, D.; Csucsb, G.; Grandina H.M.; Textor, M. *Biomaterials,* **2006**, *27,* 3044

[37] Sleyto, U.B.; Sára, M.; Pum, D.; Schuster, B. *Prog. Surf. Sci.* **2001,** *68*, 231

[38] Ito, Y. *Biomaterials* **1999**, *20,* 2333

[39] Bhatia, S.K.; Hickman, J.J; Ligler, F.S. *J. Am. Chem. Soc.* **1992**, *114*, 4432

[40] Matsuda, T.; Inoue, K.; Tani, N. U.S. Patent 5202227, **1993**

[41] Kleinfeld, D.; Kahler, K.H.; Hockberger, P.E. *J. Neurosci*, **1988**, *8*, 4098

[42] Britland, S.; Perez-Arnaud, E.; Clark, P.; McGinn, B.; Connolly, P.; Moores, G. *Biotechno. Prog.* **1992**, *8*, 155

[43] Kane, R.; Takayama, S.; Ostuni, E.; Ingber, D.E.; Whitesides, G.M. *Biomaterials* **1999**, *20*, 2363

[44] Park, T.H.; Shuler, M.L. *Biotechnol. Prog.* **2003,** *19*, 243

[45] Reichmanis, E.; Houlihan, F.; Nakamasu, O.; Neeham, T. *Chem. Mater.* **1991,** *3*, 394

[46] Groves, T. R.; Pickard, D.; Rafferty, B.; Crosland, N.; Adam, D.; Schubert, G. *Microelec. Eng.* **2002**, *61*, 285

[47] Merhari, L.; Gonsalves, K.E.; Hu, Y.; He, W.; Huang, W.-S.; Angelopoulos, M.; Bruenger, W.H.; Dzionk, C.; Torkler, M. *Microelec. Eng.* **2002**, *63*, 391

[48] Wallraff, G.M.; Hinsberg, W.D. *Chem. Rev.* **1999**, *99*, 1801

[49] Malaquin, L.; Carcenac, F.; Vieu, C.; Mauzac, M. *Microelec. Eng.* **2002**, *61*, 379

[50] Casey, B.G.; Cumming, D.R.S.; Khandaka, I.I.; Curtis, A.S.G.; Wilkinson, C.D.W. *Microelec. Eng.* **1999**, *46*, 125

[51] Wilbur, J.L.; Kumar A.; Biebuyck H.A.; Kim E.; Whitesides G.M. *Nanotech.* **1990**, *7*, 452

[52] Chilkoti, A.; Yang, Z. US 6444254, **2002**

[53] Kumar, A.; Whitesides, G.M. *Appl. Phys. Lett.* **1993**, *273*, 347

[54] Jackman, R.; Wilbur, J.; Whitesides, G.M. *Science* **1995**, *269*, 664

[55] Zhao, X.-M.; Xia, Y.; Whitesides, G.M. *Mater. Chem* .**1997,** *7*, 1069

[56] López, G.P.; Biebuyck, H.A.; Härter, R.; Kumar, A.; Whitesides, G.M. *J. Am. Chem. Soc.* **1993**, *115*, 10774

[57] Xia, X.; McClelland, J.J.; Gupta, R.; Qin, D.; Zhao, X. –M.; Sohn. L.L.; Celotta, R.J.; Whitesides, G.M. *Adv. Mater.* **1997**, *9*, 147

[58] Kim, E.; Xia, Y.; Whitesides, G.M. *Nature* **1995**, *376*, 581

[59] Delamarche, E.; Bernard, A; Schmid, H.; Michael, B.; Biebuyck, H. *Science* **1997**, *276*, 779

[60] Xia, Y.; Kim, E.; Whitesides, G.M. *Chem. Mater.* **1996**, *8*, 1558

[61] Thissen, H.; Hayes, J.P.; Kingshott, P.; Johnson, G.; Harvery, E.C.; Griesser, H.J. *Smart Mater. Struct.* **2002**, *11*, 792

[62] Biebuyck, H.A.; Larsen, N.B.; Delamarche, E.; Michael, B. *IBM J. Res. Dev.,* **1997**, *41*, 159

[63] Liu, J.-F.; Zhang, L.-G.; Gu, N.; Ren, J.-Y., Wu, Y.-P.; Lu, Z.-H.; Mao, P.-S.; Chen, D.-Y. *Thin Solid Films* **1998**, *327*, 176

[64] Dai, L.; Grieseer, H.J.; Mau, A.W.H. *J. Phys. Chem. B* **1997**, *101*, 9548

[65] Dai, L.; Mau, A.W.H.; Gong, X.; Grieseer, H.J. *Syn. Mater.* **1997**, *85*, 1379

[66] Chan, C.-M.; Ko, T.-M.; Hiraoka, H. *Sur. Sci. Rep.* **1996**, *24*, 1

[67] Dewez, J.L.; Lhoest, J.B.; Detrait, E.; Berger, V.; Dupont-Gillain, C.C.; Vincent, L.M.; Schneider, Y.J.; Bertrand, P.; Rouxhet, P.G. *Biomaterials* **1998,** *19*, 1441

[68] Ostuni, E.; Chen, C.S.; Ingber, D.E.; Whitesides, G.M. *Langmuir* **2001,** *17*, 2828

[69] Nolan, J.P.; Sklar L.A. *Trends Biotech.* **2002**, *1*, 9

[70] Krishan, C.; Tiecheng Q.; Lincoln V.D. EP 1287883, **2003**

[71] Harvey T.B. US 20030044801, **2003**

[72] Epstein, J.R.; Leung, A.P.K.; Lee, K.-H.; Walt, D.R. *Biosens. Bioelec.* **2003,** *18*, 541

[73] Blohm, D.H.; Guiseppi-Elie, A. *Curr. Opin. Biotech.* **2001**, *12*, 41

[74] Qin, D.; Xia, Y.; Xu, B.; Yang, H.; Zhu, C.; Whitesides, G.M. *Adv. Mater.* **1999,** *11*, 1433

[75] Becker, H.; Gärtner, C. *Rev. Mol. Biotech.* **2001**, *82*, 89

[76] Boone, T.D.; Fan, Z.H.; Hooper, H.H.; Ricco, A.J.; Tan, H.; Williams, S.J. *Anal. Chem.* **2002**, *74*, 78A

[77] Parker, A.R.; Lawrence, C.R. *Nature* **2001,** *414*, 33

[78] Dai, L.; Griesser, H.J.; Hong, X.; Mau, A.W.H.; Spurling, T.H.; Yang, Y.; White, J.W. *Macromolecules* **1996**, *29*, 282

[79] Beh, W.S.; Kim, I.T.; Qin, D.; Xia, Y.; Whitesides, G.M. *Adv. Mater.* **1999**, *11*, 1038

[80] Gardner, J.W.; Bartlett, P.N. *Sensors Actuators A.* **1995,** *51*, 57

[81] Horowitz, G. *Adv. Mater.* **1998**, *10*, 365

[82] Gangopadhyay, R.; De, A. *Chem. Mater.* **2000**, *12*, 608

[83] Arefi-Khonsari, F.; Kurdi, J.; Tatoulian, M.; Amouroux, J. *Surf. Coat. Tech.* **2001,** *142*, 437

[84] Doppelt, P.; Combellas, C.; Kanoufi, F.; Chen, T.Y.; Richardson, S.; Thiébault A. *Microelec. Eng.* **2000**, *50*, 383

[85] Esrom, H. *Appl. Surf. Sci.* **2000,** *168*, 1

[86] Yang, G.H.; Lim, C.; Tan, Y.P.; Zhang, Y.; Kang, E.T.; Neoh, K.G. *Eur. Poly. J.* **2002,** *38*, 2153

[87] Kang, E.T.; Tan, K.L.; Kato, K.; Uyama, Y.; Ikada, Y. *Macromolecules* **1996,** *29*, 6872

[88] Ji, Y.L.; Kang, E.T.; Neoh, K.G.; Tan, K.L. *Macromolecules* **1999,** *32*, 8183

[89] Wu, S.; Kang, E.T.; Neoh, K.G.; Tan, K.L. *Langmuir* **2000,** *16*, 5192

[90] Yang, G.H.; Kang, E.T.; Neoh, K.G.; Zhang, Y.; Tan, K.L. *Langmuir* **2001**, *17*, 211

[91] Whang, Z.; Zhang, J.; Xing, R.; Yuan, J.; Yan, D.; Han, Y. *J. Am. Chem. Soc.* **2003**, *125*, 15278

[92] Jiang, P.; McFarland, M.J. *J. Am. Chem. Soc.* **2005**, *127*, 3710

[93] Georgiadis, R.; Peterlinz, K.P.; Peterson, A.W. *J. Am. Chem. Soc.* **2000**, *122*, 3166

[94] Zhou, H.; Baldini, L.; Hong, J.; Wilson, A.J.; Hamilton, A.D. *J. Am. Chem. Soc.* **2006**, *128*, 2421

[95] Filho, F.H.D.; Mauricio, M.H.P.; Ponciano, C.R.; Prioli, R. *Mater. Sci. Eng., B* **2004**, *112*, 194

[96] Wei, C.; Dai, L.; Roy, A.; Tolle, T.B. *J. Am. Chem. Soc.* **2006**, *128*, 1412

[97] Kline, R.T.; Paxton, F.W.; Wang, Y.; Velegol, D.; Mallouk, T.E.; Sen, A. *J. Am. Chem. Soc.* **2005**, *127*, 17150

[98] Friebel, S.; Aizenberg, J.; Abad, S.; Wiltzius, P. *Appl. Phys. Let.* **2000**, *77*, 2406

[99] Mendes, P.M.; Jacke, S.; Critchley, K.; Plaza, J.; Chen, Y.; Nikitin, K.; Palmer, R.E.; Preece, J.A.; Evans, S.D.; Fitzmaurice, D. *Langmuir* **2004**, *20*, 3766

[100] Callewaert, K.; Martele, Y.; Breban, L.; Naessens, K.; Van Daele, P.; Baets, R.; Geuskens, H.; Schacht, E. *Appl. Sur. Sci.* **2003**, *208-209*, 218

[101] Bouaidat, S.; Winther-Jensen, B.; Jonsmann, J.; EP 1260863, **2002**

[102] Park, C.; Yoon, J.; Thomas, E.L.; *Polymer*, **2003**, *44*, 6725

[103] Cox, J.K.; Eisenberg, A.; Lennox, R.B. *Curr. Opin. Coll. Inter. Sci.,* **1999**, *4*, 52

[104] Xia, Y.; Whitesides, G.M. *Angew. Chem. Int. Ed.* **1998**, *37*, 550

[105] Whitesides, G.M.; Ingber, D.E.; Ostuni, E.; Chen, C.S.; WO 02086452

[106] Chen, Y.; Lebib, A.; Carcenac, F.; Launois, H.; Schmidt, G.; Tormen, M.; Muller, G.; Molenkamp, L.W.; Liebau, M.; Huskens, J.; Reinhoudl, S.N. *Microelec. Eng.* **2000**, *53*, 253

[107] Yu, A.A.; Savas, T.; Cabrini, S.; diFabrizio, E.; Smith, H.I.; Stellacci, F. *J. Am. Chem. Soc.* **2005**, *127*, 16774

[108] Jaszewski, Schift, Gobrecht, Smith *Microelect. Eng.* **1998**, *41/42*, 575

[109] Chou, S.Y.; Krauss, P.R.; Renstrom, P.J.; *Appl. Phys. Lett.* **1995,** *67,* 3114

[110] Khang, D.-Y.; Hyunsik, Y.; Lee, H.H.; Adv. Mater. **2001**, *13*, 749

[111] Carr, T.W.; Needham, C.D.; Villetto, R.T.Jr.; EP 0031463, **1980**

[112] Severin, J.W.; Meeuwsen, F.A.; WO 9837740, **1998**

[113] Jacobs, O.; Hamm, U.W.; Kasparek, M.; US 2002164882, **2002**

[114] Neckers, D.C.; Specht, K.G.; Grinevich, O.V.; Mejiritski, A.; WO 0114460, **2001**

[115] Russo, A.P.; Apoga, D.; Dowell, N.; Shain, W.; Turner, A.M.P.; Craighead, H.G.; Hoch, H.C.; Turner, J.N. Biomed. Microdevices, **2002,** *4*, 277

[116] Liang, Z.; Rackaitis, M.; Li, K.; Manias, E.; Wang, Q. Chem. Mater. **2003**, *15*, 2699

[117] Ulsh, M.J.; Strobel, M.A.; Serion, D.F.; Keller, J.T. US 6096247, **2000**

[118] Chen, Q.; Dai, L.; *Appl. Phys. Lett.* **2000,** *76,* 2719

[119] Mitchell, S.A.; Emmison, N.; Shard, A.G.; Eur. Cell Mater. 2002, 4, 52

[120] Frey, W.; Woods, C.K.; Chilkoti, A.; *Adv. Mater.* **2000**, *12*, 1515

[121] Rinsch, C. L.; Chen, X.; Panchalingham, V.; Eberhart, R.C.; Wang, J. H.; Timmons, R. B. *Langmuir* **1996**, *12*, 2995

[122] Coulson, S. R.; Woodward, I. S.; Brewer, S. A.; Willis, C.; Badyal, J. P. S. *Chem. Mater.* **2000**, *12*, 2031

[123] Tarducci, C.; Kinmond, E.J.; Brewer, S. A.; Willis, C.; Badyal, J. P. S. *Chem. Mater.* **2000**, *12*, 1884

[124] Ryan, M. E.; Hynes, A. M.; Badyal, J. P. S. *Chem. Mater.* **1996**, *8*, 37

[125] Hutton, S. J.; Crowther, J. M.; Badyal, J. P. S. *Chem. Mater.* **2000**, *12*, 2282

[126] Tarducci, C.; Schofield, W. C. E.; Brewer, S.; Willis, C.; Badyal, J. P. S. *Chem. Mater.* **2001**, *13*, 1800.

[127] Oye, G.; Roucoules, V.; Oates, L.J.; Cameron, A.M.; Cameron, N.R.; Steel, P.G.; Davis, B.G.;

Coe, D.M.; Cox, R.A.; Badyal, J.P.S. *J. Phys. Chem. B* **2003**, *107*, 3496.

[128] Teare, D.O.H.; Barwick, D.C.; Schofield, W.C.E.; Garrod, R.P.; Ward, L.J.; Badyal, J.P.S. *Langmuir* **2005**, *21*, 11425.

[129] Tarducci, C.; Brewer, S.A.; Willis, C.; Badyal, J.P.S. *Chem. Commun.* **2005**, *3*, 406.

[130] Schofield, W.C.E.; McGettrick, J.; Bradley, T.J.; Przyborski, S.; Badyal, J.P.S. *J. Am. Chem. Soc.* **2006**, *128*, 2280

[131] Rogers, J.A.; Bao, Z.; Meier, M.; Dodabalapur, A.; Schueller, O.J.A.; Whitesides, G.M. *Syn. Metals* **2000**, *115*, 5

[132] Dai, L.; Griesser, H.J.; Mau, A.W.H.; J.Phys. Chem. B, **1997**, *101*, 9548

[133] Ito, Y. *Biomat.* **1999**, *20*, 2333

[134] Nygren, N. *Coll. Surf. B. Biointer.* **1996**, *6,* 329

[135] Xu, Y.; Watson, T.; Bruening, M. L. *Anal. Chem.* **2003**, *75*, 185

[136] Gilmor, S. D.; Thgiel, A. J.; Strother, T. C.; Smith, L. M.; Lagally, M. G. *Langmuir* **2000**, *16*, 7223

[137] Zhang, G.; Yan, X.; Hou, X.; Lu, G.; Yang, B.; Wu, L.; Shen, J. *Langmuir* **2003**, *19*, 9850

[138] Handique, K.; Burke, D. T.; Mastrangelo, C. H.; Burns, M. A. *Anal. Chem.* **2000**, *72*, 4100

[139] Huang, Z.; Wang, P.-C.; Feng, J.; MacDiarmid, A. G.; Xia, Y.; Whitesides, G. M. *Synth. Metals* **1997**, *85*, 1375

[140] Wojtyk, J. T. C.; Tomietto, M.; Boukherroub, R.; Wayner, D. D. M.; *J. Am. Chem. Soc.* **2001**, *123*, 1535

[141] Karthaus, O.; Gråsjö, L.; Maruyama, N.; Shimomura, M. *Thin Solid Films* **1998**, *327-329*, 829-832

[142] Krautter, J.; Dzialas, W. US 4576864, **1986**; Taniguchi, T.; Mibae, J. US 4478909, **1984;** Hosono, H.; Taniguchi, T. US 5134021, **1992;** Swerdlow, M. S. US 4409285, **1983**

[143] Kamio, H.; Uejima, T.; Abe, K.; Itoh, H.; Kobayashi, S.; Nitta, A.; Ouchi, T.; Tanaka, T.; Enoshita, R.; Nakagawa, T. US 4683258, **1987**

[144] Oshibe, Y.; Yamamoto, Y.; Ohmura, H.; Kumazawa, K. US 5244935, **1993**

[145] Dettre, R. H.; Johnson, R. E. *Adv. Chem. Ser.* **1964**, *43*, 136

[146] Zhai, L.; Berg, M.C.; Cebeci, F.Ç.; Kim, Y.; Milwid, J.M.; Rubner, M.F.; Cohen, R.E. *Nano Lett.,* **2006,** *6*, 1213

[147] Woodward, I.; Schofield, W. C. E.; Roucoules, V.; Badyal, J. P. S. *Langmuir* **2003**, *19*, 3432

[148] Morra, M.; Occhiello, E.; Garbassi, F. *Surf. Interface Anal.* **1990**, *16*, 412

[149] Ryan, M. E.; Badyal, J. P. S. *Macromolecules* **1995**, *28*, 1377

[150] Morra, M.; Occhiello, E.; Garbassi, F. *Langmuir*, **1989**, *5*, 872

[151] Coulson, S. R.; Woodward, I.; Badyal, J. P. S.; Brewer, S. A.; Willis, C. *J. Phys. Chem. B* **2000**, *104*, 8836

[152] www.fogquest.org

[153] Chung, B.-J.; Kim, S.; Kim, M. C. *Int. Comm. Heat Mass Transfer* **2005**, *32*, 233

[154] Mittal, K.L., Ed.: *Contact Angle, Wettability and Adhesion*; VSP, **1993**, Zeist, Netherlands

[155] Furnidge, G.C.L. *J. Colloid Interface Sci.* **1962**, *17*, 309

[156] Healy, K.E. *Curr. Opin. Solid State Mater. Sci.* **1999**, *4*, 381

[157] Higham, M.; Short, R.; Szabo, M.; Dawson, R.; MacNeil, S. *Eur. Cell Mater.* **2002**, *4*, 36

[158] Hutmach, D.W. *Biomaterials*, **2000**, *21*, 2529

[159] Webb, R.; Hlady, W.; Tresco, P.A. *J. Biomed. Mater. Res.* **1998**, *41*, 422

[160] Dewez, J.-L.; Doren, A.; Schneider, Y.-J.; Rouxhet, P.G. *Biomaterials*, **1999**, *20*, 547

[161] Altankov, G.; Thom, V.; Groth, Th.; Jankova, K.; Jonsson, G.; Ulbricht, M. *J. Biomed. Mater. Res.* **1999**, *52*, 219

[162] Salloum, D.S.; Olenych, S.G.; Keller, T.C.S.; Schlenoff, J.B. *Biomacromolecules*, **2005**, *6*, 161

[163] Bisson, I.; Koskinski, M.; Ruault, S.; Gupta, B.; Hilborn, J.; Wurm, F.; Frey, P. *Biomaterials*, **2002**, *23*, 3149

[164] Pierschbacher, M.D.; Ruoslahti, E. *Nature*, **1984**, *209*, 30

[165] Franco, M.; Nealey, P.F.; Campbell, S.; Teixeira, A.I.; Murphy, C.J. *J. Biomed. Mater. Res.* **2000**, *52*, 261

[166] Evans, M.D.M.; Steele, J.G. *Exp. Cell Res.* **1997**, *233*, 88

[167] Ohji, M.; Mandarino, L.; Sundarraj, N.; Throft, R.A. *Invest. Ophthal. Vis. Sci.* **1993**, *34*, 2487

[168] Sanborn, S.I.; Murugesan, G.; Marchant, R.E.; Kottke-Marchant, K. *Biomaterials*, **2002**, *23*, 1

[169] Grinnell, F.; Feld, M.K. *J. Biol. Chem.* **1982**, *257*, 4888

[170] Kaibara, M.; Iwata, H.; Wada, H.; Kawamoto, Y.; Iwaki, M.; Suzuki. Y. *J. Biomed. Mater. Res.* **1996**, *31*, 429

[171] Tamada, Y.; Ikada, Y. *J. Coll. Int. Sci.*, **1993**, *155*, 334

[172] Nath, N.; Hyun, J.; Ma, H.; Chilkoti, A. *Sur. Sci.*, **2004**, *570*, 98

[173] Brash, J.L.; Horbett, T.A. *Proteins and Interfaces*, ACS Symposium Series, **1995**, *602*, 1

[174] Tidwell, C.D.; Ertel, S.I.; Ratner, B.D.; Tarasevich, B.J.; Atre, S.; Allara, D.L. *Langmuir*, **1997**, *13*, 3404

[175] Chapman, R.G.; Ostuni, E.; Takayama, S.; Holmlin, R.E.; Yan, L.; Whitesides, G.M. *J. Am. Chem. Soc.* **2000**, *122*, 8303

[176] Curtis, A.S.G.; Forrester, J.V.; Clark, P. *J.Cell. Sci.* **1986**, *86*, 9

[177] Ertel, S.I.; Chilkoti, A.; Horbett, T.A.; Ratner, B.D. *J. Biomater. Sci. Polym. Ed.* **1991**, *3*, 163

[178] Chinn, J.A.; Horbett, T.A.; Ratner, B.D.; Schqay, M.B.; Haque, Y.; Hauschka, S.D. *J. Colloid Interface Sci.* **1989**, *127*, 67

[179] Nuzzo, R.G.; Dubois, L.H.; Allara, D.L. *J. Am. Chem. Soc.* **1990**, *112*, 558

[180] Lewandowska, K.; Pergament, E.; Sukenik, C.N.; Culp, L.A. *J. Biomed. Mater. Res.* **1992**, *26*, 1343

[181] Prime, K.L.; Whitesides, G.M. *J. Am. Chem. Soc.* **1993,** *115*, 10714

[182] Gumpenberger, T.; Heitz, J.; Bäuerle, D.; Kahr, H.; Graz, I.; Romanin, C.; Svorcik, V.; Leisch, F. *Biomaterials,* **2003,** *24*, 5139

[183] Suzuki, Y. *Nucl. Instr. And Meth. In Phys. Res. B* **2003,** *206*, 501.

[184] Hsu, S.-H.; Chen, W.-C. *Biomaterials* **2000**, *21*, 359

[185] Hayman, M.W.; Smith, K.H.; Cameron, N.R.; Przyborski, S.A. *J. Biochem. Biophys. Methods,* **2004**, *31*, 231

[186] Feng, X.; Zhang, J.; Xie, H.; Hu, Q.; Huang, Q.; Liu, W. *Surf. Coat. Technol.* **2003,** *171*, 96

[187] Absolom, D.R.; Hawthorn, L.A.; Chang, G. *J. Biomed. Mater. Res.* **1988**, *22*, 271

[188] Van Wachem, P.B.; Hogt, A.H.; Beugeling, T.; Feijen, J.; Bantjes, A.; Detmers, J.P.; Van Aken, W.G. *Biomaterials,* **1987,** *8,* 323

[189] Lee, J.H.; Khang, G.; Lee, J.W.; Lee, H.B. *J. Colloid. Inter. Sci.* **1998,** *205*, 323

[190] Van Kooten, T.G.; Schakenraad, J.M.; Van der Mei, H.C.; Busscher, H.J. *Biomaterials,* **1992,** *13*, 897

[191] Griesser, H.J.; Chatelier, R.C.; Gengenbach, T.R.; Vasic, Z.R.; Johnson, G.; Steele, J.G. *Polym. Int.* **1992,** *27*, 109

[192] Teare, D. O. H.; Barwick, D. C.; Schofield, W. C. E.; Garrod, R. P.; Beeby, A.; Badyal, J. P. S.; *J. Phys. Chem. B* **2005**, *109*, 22407

[193] Higham, M.; Short, R.; Szabo, M.; Dawson, R.; MacNeil, S. *Eur. Cell Mater.* **2002,** *4*, 36

[194] Dahm, M.; Chang, B.-J.; Prucker, O.; Pierkes, M.; Alt, T.; Mayer, E.; Rühe, J.; Oelert, H. *Ann. Thora. Surg.***2001,** *71*, S437

[195] Daw, R.; Candan, S.; Beck, A.J.; Devlin, A.J.; Brook, I.M.; MacNeil, S.; Dawson, R.A.; Short, R.D. *Biomaterials,* **1998,** *19*, 1717

[196] Young, C.-D.; Wu, J.-R.; Tsou, T.-L. *J. Membrane Sci.* **1998,** *146*, 83

[197] France, R.M.; Short, R.D.; Dawson, R.A.; MacNeil, S. *J. Mater. Sci.* **1998**, *8*, 37

[198] Yang, J.-Y.; Huang, M.J.; Yeh, T.-S. J. Biomed. Mater. Res. **1999**, *45*, 133

[199] Ertel, S.I.; Ratnoer, B.D.; Horbett, T.A. *J. Biomed. Mater. Res.* **1990,** *24*, 1637

[200] Stenger, D.A.; Georger, J.H.; Dulcey, C.S.; Hickmann, J.J.; Rudolph, A.S.; Nielson, T.B.; McCort, S.M.; Calvert, J.M. *J. Am. Chem. Soc.* **1992,** *114*, 8435

[201] Pignataro, B.; Conte, E.; Scandurra, A.; Marletta, G. *Biomaterials* **1997,** *18*, 1461

[202] Maroudas, N.G. *J. Theoret. Biol.* **1975,** *49*, 417

[203] Sutherland, D.S.; Brink, J.; Olsson, P.; Lidberg, U.; Andersson, A.-S. *Eur. Cell Mater.* **2002,** *4*, 28

[204] Dalby, M.; Riehle, M.; Yarwood, S.J.; Johnstone, H.J.H.; Affrossman, S.; Curtis, A.S.G. *Eur. Cell Mater.* **2002**, *4*, 47

[205] Lampin, M.; Warocquiere-Clérout, R.; Legris, C.; Degrange, M.; Sigot-Luizard, M.F. *J. Biomed. Mater. Res.* **1997,** *36*, 99

[206] Rinsch, C. L.; Chen, X.; Panchalingham, V.; Eberhart, R.C.; Wang, J. H.; Timmons, R. B. *Langmuir* **1996**, *12*, 2995

[207] Coulson, S. R.; Woodward, I. S.; Brewer, S. A.; Willis, C.; Badyal, J. P. S. *Chem. Mater.* **2000**, *12*, 2031.

[208] Tarducci, C.; Kinmond, E.J.; Brewer, S. A.; Willis, C.; Badyal, J. P. S. *Chem. Mater.* **2000**, *12*, 1884

[209] Ryan, M. E.; Hynes, A. M.; Badyal, J. P. S. *Chem. Mater.* **1996**, *8*, 37.

[210] Hutton, S. J.; Crowther, J. M.; Badyal, J. P. S. *Chem. Mater.* **2000**, *12*, 2282.

[211] Tarducci, C.; Schofield, W. C. E.; Brewer, S.; Willis, C.; Badyal, J. P. S. *Chem. Mater.* **2001**, *13*, 1800

[212] Ertel, S.I.; Ratner, B.D.; Horbett, T.A. *J. Colloid Interface Sci.* **1991**, *147*, 433

[213] Lhoest, J.-B.; Detrait, E.; Van den Bosch de Aguilar, P.; Bertrand, P. *J. Biomed. Mater. Res.* **1998**, *41*, 95

[214] http://users.path.ox.ac.uk/~vdmerwe/Internal/spr.PDF

[215] Bradley, T.J.; Schofield, W.C.E.; Garrod, R.P.; Badyal, J. P. S.; *Langmuir* **2006**, *22*, 7552

[216] Badyal, J. P. S.; Schofield, W.C.E. EP 1492630, **2005**

[217] Evenson, S.A.; Fail, C.A.; Badyal, J. P. S. *Chem. Mater.* **2000**, *12*, 3038

[218] Teare, D.O.H.; Schofield, W.C.E.; Garrod, R.P.; Badyal J.P.S. *J. Phys. Chem. B* **2005**, *109*, 20923

[219] Schofield, W. C. E.; McGettrick, J.; Bradley. T. J.; Badyal, J. P. S.; Przyborski, S.; *J. Am. Chem. Soc.* **2006**, *128*, 2280

[220] Teare, D.O.H.; Schofield, W.C.E.; Garrod, R.P.; Ward, L.J.; Badyal J.P.S. *Langmuir* **2005**, *21*, 11425

[221] McGettrick, J.D.; Schofield, W. C. E.; Badyal, J. P. S, WO 2006100480, **2006**

[222] Coulson S.R.; Badyal, J.P.S. WO 0005000, **2000**

[223] Tarducci, C.; Schofield, W. C. E.; Badyal, J. P. S.; Brewer, S. A.; Willis, C. *Chem. Mater.* **2002**, *14*, 2541

[224] Han, L.M.; Timmons, R.B. *J. Polym. Sci. A Polym. Chem.* **1998**, *36*, 3121

[225] Kottke-Marchant, K.; Veenstra, A.A.; Marchant, R.E. *J. Biomed. Mater. Res.* **1996**, *30*, 209

[226] Akiyama, Y.; Kikuchi, A.; Yamato, M.; Okano, T. *Langmuir,* **2004**, *20*, 5506

[227] Rowe, A.J. *Biophys. Chem.* **2001**, *93*, 93

[228] Kitano, H.; Imai, M.; Sudo, K.; Ide, M. *J. Phys. Chem. B,* **2002**, *106*, 11391

[229] Kitano, H.; Sudo, K.; Ichikawa, K.; Ide, M.; Ishihara, K. *J. Phys. Chem. B,* **2000**, *104*, 11425

[230] Vogler, E.A. *Adv. Coll. Int. Sci.* **1998**, *74*, 69

[231] Cicero, G.; Grossman, J.C.; Catellani, A.; Galli, H. *J. Am. Chem. Soc.* **2005**, *127*, 6830.

[232] Stewart, R.; Christie, V.B.; Przyborski, S. *Stem Cells,* **2003**, *21*, 246

[233] Konno, T.; Kawazoe, N.; Chen, G.; Ito. Y. *J. Biosci. Bioeng.* **2006,** *102*, 304

[234] Konno, T.; Akita, K.; Kurita, K.; Ito, Y. *J. Biosci. Bioeng.* **2005,** *100*, 88

[235] Kurosava, H.; Imamura, T.; Koike, M.; Sasaki, K.; Amano, Y. *J. Biosci. Bioeng.* **2003,** *96*, 409

[236] Horak, D.; Kroupova, J.; Slouf, M.; Dvorak, P. *Biomaterials,* **2004,** *25*, 5249